



UNIVERSITÀ
POLITECNICA
DELLE MARCHE

FACULTY OF ENGINEERING
MASTER'S DEGREE IN BIOMEDICAL ENGINEERING

USE OF 3D PRINTING TECHNOLOGY AS
HEART SURGICAL GUIDE IN ISCHEMIC
SCAR ABLATION TREATMENT:
A FEASIBILITY STUDY

THESIS SUPERVISOR:

PROF. MARCO MANDOLINI

MASTER THESIS OF:

MARA CANDELARI

THESIS CO-SUPERVISORS:

PROF. BERNARDO INNOCENTI

PROF. CARLO DE ASMUNDIS

ANNO ACCADEMICO 2020-2021

ABSTRACT

In last decades 3D printing has had rapid developments in medicine, especially in orthopedy and dentistry, where it is used as surgical guide for implantation with an improvement of treatment outcomes. Thus, the purpose of this work is to propose a cardiac surgical guide as improved solution for ischemic scar treatment, reducing the medical procedure timing, and enhancing the treatment. The work is done at the cardiology department of UZ Brussel Hospital in Bruxelles, under the guidance of Prof. Marco Mandolini, Prof. Bernardo Innocenti and Prof. Carlo de Asmundis.

The treatment of ischemic scar in patients with post myocardial infarction (MI) is clinically important because it leads to malignant arrhythmias, like ventricular tachycardia (VT), which represent a common cause of morbidity and mortality. Because of MI, the border zone between scarred and normal myocardium is the predominant substrate for the majority of VT post-MI. Nowadays, the treatment consists of a long iterative method, which alternes heart electrical activity mapping and ablation procedure until the sinus rhythm is restored. The concept of surgical guide for ischemic scar treatment derived from the need to have a precise visualization of pathological area to make sure to assess the necrotic extent of ablation lesions because an incomplete ablation of arrhythmogenic substrate allows subsequent recovery of tissue with restoration of arrhythmias.

To build a surgical guide to indicate directly on the heart the target area to be treated by ablation procedure, it is necessary to consider surgeon's and engineer's requirements in terms of biocompatibility, efficiency, temperature resistance, manufacturing time and cost. For the model realization, computed tomography (CT) and cardiac magnetic resonance (CMR) images are processed in 3D Slicer Software to extract anatomical structure and pathological information, and then, the models are merged in Meshmixer Software to realize the 3D virtual model. The material selection is crucial: it depends on surgical guide action, and 3D printer, considering workspace and surgical procedures associated to, such as packaging and sterilization through Vaporized Hydrogen Peroxide Gas (VHP).

The second part of this work is focused on demonstrating the product functionality and feasibility, thought conducting of the geometry and thermal tests. The geometry test has demonstrated that the VHP sterilization does not affect either geometric structure (about a millimeter) and mechanical properties. Though the overcomes of nondestructive tests have demonstrated that safe conditions (below 40-45°C during RF and LRF and, above -40°C during cryoablation) are guaranteed in all trials, except for T1 at 0 s during RF, which warms the guide material, leading to cell damaging. Thus, it is

recommended to not be in contact with the surgical mask and maintain at least 1 mm of distance from the mask during ablation. Instead, through the comparison between samples before and after ablation procedures, it is possible to appreciate that all samples have not any visible changes. Finally, the simulation test on porcine heart has demonstrated the surgical mask functionality and the easy application: during LRF procedure, the ablator acts within the surgical mask target area, creating a visible grey lesion which precisely follows the guide perimeter with tolerances in the order of millimeter, considered acceptable.

In conclusion, work findings indicate that the 3D surgical guide is a reliable technology that contributes to more precise and rapid treatment of ischemic scar post MI, but a medical support for identification of target area to treat from diagnostic images is still essential. Further studies are needed to make a trustworthy evaluation of position accuracy and to demonstrate the efficiency in terms of time and quality for the ischemic scar ablation treatment.

ABSTRACT (Italian version)

Negli ultimi decenni la stampa 3D ha subito rapidi sviluppi in diversi campi della medicina, in particolare in ortopedia e in ortodonzia, in cui sono state sviluppate guide chirurgiche per migliorare l'impianto di protesi. Per questo motivo, lo scopo di questo progetto è di proporre una guida chirurgica in ambito cardiologico, per il trattamento di cicatrici ischemiche, minimizzando i tempi della procedura operatoria e migliorandone i risultati. L'intero lavoro è stato svolto a Bruxelles, presso il reparto di cardiologia dell'ospedale UZ Brussel, sotto la supervisione dei professori Marco Mandolini, Bernardo Innocenti e Carlo de Asmundis.

Il trattamento delle cicatrici ischemiche in pazienti affetti da infarto miocardico è di cruciale importanza perché porta ad aritmie cardiache, quali tachicardie ventricolari, che rappresentano una delle più comuni cause di mortalità. In seguito ad un infarto, la zona compresa tra il tessuto cardiaco totalmente danneggiato e quello sano è considerata la zona da trattare.

Attualmente, il trattamento consiste in un processo iterativo che alterna il mappaggio dell'attività elettrica cardiaca e il trattamento di ablazione di piccole zone finché non viene restaurato il ritmo sinusale. Il concetto di guida chirurgica per il trattamento di questa patologia, deriva del bisogno di avere una precisa visualizzazione dell'area patologica che permetta un rapido accesso alla zona da trattare, affinché l'aritmia venga risolta senza rischio di ricadute.

Per costruire una guida che indichi direttamente sulla superficie cardiaca la zona da trattare, è necessario tenere in considerazione diversi requisiti quali la biocompatibilità, la stabilità, la resistenza alla temperatura, i tempi e i costi di realizzazione.

Per la realizzazione del modello, le immagini della TC e della RM sono state processate attraverso il Software 3D Slicer per l'estrazione della struttura anatomica e della patologia. Successivamente, i modelli ottenuti sono stati sovrapposti attraverso il software Meshmixer, ottenendo il modello 3D virtuale. Di cruciale importanza è stata la scelta del materiale, il quale deve essere funzionale al trattamento, compatibile con il tipo di stampante 3D, considerando lo spazio di lavoro, e le procedure associate, tra cui la sterilizzazione attraverso il Perossido di Idrogeno e l'impacchettamento, per il mantenimento delle condizioni sterili fino alla sala operatoria.

La seconda parte del progetto è incentrata a dimostrare la fattibilità e la funzionalità del prodotto, attraverso test termici e sulla geometria. I risultati dei test hanno dimostrato che la guida chirurgica ha risposto positivamente alla maggior parte delle prove a cui è stata sottoposta: la sterilizzazione

VHP non ha avuto effetti né sulla struttura né sulle proprietà meccaniche del materiale. Il materiale ha dimostrato di poter garantire le condizioni di sicurezza quando sottoposto all'ablazione, tranne nella prova di RF, in cui il materiale si surriscalda, portando ad una temperatura di +50°C il tessuto sottostante sano, danneggiandolo. Pertanto, si raccomanda di mantenere lo strumento di ablazione ad una distanza di 1 mm. Al termine dei test termici, i campioni di materiale sono stati paragonati e non è stato rilevato alcun cambiamento. Inoltre, il test di simulazione sul cuore di maiale ha confermato la rapida modalità di applicazione e la funzionalità della guida: l'effetto dell'ablatore sul tessuto cardiaco segue fedelmente il perimetro della zona target indicata dalla guida.

In conclusione, i risultati ottenuti indicano che la guida chirurgica stampata 3D è un'affidabile tecnologia che potrebbe contribuire ad un trattamento più preciso delle cicatrici ischemiche riducendo i tempi della procedura; tuttavia, il supporto medico è ancora essenziale per l'identificazione dell'area patologica dalle immagini diagnostiche. Ulteriori studi sono necessari per valutarne l'accuratezza e l'efficienza specifica per ogni paziente.

Index

- I. Figures List 3
- II. Tables List 7
- 1. Introduction 9
- 2. State of the Art and Theoretical Background 11
 - 2.1. Heart Failure and Myocardial Infarction 11
 - 2.1.1. Arteriosclerosis, the main cause of Myocardial Infarction 12
 - 2.1.2. Pathophysiology of Myocardial Infarction-induced HF 14
 - 2.2. Medical Diagnostic Imaging and Treatment Techniques 15
 - 2.2.1. Physical Principles of Computed Tomography 16
 - 2.2.2. Computed Tomography for Myocardial Perfusion Evaluation 19
 - 2.2.3. Physical Principles of Magnetic Resonance 20
 - 2.2.4. Cardiac Magnetic Resonance for Ischemic Scar Diagnosis 22
 - 2.2.5. Radiofrequency Ablation for Scar-related Ventricular Tachycardia Treatment 23
 - 2.2.6. Cardiac Cryoablation for Scar-related Ventricular Tachycardia Treatment 26
- 3. Design of Surgical Guide for Ischemic Scar Treatment 28
 - 3.1. Needs and Market Analysis 28
 - 3.2. Aim of study 29
 - 3.3. Requirements 30
 - 3.4. Function 32
 - 3.5. Specifications 33
 - 3.6. Quality Function Deployment Method 34
 - 3.7. Conceptualization 36
 - 3.8. Evaluating Alternatives 38
 - 3.8.1. Concepts and Parameters Evaluation 40
- 4. Case Report 41

4.1.	Virtual Prototyping Algorithm	41
5.	Detailed Design	47
5.1.	Process Selection: 3D printing.....	47
5.1.1.	Stratasys Objet260 Connex1 3D printer	48
5.1.2.	PRUSA 3D printer	50
5.2.	Material Selection	52
5.3.	Cleaning, Packaging and Sterilization.....	52
5.4.	Cost Estimation.....	55
6.	Design Analysis	56
6.1.	The First Physical Prototype	56
6.2.	The Second Physical Prototype	59
6.3.	Comparative Analysis between the first and the second prototype	61
7.	Experimental Validation Tests	63
7.1.	Geometry Test.....	64
7.1.1.	Methodology of Geometry Test of Cardiac Surgical Guide for ischemic scar treatment 64	
7.1.2.	Results of Geometry Test.....	64
7.2.	Nondestructive Tests: Thermal and Contact Safe evaluation in Wet Lab	67
7.2.1.	Methodology of Nondestructive Tests	67
7.2.2.	Results of Nondestructive Tests.....	72
8.	Discussion	76
9.	Conclusion and Future Developments	79
	Appendix A.....	81
III.	References.....	91

I. Figures List

Figure 1. Schematic diagram of acute myocardial infarction: when blood clots build up, the blood flow is obstructed, causing hypoxia and a consequent necrotic myocardium [6]. 12

Figure 2. A) In normal artery and related artery cross-section allows a normal blood flow. B) Atherosclerosis can result from plaques formed by the buildup of fatty, calcium deposits in an artery. C) A total blockage completely obstructs the bloodstream, leading to ischemia to the tissues. 13

Figure 3. Reentrant ventricular tachycardia usually arises as the result of reentry within the border zone of myocardial infarction [3]..... 15

Figure 4. illustration showing the progressive pathological conditions in the myocardial ischemic cascade. Coronary Artery atherosclerosis progresses and leads to myocardial hypoperfusion because of plaque progression and laminar stenosis. Myocardial hypoperfusion is followed by metabolic abnormalities, diastolic and systolic dysfunction, ECG abnormalities, culminating in chest pain. In the right part are listed the modalities to detect abnormalities at each step: Computed Tomography (CT), Magnetic Resonance Imaging (MRI), Positron Emission Tomography (PET), Single-Photon Emission Computed Tomography (SPECT), Echo, and ECG [8]. 16

Figure 5. The main components of CT are represented. 17

Figure 6. Two algorithms to rebuild the image are represented: Radon transform in the left, and back-projection algorithm in the right side are shown. 18

Figure 7. Cardiac CT reformatted into a four-chamber view demonstrating normal anatomy. The contrast bolus timing was optimized to predominantly opacify the left heart (LA, left atrium; LV, left ventricle) for this examination. CT can provide exquisite high-resolution detail of anatomic structures. 19

Figure 8. H atom processing in a magnetic field (B_0) [11]. 20

Figure 9. Generation of MRI signal. 21

Figure 10. In the late enhancement imaging the myocardial infarction is indicated by the yellow arrow..... 22

Figure 11. Gadolinium kinetics in normal myocardium and acute and chronic myocardial infarction. A. Normal myocardium properly washes out the gadolinium. B. In acute myocardial infarction, the gadolinium is washed out less quickly than normal due to an expanded volume as a result of cell membrane disruption. C. Chronic myocardial infarction with collagen matrix scar formation slowly washed out the gadolinium due to increased interstitial space within the scar [13]. 23

Figure 12. Draw of RF generator providing a continuous unmodulated sine wave output to the metal electrode, causing a temperature increase through the Joule Heat in the surrounding tissue and in the catheter tip. The temperature of the electrode tip at an optimal ablation heating of the desired tissue is above +50°C.....24

Figure 13. Cardiac ablation catheter. A. Closed loop catheter with 7 Fr, 4 mm of diameter electrode. B. Open irrigated catheter with 7.5 Fr, 3.5 mm of diameter electrode.24

Figure 14. Radiofrequency Ablators: A) Radiofrequency ablation Catheter for endocardium treatment, B) Radiofrequency Ablator for epicardium treatment in open chest surgery.25

Figure 15. A) Three types of cryoablation catheters are represented for endocardium treatment: 8mm, 6mm and 4mm, and the treatment area reached is directly proportional to the catheter diameter. B) Cryoablator for epicardium treatment.27

Figure 16. The workflow describes the main steps of surgical guide development process from the acquisition data to 3D printing.30

Figure 17. House of Quality.....35

Figure 18. The sketch of green solution: the main reference landmarks are the Aorta the Pulmonary Artery, and the apex, and the thicker border, drawn in black, surrounds and identifies the target zone.....39

Figure 19. The sketch of blue solution: the basket shape. The reference points that give the stability are the heart surface fitting and the apex. A thicker border, drawn in black, identifies the scar perimeter, distinguishing from other holes.....39

Figure 20. Axial, Sagittal, Coronal and 3D views of CT Segmentation on 3D Slicer Software.43

Figure 21. Axial, Sagittal, Coronal and 3D views of MRI Segmentation on 3D Slicer Software.....43

Figure 22. 3D model of heart phantom with additional components to stabilize the model to avoid the collapse during printing.44

Figure 23. CT and MRI models merging on Autodesk Meshmixer Software.....45

Figure 24. Anterior, lateral and posterior view of the 1st virtual prototype of surgical guide for ischemic scar treatment.....46

Figure 25. The main virtual prototyping steps from the acquisition data, volume segmentation in 3D Slicer Software, to 3D model visualization in Autodesk Meshmixer Software.46

Figure 26. Anterior and posterior view of virtual simulation of surgical guide fitting on the heart phantom in Autodesk Meshmixer Software.....47

Figure 27. Stratasys Objet260 Connex1.....48

Figure 28. Illustration of Polyjet 3D printing.....	48
Figure 29. The WaterJet, a compact system enables to efficiently clean any type of 3D model or prototype from support material.	50
Figure 30. PRUSA 3D printer.	51
Figure 31. The 3D heart phantom is printed in PLA by PRUSA.	51
Figure 32. Pouch packaging on the top, Sterrad Vaporized Hydrogen Peroxide Gas Sterilization machine on the bottom.	54
Figure 33. The scheme of VHP sterilization system components.....	55
Figure 34. The first prototype representation during printing.....	56
Figure 35. The 1 st prototype of surgical guide during cleaning in Waterjet to remove the support material.....	57
Figure 36. The first prototype of surgical guide for treatment of ischemic scar printed in MED625FLX by Stratasys Objet260 Connex1.	58
Figure 37. Surgical mask fitting simulation on the heart phantom, previously printed in PLA by PRUSA 3D printer.	59
Figure 38. Three views of the 2 nd virtual prototype of surgical guide for ischemic scar treatment.	60
Figure 39. Three views of the 2 nd physical prototype of virtual surgical guide for ischemic scar treatment.	61
Figure 40. The 2 nd physical prototype of surgical mask fitting simulation on the heart phantom, previously printed in PLA by PRUSA 3D printer.	61
Figure 41. Pouch packaging of the first prototype after the VHP sterilization.....	64
Figure 42. Half circular sector samples of 1 mm, 2.5 mm and 3 mm+ 3 mm of thickness.....	68
Figure 43. The figure represents the material samples to be tested with different thickness: a. 1 mm, b. 2.5 mm, c. 3 mm + 3 mm. D1 and D2 are the distances from the sources. The black circles represent the cryoablator and the RF ablator, while the rectangle represents the linear RF ablator.	69
Figure 44. The figure represents the material samples to be tested with different thickness: a. and d. 1 mm, b. and e 2.5 mm, c. and f. 3 mm + 3 mm. D1 and D2 are the distances from the sources. The black dots represent the cryoablator and the RF ablator, while the black rectangle represents the linear RF ablator, during the ablation performance not in contact with the material samples (a., b., and c.). The blue dots represent the cryoablator and the RF ablator, while the blue rectangle	

represents the linear RF ablator, during the ablation performance in contact with the material samples.	71
Figure 45. The AM Scar-VT Prototype. The area to be ablated is in purple.	72
Figure 46. Application of first prototype of surgical guide on the porcine heart for the LRF treatment. The black arrow indicates the area to treat.....	74
Figure 47. LRF ablation procedure on porcine heart with the first prototype of surgical guide.....	74
Figure 48. Porcine heart after the LRF procedure with mask. The red arrow shows the effect of ablation.	75
Figure 49. Porcine heart after the LRF ablation. The green arrow indicates the grey lesion created by the LRF ablator.	75
Figure 50. 3mm+3mm (sample 7), 2.5 mm (sample 10) and 1 mm (sample 13) of MED625FLX samples are tested in response to the RF ablation.....	82
Figure 51. 3mm+3mm (sample 9), 2.5 mm (sample 12) and 1 mm (sample 15) of MED625FLX samples are tested response to the cryoablation procedure.....	84
Figure 52. 3mm+3mm (sample 8), 2.5 mm (sample 11) and 1 mm (sample 14) of MED625FLX samples are tested response to the Linear Radiofrequency ablation procedure.	85
Figure 53. Radiofrequency effect on MED625FLX of 2.5 mm at 1 mm (T1) and 10 mm (T2).	86
Figure 54. Linear Radiofrequency effect on MED625FLX of 2.5 mm at 1 mm (T1) and 10 mm (T2).	86
Figure 55. Cryoablation effect on MED625FLX of 2.5 mm at 1 mm (T1) and 10 mm (T2).	87
Figure 56. Radiofrequency effect at 1 mm (T1).	87
Figure 57. Linear Radiofrequency effect at 1 mm (T1).	88
Figure 58. Cryoablation effect at 1 mm (T1).	88
Figure 59. Radiofrequency effect at 10 mm (T2).	89
Figure 60. Linear Radiofrequency effect at 10 mm (T2).	89
Figure 61. Cryoablation effect at 10 mm (T2).	90

II. Tables List

Table 1. In priory order the main requirements are listed distinguishing the medical from the engineering ones.....32

Table 2. Engineering action performed by surgical guide.32

Table 3. Surgical guide Specifications.33

Table 4. Morphological chart provides three options for each item to realize the surgical guide. Among all possible combinations, the green and the blue are considered and analyzed. Other combinations are possible.37

Table 5. Decision Matrix.....40

Table 6. Cost Estimation of the 1st physical prototype of surgical guide.....55

Table 7. Comparative analysis between the first and the second prototype. The final score confirms the superiority of the second with respect to the first one. In the last column come notes are reported.62

Table 8. Results of geometry test: surgical guide features before (No sterilization) and after sterilization (VHP Sterilization) are reported.....65

Table 9. On the left side the picture of surgical guide is represented before VHP sterilization (No sterilization is performed yet). On the right side the picture of surgical guide after VHP sterilization. In both cases grey marker defines the surgical guide perimeter.65

Table 10. The grey marker on the heart phantom, printed in PLA, defines the surgical guide perimeter before (No sterilization) and after sterilization (VHP Sterilization).....66

Table 11. surgical guide is shown before (No sterilization) and after sterilization (VHP Sterilization). After sterilization technique the bottom part of surgical guide has reported a rupture in correspondence to critical point.....66

Table 12. AM scar-VT features.....67

Table 13. Material samples feaures.....67

Table 14. Ablators settings.....68

Table 15. The table describes the distances (D1 and D2) from the source, depending on the ablation procedures.69

Table 16. The table describes the distances (D1 and D2) from the Ablation Point (AP) when the procedure is performed not in contact with the material sample, and from the Ablation Point contact (AP_{contact}), when the procedure is performed in contact with the material sample.70

Table 17. Radiofrequency Ablation (RF) Procedure. 3mm+3mm, 2.5 mm and 1 mm of MED625FLX samples are tested. T1 and T2 are the temperatures of underlying tissue measured at different distances from the source at 0 s, 10 s, at 15 s, 30 s and 60 s after ablation. The control refers to temperatures' measurement of meat sample without material sample. Each star (*) identifies the number of ablations performed. For the first two stars (* and **) the ablations were performed not in contact with material sample, while for the last stars (***) and ****) the ablations were performed in contact with material sample.81

Table 18. Cryoablation Procedure. 3mm+3mm, 2.5 mm and 1 mm of MED625FLX samples are tested. T1 and T2 are the temperatures of underlying tissue measured at different distances from the source at 0 s, 10 s, at 15 s, 30 s and 60 s after ablation. The control refers to temperatures' measurement of meat sample without material sample. Each star (*) identifies the number of ablations performed. For the first two stars (* and **) the ablations were performed not in contact with material sample, while for the last stars (***) and ****) the ablations were performed in contact with material sample.82

Table 19. Linear Radiofrequency Ablation Procedure. 3mm+3mm, 2.5 mm and 1 mm of MED625FLX samples are tested. T1 and T2 are the temperatures of underlying tissue measured at different distances from the source at 0 s, 10 s, at 15 s, 30 s and 60 s after ablation. The control refers to temperatures' measurement of meat sample without material sample. Each star (*) identifies the number of ablations performed. For the first two stars (* and **) the ablations were performed not in contact with material sample, while for the last stars (***) and ****) the ablations were performed in contact with material sample.84

1. Introduction

In last decades 3D printing has had rapid developments in medicine, with applications in many different fields ranging from orthopedics, dentistry to cardiovascular disease. 3D reconstruction models aim to replicate anatomical structures and pathology with high accuracy, starting from medical imaging data acquisition like computed tomography (CT) and magnetic resonance (MR), to assist preoperative planning, simulate surgical or interventional procedures to achieve precision medicine for improvement of treatment outcomes, provide medical education to medical students [1].

The novel 3D reconstruction of cross-sectional imaging is an advanced technique not only in preoperative planning and operative simulating but also in execution of medical management in many fields, such as orthopedic surgery, accounting for the biggest population, neurological surgery, and cardiovascular surgery, but only in hemodynamics, e.g., cardiac valves implantation [2].

Since there is not the 3D printing applications as cardiac surgery guide, the purpose of this project is to create a specific-patient surgical mask to be applied directly on the heart surface for the treatment of ischemic scar, caused by post-myocardial infarction (MI), in order to reduce the medical procedure timing, improving the treatment result.

The treatment of ischemic scar in patients post-myocardial infarction is clinically important because it leads to malignant arrhythmias, like ventricular tachycardia (VT), which represent a common cause of morbidity and mortality: in the most cases, the pathological area is not the only part to be treated, in fact, when a coronary artery is occluded by stenosis, obstructing the blood flow and causing the lack of nutrients and oxygen to the cardiac tissue, the myocardium cells are damaged in different ways, according to the time of oxygen lacking and the level of oxygen supply. It means that there will be a completely damaged cardiac cells, called fibrotic cells, which are unable to conduct the heart electrical activity anymore, that are surrounded by partial damaged cells, characterized by a slower conductive capacity, that leads to arrhythmias.

Thus, the border zone between scarred myocardium and normal myocardium is the predominant substrate for the majority of ventricular tachycardias (VT) post-MI. This zone is characterized by small islets of viable myocardium interspersed with scarred tissue that create an opportunity for

electrical reentry. For these reasons, both completely and partially damaged cells are treated in operating room, and they take part of what is defined “target zone”.

Nowadays, the method uses electro-anatomical mapping to define regions of scar and viable myocardium in sinus rhythm, followed by ablation in the border zone regions: it consists of a long iterative method, which alternates heart electrical activity and ablation procedure until the sinus rhythm is restored [3].

The concept of surgical guide for ischemic scar treatment derived from the need to have a precise visualization of pathological area to make sure to assess the necrotic extent of ablation lesions because an incomplete ablation of arrhythmogenic substrate causes subsequent recovery of tissue with restoration of conduction and recurrent arrhythmias.

Once having transformed the medical and engineering requirements into specifications, the product development process involves in different steps: it starts from the medical imaging data acquisition from Computed Tomography (CT), for a reliable anatomy of the specific patient heart and from Cardiac Magnetic Resonance (CMR), for the identification of pathological area.

Successively, using post-processing software, the region of interest undergoes segmentation, and thus the 3D model of cardiac surgery guide is performed and converted into a file format, usually into the standard tessellation language (STL) format, which the 3D printer can interpret. Currently, different printing technologies are used to create the models, especially to assist in planning complex cardiac surgery and not for the time being as surgical guides, which could provide a better view of the complex and variable pathology. In fact, using cardiac guides, physicians will be able to prepare and operate precisely executing the surgery, optimizing operation time, and enhancing the treatment result.

Moreover, whereas the large number of materials, characterized by mechanical and chemical properties, the choose of material is critically important, because not only the 3D printer availability and surgical guide task must be considered, but also the washing and sterilization processes to make it suitable for the surgery. Before surgical use in the operating room, indeed, the mask must be cleaned and sterile, and then correctly placed on the heart patient, in order to proceed with the ablation for the ischemic scar treatment [4].

2. State of the Art and Theoretical Background

2.1. Heart Failure and Myocardial Infarction

Heart failure (HF) is a progressive disorder of myocardial remodeling characterized by impaired cardiac function and circulatory congestion. HF is often the end stage in the cardiovascular disease continuum. Risk factors for HF include genetic factors, diet, smoking, sedentary lifestyle, stress, dyslipidemia, type 2 diabetes mellitus, obesity, and metabolic syndrome. Epidemiologically, HF is a major cause of morbidity and mortality worldwide, and it is associated with high hospitalization rates and high related healthcare expenses. HF manifests as an abnormality of the cardiac structure and/or function that impairs the heart to maintain adequate blood flux to peripheral tissues or to do it at the expense of increased filling pressures.

Myocardial infarction (MI) is a syndrome where myocardial cells die due to imbalances between myocardial oxygen supply and demand. The main cause of MI is the presence of atherosclerotic plaque, and its severity of concomitant coronary artery disease (CAD) likely defines the extent of supply-demand imbalance necessary to evoke ischemia, a reduced blood flow in the coronary circulation, which may provoke, if the hypoxia period is prolonged, the irreversible cell death (Figure 1). The dimension of affected area depends on the time period of hypoxia, but also on the vessels involved: larger is the diameter of coronary artery occluded, higher is the damaged area.

Post-MI factors, which influence myocardial dysfunction, are the myocardial ischemia, infarct size, LV remodeling, myocardium mechanical complications, and hibernating myocardium. Pursuant to the increasing prevalence of ischemic heart disease and MI, the acute management of these conditions has been advanced by the use of rapid percutaneous revascularization. However, although this approach has reduced mortality rates, it has also resulted in a high incidence of chronic HF, with the consequent overloading of healthcare systems. Thus, knowledge of the mechanisms related to the progression of MI to HF is essential for the development of novel treatments for its management [5,6].

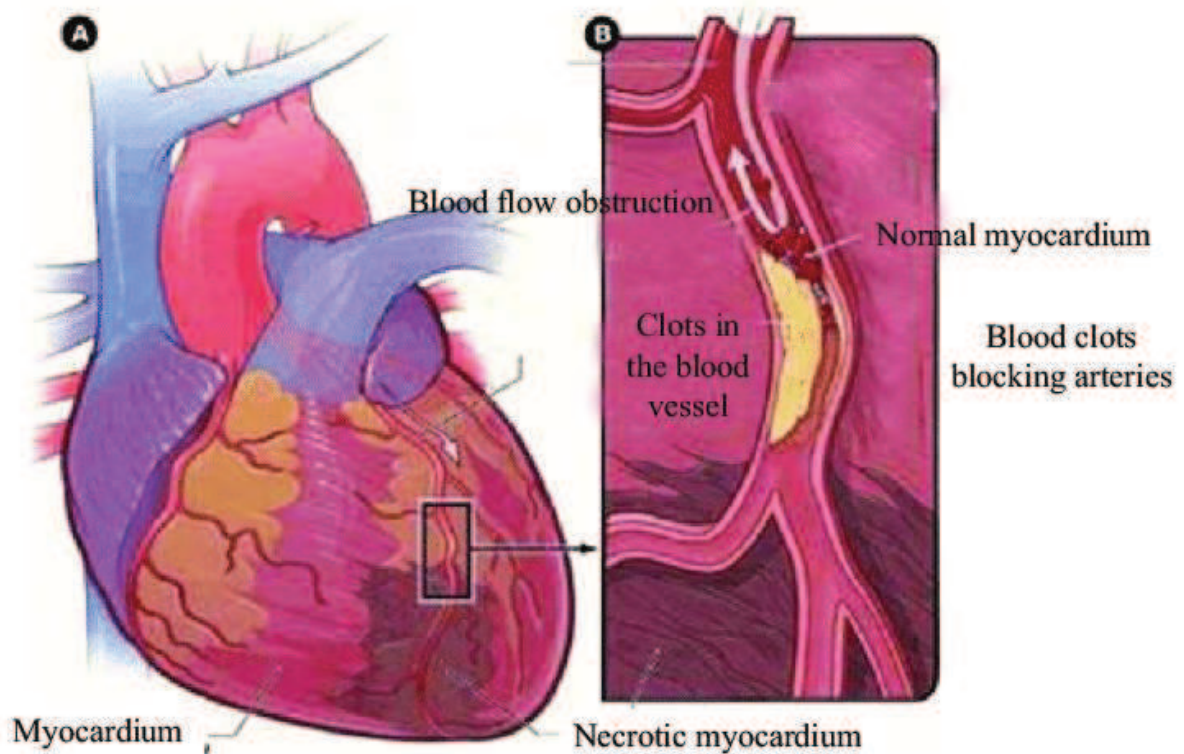


Figure 1. Schematic diagram of acute myocardial infarction: when blood clots build up, the blood flow is obstructed, causing hypoxia and a consequent necrotic myocardium [6].

2.1.1. Arteriosclerosis, the main cause of Myocardial Infarction

The main function of coronary arteries is to pump blood to cardiac cells, and it is allowed thanks to the compliance, a factor which provides expansion when blood is pumped through it from the heart, and then contraction after the surge has passed. This helps promote blood flow. In arteriosclerosis, the main cause of myocardial infarction, compliance is reduced, and pressure and resistance within the vessel increase. This is a leading cause of hypertension and coronary heart disease, as it causes the heart to work harder to generate a pressure great enough to overcome the resistance. Arteriosclerosis begins with injury to the endothelium of an artery, which may be caused by irritation from high blood glucose, infection, tobacco use, excessive blood lipids, and other factors. Artery walls that are constantly stressed by blood flowing at high pressure are also more likely to be injured—which means that hypertension can promote arteriosclerosis, as well as result from it. Tissue injury causes inflammation, which spreads into the artery wall, it weakens and scars it, leaving

it stiff (sclerotic). As a result, compliance is reduced. Moreover, circulating triglycerides and cholesterol can seep between the damaged lining cells and become trapped within the artery wall, where they are frequently joined by leukocytes, calcium, and cellular debris. Eventually, this buildup, called plaque, can narrow arteries enough to impair blood flow. The term for this condition, atherosclerosis (athero- = “porridge”) describes the mealy deposits.

Sometimes a plaque can rupture, causing microscopic tears in the artery wall that allow blood to leak into the tissue on the other side. When this happens, platelets rush to the site to clot the blood. This clot can further obstruct the artery and, if it occurs in a coronary artery, an immediate intervention is needed to restore the blood flow. Alternatively, plaque can break off and travel through the bloodstream as an embolus until it blocks a more distant, smaller artery. Even without total blockage, vessel narrowing leads to ischemia—reduced blood flow—to the tissue region “downstream” of the narrowed vessel. Ischemia in turn leads to hypoxia—decreased supply of oxygen to the tissues. Hypoxia involving cardiac muscle can lead to cell death and severe impairment of heart function (Figure 2) [7].

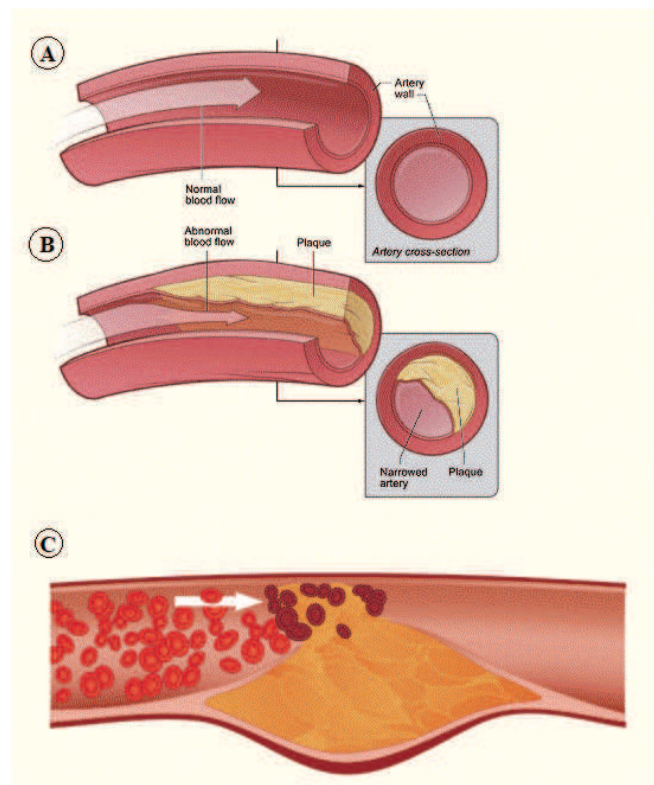


Figure 2. A) In normal artery and related artery cross-section allows a normal blood flow. B) Atherosclerosis can result from plaques formed by the buildup of fatty, calcium deposits in an artery. C) A total blockage completely obstructs the bloodstream, leading to ischemia to the tissues.

In case of complete occlusion, an emergency action is needed to restore the vascularization; instead, in less dangerous situations with a decreased perfusion, followed by myocardial dysfunction, medical procedures are performed, according to the occlusion severity, e.g., coronary artery bypass grafting.

Although the vascularization procedures can restore the blood flow, the previous decreased supply of oxygen to the tissues causes cell death and severe impairment of heart function.

2.1.2. Pathophysiology of Myocardial Infarction-induced HF

MI can be defined as the necrosis of cardiac cells due to reduced O₂ supply as a consequence of the occlusion of coronary arteries, the heart blood vessels, because of stenosis. Cardiac energy synthesis relies mostly on oxidative metabolism and is therefore highly sensitive to changes in the intracellular O₂ levels. Coronary artery occlusion reduces O₂ concentration and upregulates anaerobic-dependent ATP synthesis, leading to energy starvation and cardiac cell necrosis. This scenario generates several deleterious outcomes, including increased cytosolic calcium (Ca²⁺) concentrations and reduced pH, which together culminate in the loss of cell membrane integrity and an uncontrolled release of the intracellular content into the extracellular space. The primary consequences of cardiac cell necrosis are the abrupt reduction of cardiac output (CO) and development of severe cardiac arrhythmias due to the loss of functional contractile muscle mass and the electrolyte imbalance generated during cell lysis. MI can be fatal if clinicians do not intervene in time [5].

However, even though patient survives an ischemic attack, MI result in cardiomyocyte death, tissue remodeling, and often a heterogeneous fibrous scar. Despite the scar is believed to preserve tissue integrity, preventing wall rupture after the loss of myocytes, the fibrous scar may result in decreased mechanical contractility, heart failure, and arrhythmogenesis, which must be, therefore, surgically treated.

Thereby, the treatment of ischemic scar in patients post-myocardial infarction is clinically important because it leads to malignant arrhythmias, like ventricular tachycardia (VT), which represent a common cause of morbidity and mortality: in the most cases, the pathological area is not the only part to be treated, in fact, when a coronary artery is occluded by stenosis, obstructing the blood

flow and causing hypoxia to the cardiac tissue, the myocardium cells are damaged in different ways, according to the time of oxygen lacking and the level of oxygen supply. This zone is characterized by small islets of viable myocardium interspersed with scarred tissue that create an opportunity for electrical reentry (Figure 3).

Thus, the border zone between scarred myocardium and normal myocardium is the predominant substrate for the majority of ventricular tachycardias (VT) post-MI. For these reasons, both fibrotic and arrhythmogenic tissue must be treated in operating room, by ablation procedure in order to reestablish the sinus rhythm.

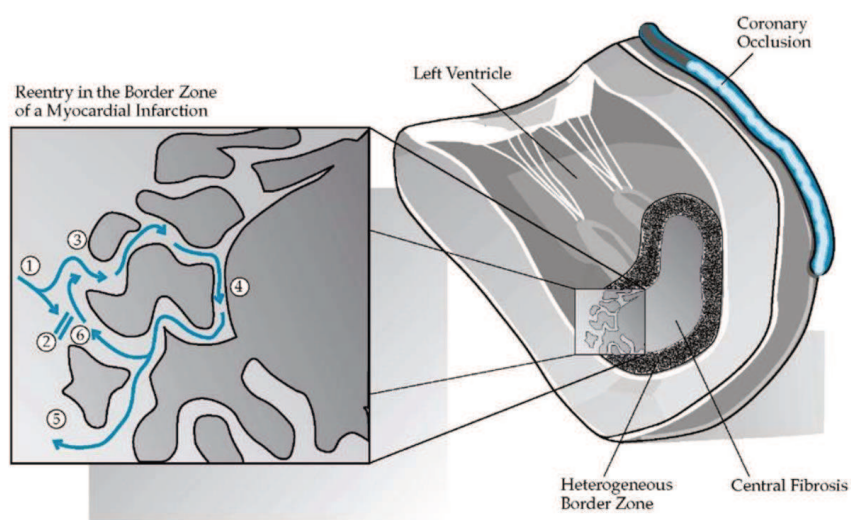


Figure 3. Reentrant ventricular tachycardia usually arises as the result of reentry within the border zone of myocardial infarction [3].

2.2. Medical Diagnostic Imaging and Treatment Techniques

Coronary artery atherosclerosis progresses asymptotically in the early stage and leads to luminal stenosis and myocardial ischemia. The ischemic cascade illustrates the progressive pathological conditions that develop from hemodynamically significant stenosis, evolving from subclinical to clinical stages (Figure 4). Decreased perfusion leads to metabolic changes, followed by diastolic and then systolic dysfunction, electrocardiographic (ECG) changes, and anginal chest pain. The evaluation of different stages along the ischemic cascade can be achieved by invasive and noninvasive tests including exercise ECG, echocardiography, nuclear imaging, magnetic resonance imaging (MRI), and computed tomography (CT).

The following paragraphs describe the medical techniques related to diagnosis of ischemic scar, i.e., the MRI and CT, and the procedures for treatment of scar-related Ventricular Tachycardia, i.e., Radiofrequency ablation and Cryoablation [8].

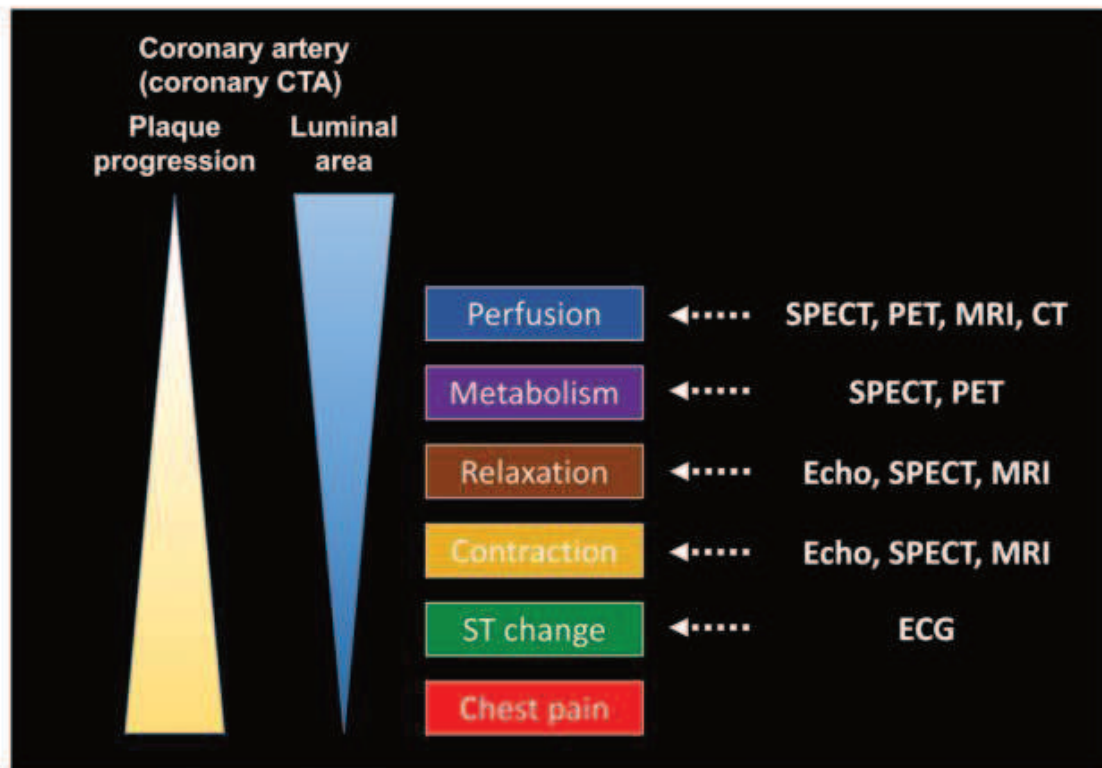


Figure 4. illustration showing the progressive pathological conditions in the myocardial ischemic cascade. Coronary Artery atherosclerosis progresses and leads to myocardial hypoperfusion because of plaque progression and laminar stenosis. Myocardial hypoperfusion is followed by metabolic abnormalities, diastolic and systolic dysfunction, ECG abnormalities, culminating in chest pain. In the right part are listed the modalities to detect abnormalities at each step: Computed Tomography (CT), Magnetic Resonance Imaging (MRI), Positron Emission Tomography (PET), Single-Photon Emission Computed Tomography (SPECT), Echo, and ECG [8].

2.2.1. Physical Principles of Computed Tomography

Computed tomography (CT) is a diagnostic imaging procedure in which anatomical information is digitally reconstructed from x-ray transmission data obtained by scanning an area from many directions in the same plane to visualize information in that plane. In concept, CT solves the set of simultaneous equations involving several attenuation coefficients, for each element over different

directions used. Along a line given by a direction, the total attenuation is related to a sum of individual attenuation coefficients: for a single element $I = I_0 e^{-\mu x}$. For a series of elements of equal thickness:

$$\ln(I/I_0) = -\Delta x e - D x (\mu_1 + \mu_2 + \mu_3 + \mu_4 + \dots)$$

where I is the exit beam intensity, I_0 is the initial intensity, x is the layer thickness. Dx is the thickness of an element of constant size, μ is the attenuation coefficient, μ_i is the absorption coefficient of a particular series element.

In the CT machines a collimated beam of x ray is passed through the patient in a direction transverse to the longitudinal axis. The emerging beam flux cross the patient body and reaches the sensors of the linear detector on the opposite side, at the solid state with a high efficiency for the low energies of the CT systems. The configuration of x ray beam source and detector is then rotated through a small angle, and the procedure is repeated. The x ray source and detector move together around the patient, perpendicular to the beam direction, while the patient is in motion from a translating table in the scanner system (gantry): this produces a spiral data collection of total attenuation of the x-ray beam (Figure 5).

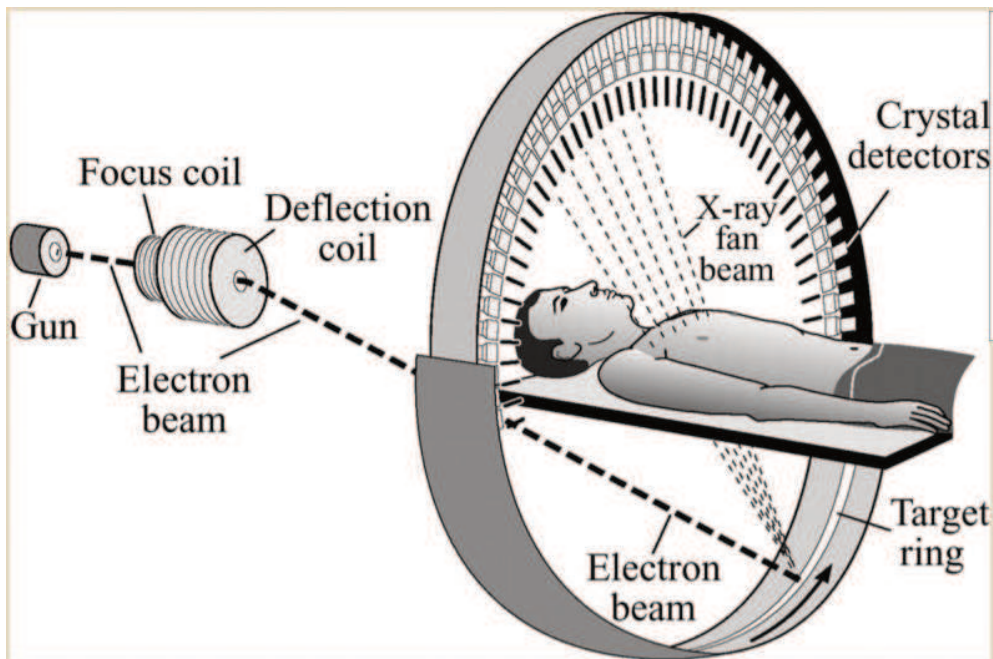


Figure 5. The main components of CT are represented.

The procedure is called tomography because those structures lying in the narrow anatomical slice traversed by the beam are imaged. A sampling of projections at angle uniformly distributed about the origin can provide an approximate reconstruction of image and the level of detail is straightforwardly dependent on the number of angles sampled and the sampling coarseness at each angle.

After performing numerous projections along different directions, it is possible - through appropriate algorithms (Radon transform and back-projection algorithm) - to rebuild the image (Figure 6).

Among numerous reconstruction algorithms, most widely used, the Filtered Back-projection reconstruction consists of building up the CT image by essentially reversing the acquisition steps. The μ value for each ray is smeared along this same path in the image of the patient and, as data from a large number of rays are back projected onto the image matrix, areas of high attenuation tend to reinforce one another, as do areas of low attenuation, building up the image [9].

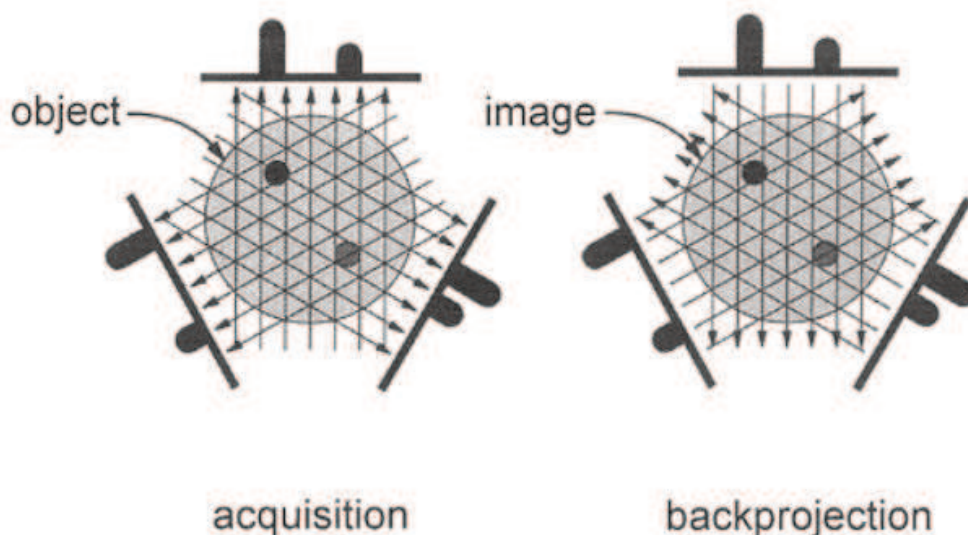


Figure 6. Two algorithms to rebuild the image are represented: Radon transform in the left, and back-projection algorithm in the right side are shown.

Phases of CT imaging are scanning the patient, data acquisition (Tube or tube and detector move, or multiple attenuation measurements are taken around the object), image reconstruction, image archival (recording), usually in DICOM format.

2.2.2. Computed Tomography for Myocardial Perfusion Evaluation

Computed Tomography (CT) provides important information about cardiac morphology, function, viability, and perfusion with a short acquisition time and a high spatial resolution (Figure 7). Coronary CT angiography (CTA) is widely used in the diagnosis of CAD, in fact, high-resolution CT imaging allows for better visualization and assessment of coronary lumen stenosis caused by calcified plaques, thus further validating previous findings about the effect of spatial resolution on diagnostic assessment of calcified coronary plaques [1].

To acquire CT data, ionizing radiation and contrast media are needed. Although CT coronary angiography is widely used and gives important anatomical information, it does not provide information about the hemodynamic effects of a stenosis. For this reason, other non-invasive tests can evaluate myocardial ischemia like Cardiac Magnetic Resonance, described in the following paragraphs [10].

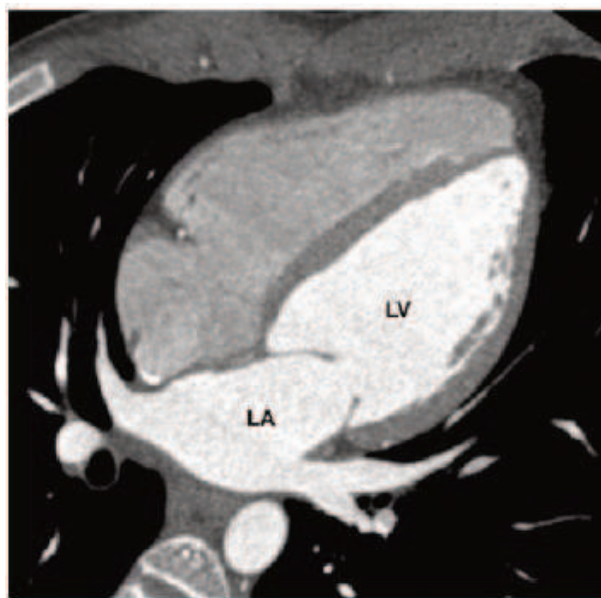


Figure 7. Cardiac CT reformatted into a four-chamber view demonstrating normal anatomy. The contrast bolus timing was optimized to predominantly opacify the left heart (LA, left atrium; LV, left ventricle) for this examination. CT can provide exquisite high-resolution detail of anatomic structures.

2.2.3. Physical Principles of Magnetic Resonance

In Magnetic Resonance Imaging (MRI), magnetic properties of hydrogen (H) atoms, are utilized because they are abundant in tissues and have the simplest atomic configuration containing only one proton in the nucleus and an orbiting electron. Protons and neutrons possess an intrinsic angular momentum called “spin” which is a purely quantum mechanical phenomenon. Its speed cannot be changed, the only feature that can change is the axis of spin (the direction of the angular momentum). When placed in a magnetic field (B_0) the proton rotates into alignment with the field because of its magnetic dipole moment. Because the proton also has angular momentum, the spin axis of the proton processes around the field axis and creates its own magnetic field (M_0) that is parallel to and smaller than the main magnetic field B_0 (Figure 8) [11].

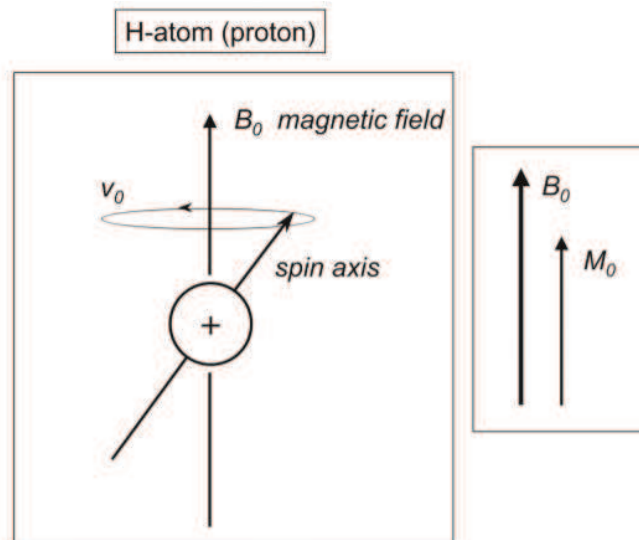


Figure 8. H atom processing in a magnetic field (B_0) [11].

The frequency at which the protons run is called the Larmor frequency:

$$(\omega): \omega = \gamma B / 2\pi$$

where B is the Magnetic field, γ is the gyromagnetic ratio (an intrinsic magnetic property specific to each nucleus). The Larmor frequency for H-atoms in 1.5 Tesla (T) is 64 Mhz. This is also called the resonance frequency of the H atoms in 1.5 T. In MRI, a radiofrequency (RF) pulse is applied to the protons, which forces them to rotate around 90° in the main magnetic field B_0 . This creates a dipole magnetic field that changes with time as the protons rotate. The changing magnetic field will induce

current in the receiver coil, and the MR signal can be detected as a voltage change generated by the rotating protons.

Important is that the H-atoms are targeted selectively by the RF pulse, that contains the Larmor frequency of the H-atoms must be used (64 MHz in 1.5 Tesla).

In brief, the MRI signal is generated by the RF energy at the resonance frequency of H-atoms that is first absorbed and then released by these atoms when they relax. There are two relaxation times, known as T_1 and T_2 . T_1 is the time required for M_0 to return to 63% of its original value following an excitation RF pulse. It is also called the “longitudinal” or “spin-lattice” relaxation time. When the spins return to their original position after excitation, they emit their energy to their surroundings (“lattice”). T_2 is the time required for M_1 to decay to 37% of its initial value on the horizontal plane. It is also called the “transverse” or “spin-spin” relaxation time. After the RF pulse, spins start losing their phase coherence while at the same time they reorient themselves along B_0 . The spin energy will dissipate in the form of energy exchange among nearby spins with incoherent phases. Obviously, T_2 will always be less than or equal to T_1 . In gradient echo pulse sequences T_2 is referred to as T_2^* , the asterisk indicating the contribution of extrinsic noise to T_2 (Figure 9) [12].

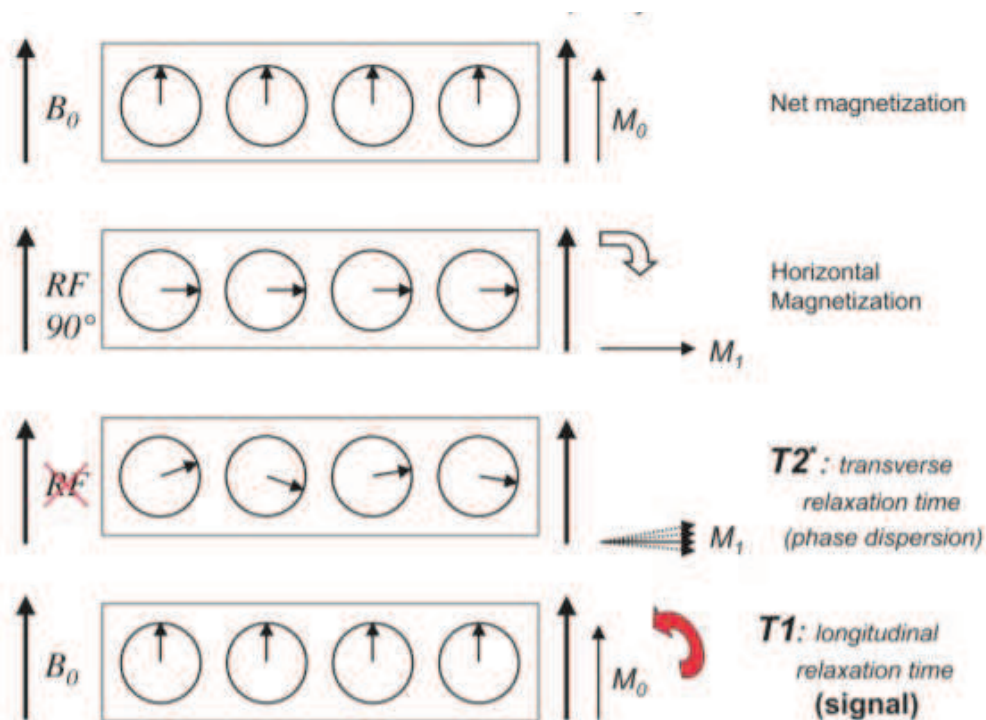


Figure 9. Generation of MRI signal.

2.2.4. Cardiac Magnetic Resonance for Ischemic Scar Diagnosis

Ischemic heart disease (IHD) is the leading cause of death worldwide. Over the last two decades, cardiac MRI (CMR) has emerged as a promising non-invasive modality in the assessment of patients with suspected and established IHD due to its good spatial resolution, high reproducibility, and myocardial tissue characterization capabilities, thereby aiding in the diagnosis, guiding clinical decision-making. CMR is non-invasive gold standard method to measure the myocardial wall thickening and left and right ventricular (LV and RV) volumes and its functionality. For CMR volumetric assessment, the ventricles are sliced from base to apex and the endocardium and epicardium subsequently contoured, resulting in a three-dimensional (3D) image. Cine CMR can also be used during low-dose and high-dose dobutamine to assess myocardial viability and inducible ischemia, respectively.

This T1-weighted technique allows myocardial tissue characterization. It can demonstrate the presence and extent of myocardial scarring (figure 10).

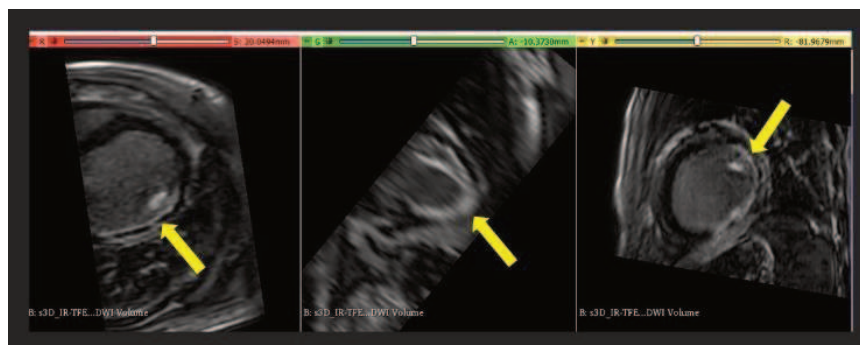


Figure 10. In the late enhancement imaging the myocardial infarction is indicated by the yellow arrow.

In brief, the gadolinium-chelate contrast agent administered intravenously promptly diffuses into the extracellular myocardial compartment. In normal myocardium, the contrast quickly washes in and out of the myocardium. The presence of myocardial scarring results in increased extracellular space, where the contrast accumulates with longer washout time compared to normal myocardium (Figure 11) [13].

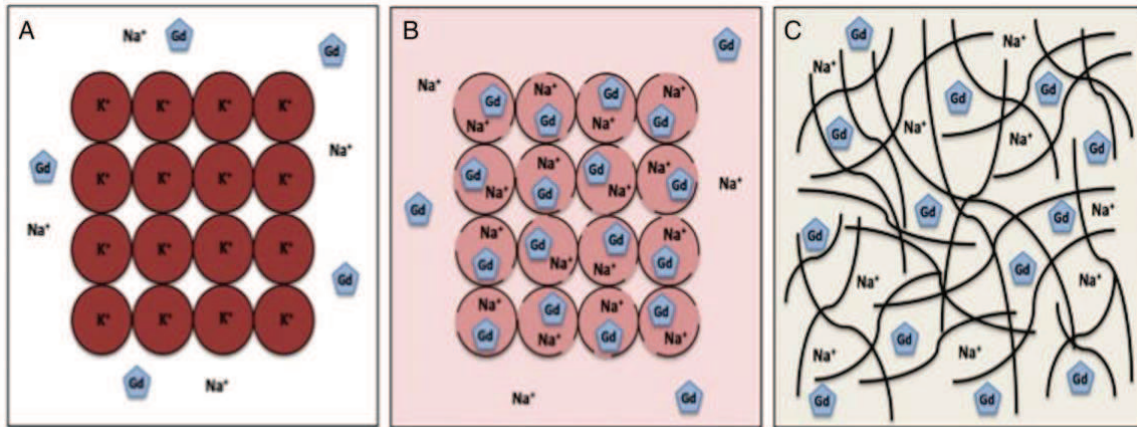


Figure 11. Gadolinium kinetics in normal myocardium and acute and chronic myocardial infarction. A. Normal myocardium properly washes out the gadolinium. B. In acute myocardial infarction, the gadolinium is washed out less quickly than normal due to an expanded volume as a result of cell membrane disruption. C. Chronic myocardial infarction with collagen matrix scar formation slowly washed out the gadolinium due to increased interstitial space within the scar [13].

2.2.5. Radiofrequency Ablation for Scar-related Ventricular Tachycardia Treatment

Substrate-based catheter ablation is an effective therapeutic option in patients with recurrent episodes of scar-related ventricular tachycardia (VT). A frequently technique to terminate the arrhythmia involves destroying the heart tissue which causes the arrhythmia by heat, e.g., applying a high frequency electrical energy, such as Radiofrequency (RF) to a desired arrhythmogenic site on the patient's heart.

RF generator usually provides a continuous unmodulated sine wave output in the frequency range of 300 kHz to 1 MHz to the metal electrode, causing a temperature increase both in the surrounding tissue and in the tip. The target tissue is hit by the RF field and raises the temperature of the electrode tip at an optimal ablation heating of the desired tissue above +50°C (Figure 12), because the threshold for thermal damage is demonstrated to be set at +43°C [14]. A cardiac ablation electrode diameter is about 2.3 mm to 4 mm, and it can be irrigated catheter or closed loop catheter (figure 13). The electrodes on the device shaft are independent, for monopolar mode use with an electrode in contact with the exterior of the patient's body. Alternatively, the electrodes may be bipolar, for use as a pair of electrodes on the shaft. Another option is represented by helical coil shaped electrodes for improved device flexibility, although other designs are suitable including cylindrical bands, arcuate bands or ribbons or the like.

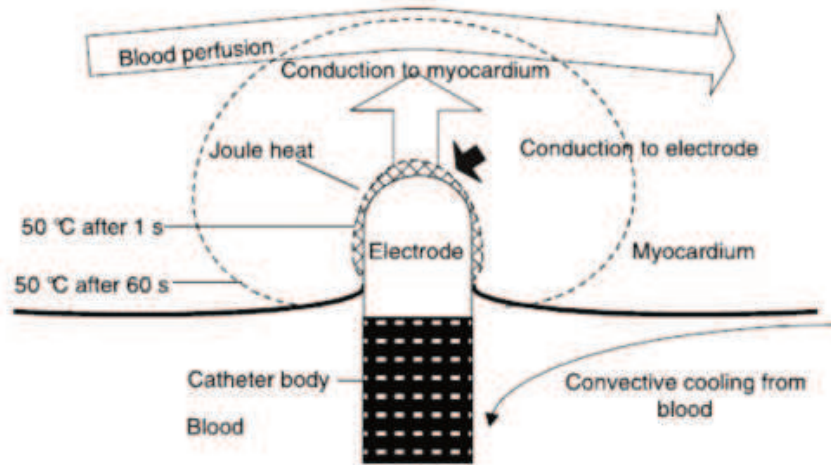


Figure 12. Draw of RF generator providing a continuous unmodulated sine wave output to the metal electrode, causing a temperature increase through the Joule Heat in the surrounding tissue and in the catheter tip. The temperature of the electrode tip at an optimal ablation heating of the desired tissue is above +50°C.

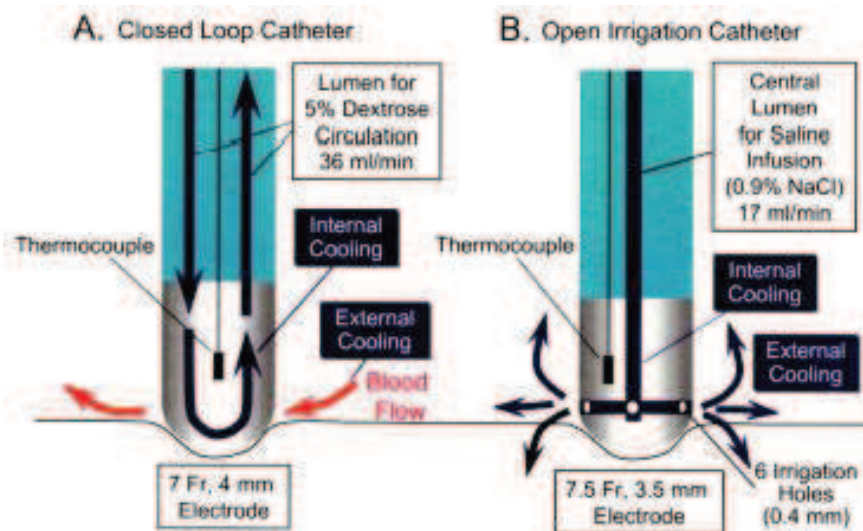


Figure 13. Cardiac ablation catheter. A. Closed loop catheter with 7 Fr, 4 mm of diameter electrode. B. Open irrigated catheter with 7.5 Fr, 3.5 mm of diameter electrode.

Usually, to perform a lesion the RF ablation for ischemic scar treatment is controlled by a temperature limit of +45°C with a power limit of 50 W at the endocardium and +70°C at the epicardium (Figure 14). Typically, the RF device is advanced within a patient through thoracoscopy, though the RF catheter or it is directly applied on the epicardium in open chest surgery, and, when RF electrical energy is emitted from electrodes of the device, a lesion is formed at the myocardium. RF ablation-produced lesions are directly proportional to diameter and source power.

Consequently, several lesions are typically formed to completely ablate an area than the average arrhythmogenic site.

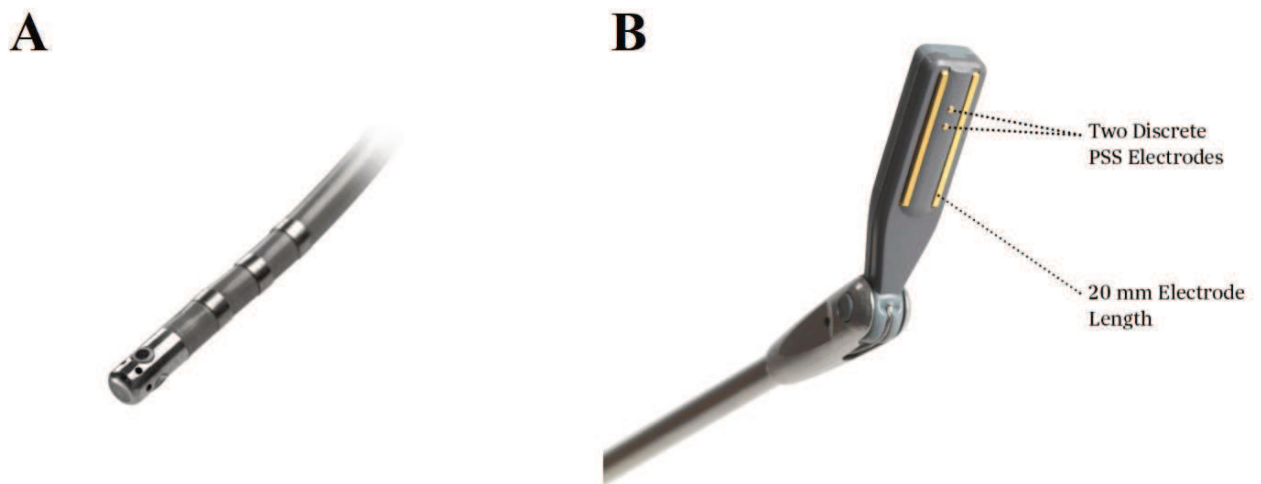


Figure 14. Radiofrequency Ablators: A) Radiofrequency ablation Catheter for endocardium treatment, B) Radiofrequency Ablator for epicardium treatment in open chest surgery.

Furthermore, the RF device is composed of probes along an outer surface of the device, sensing the temperature and the impedance of the system, and the information goes to the console.

The common temperature sensors used, are thermocouples, although other suitable temperature sensors may be used, such as thermistors or other temperature sensing means. The temperature sensors monitor the temperature of the heart wall at the edge of the adjacent lesions which meet or overlap to form one continuous lesion. By thus monitoring the temperature, together with a conducting member which rapidly equilibrates the temperature around the catheter circumference to the temperature at the patient's heart wall, the physician is able to ensure that adequate heating is produced, avoiding overheating and resulting in complete ablation of the area of interest.

Nevertheless, the real challenge is a complete treatment of area of interest because recent studies have demonstrated that a complete elimination of the scar substrate, could improve post MI results, solving the VT and avoiding subsequent hospitalization [15].

2.2.6. Cardiac Cryoablation for Scar-related Ventricular Tachycardia Treatment

Since 1970s, cryothermal ablation probes have been adapted for cardiac surgical applications because a synthesis of experiments predominantly focused on frostbite and cryopreservation demonstrated that the major mechanisms of cold-induced cellular and tissue injury result from a combination of direct cellular damage attributable to the deleterious effects of ice crystal formation during hypothermia and ischemic cell death attributable to microcirculatory failure and subsequent vascular stasis during thawing.

Moreover, since a period of reversible tissue inhibition obligatorily precedes irreversible tissue destruction, and considering an extreme freezing (i.e., tissue temperatures colder than -50°C) results in near instantaneous permanent tissue injury, the degree of permanent cellular damage with relatively warmer tissue temperatures (-10°C to -25°C) is directly related to duration of freezing. Thus, the use of milder freezing temperatures and shorter ablation times facilitates the assessment of clinical effect at the target lesion site, and confirmation that a target site does not result in adverse clinical outcomes. It is important to note that although safety and efficacy mapping may be realized using a dynamic cryomapping process will naturally occur during the course of a cryoapplication as the hypothermic wavefront spreads centrifugally from the catheter tip to the surrounding tissue.

In the last years, significant engineering advances have been required to achieve the safe and effective delivery of pressurized cryorefrigerant to the tip of a steerable percutaneous catheter. The current transvenous cryocatheter system consists of a hollow shaft deflectable catheter with a closed distal end containing a cooling electrode tip, 3 proximal ring electrodes, and a proximal thermocouple. The catheter is connected to a specialized external console via an electric cable and gas umbilical tube. Ablation is realized through the delivery of pressurized cryorefrigerant to the catheter tip via an ultrafine injection tube. Just before release into the tip, the cryorefrigerant is further pressurized through a restriction tube that is designed to maximize the temperature drop via the Joule–Thompson effect. This accelerated liquid to-gas phase change results in rapid cooling of the distal tip. The cryorefrigerant then absorbs heat from the surrounding tissue before returning to the console via a second coaxial return lumen maintained under vacuum. Although the core tenets of its design have remained largely unchanged, the transvenous cryoablation catheter has undergone significant evolutionary advances throughout the past decade: the refrigerant was

modified to the current nitrous oxide to allow lower temperatures and faster freezing rates, catheter diameter was reduced from 9F to 7F, whereas larger electrode tip sizes were introduced (4 mm to 6 mm to 8 mm). According to the epicardium treatment or endocardium treatment, different ablators are used (Figure 15). Finally, the introduction of innovative catheter configurations like focal, linear, circular, and balloon-based apparatuses, allows diverse clinical applications. Currently, modern 7F version with rapid cooling achieves temperatures below -80°C .

In conclusion, thanks to the characteristics described above, cryotherapy is a reliable technique able to assess the safety and efficacy of a potential ablation lesion site dynamically and prospectively [16].

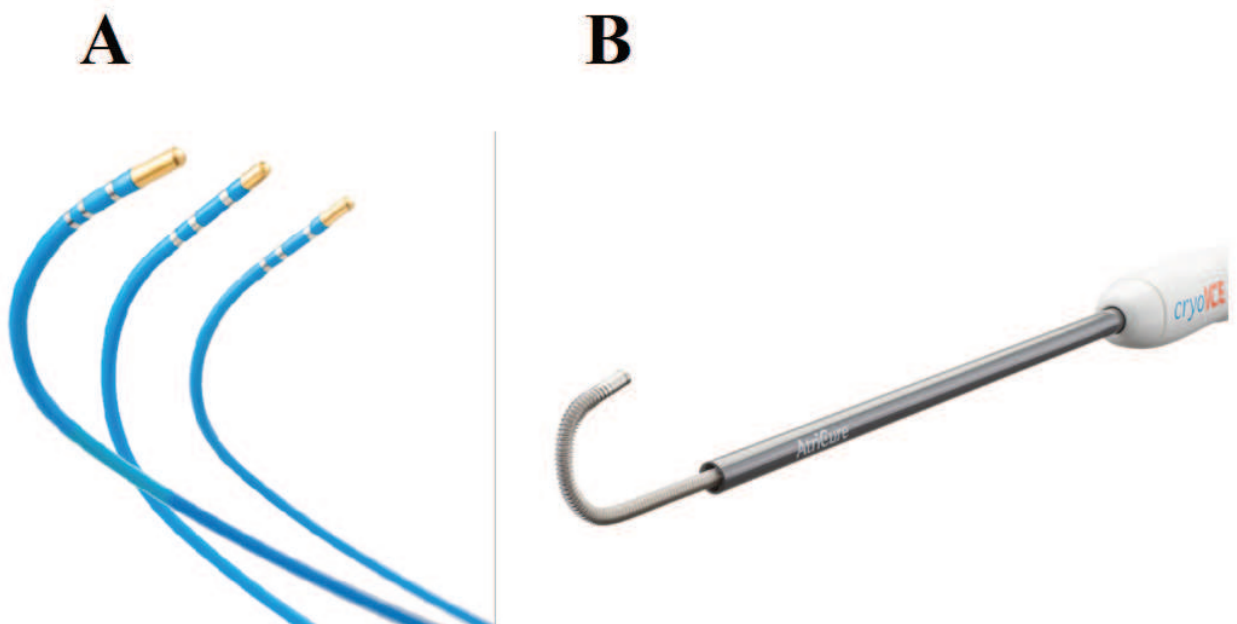


Figure 15. A) Three types of cryoablation catheters are represented for endocardium treatment: 8mm, 6mm and 4mm, and the treatment area reached is directly proportional to the catheter diameter. B) Cryoablator for epicardium treatment.

3. Design of Surgical Guide for Ischemic Scar Treatment

3.1. Needs and Market Analysis

In last decades 3D printing has had rapid developments in medicine, with applications in many different fields ranging from orthopedics, dentistry to cardiovascular disease. 3D reconstruction models aim to replicate anatomical structures and pathology with high accuracy, starting from medical imaging data acquisition like computed tomography (CT) and magnetic resonance (MR), to assist preoperative planning, simulate surgical or interventional procedures to achieve precision medicine for improvement of treatment outcomes, provide medical education to medical students [1].

The novel 3D reconstruction of cross-sectional imaging has been an advanced technique not only in preoperative planning, operative simulating, and student training but also in execution of medical management in many fields, such as orthopedic surgery, accounting for the biggest population, neurological surgery, and cardiovascular surgery, but only in hemodynamics, i.e., cardiac valves implantation [2].

In particular, the ischemic scar is surgically treated, after a diagnostic provided by medical exams such as Cardiac Magnetic Resonance with contract, which suggests and indicates the pathological area, in the operating room, where the cardiac surgeon acts on ischemic scar through ablation procedure, without any visible references. Sometimes the cardiac scar looks like light-coloured cardiac tissue, but in most cases the unhealthy tissue is covered by fat and usually it is surrounded by not completely unhealthy cells, or partially damaged tissue, characterized by arrhythmogenic behaviour causing arrhythmias, or re-entry circuits, even dangerous for the patient, like VT. This kind of partially unhealthy tissue is difficult to be visually recognized and it has to be treated by ablation. Nowadays the procedure is supported by other medical devices like electrophysiological catheter, to evaluate whether the ablation has solved the arrhythmias by measuring the electrophysiology of the heart: it is a recursive treatment, which takes time and finishes when the arrhythmia stops. In addition, since arrhythmogenic tissue is difficult to be distinguished from cardiac cells, there is a higher risk to ablate healthy tissue.

3.2. Aim of study

Since the 3D printing applications as cardiac surgery guide have not already developed, the purpose of this project is to create a specific-patient surgical mask to be applied directly on the heart surface for the treatment of ischemic scar, caused by post-myocardial infarction (MI), in order to reduce the medical procedure timing, improving the treatment result.

As fibrous tissue leads to malignant ventricular tachyarrhythmias (VT), which represent a common cause of morbidity and mortality, the treatment of ischemic scar in patients post-myocardial infarction is clinically important: in the most cases, the pathological area is not the only part to be treated, in fact, when a coronary artery is occluded by stenosis, obstructing the blood flow and causing the lack of nutrients and oxygen to the cardiac tissue, the myocardium cells are damaged in different ways, according to the oxygen supply and the time of hypoxia. When it occurs, the cardiac tissue is characterized by completely damaged cardiac cells, fibrotic cells, unable to conduct the heart electrical activity anymore, that are surrounded by partial damaged cells, characterized by a slower conductive capacity, that leads to arrhythmias.

Thus, the border zone between scarred and normal myocardium is the predominant substrate for the majority of ventricular tachycardias (VT) post-MI. This zone is characterized by small islets of viable myocardium interspersed with scarred tissue that create an opportunity for electrical reentry. For these reasons, both completely and partially damaged cells are treated in operating room, and they take part of what is defined "target zone".

Nowadays, the method uses electro-anatomical mapping to define regions of scar and viable myocardium in sinus rhythm, followed by ablation in the border zone regions: it consists of a long-time iterative method, which alternes heart electrical activity and ablation procedure until the sinus rhythm is restored [3].

The concept of surgical guide for ischemic scar treatment derived from the need to have a precise visualization of pathological area to make sure to assess the necrotic extent of ablation lesions because an incomplete ablation of arrhythmogenic substrate allows subsequent recovery of tissue with restoration of conduction and recurrent arrhythmias.

For all these reasons, the new concept is born to need to build a surgical guide to indicate directly on the heart surface the partially and completely unhealthy cells to be treated by ablation procedure.

Thus, customers' needs, the cardiac surgeons' needs, become requirements of product, which allows to precisely indicate the pathological area directly on the heart surface reducing not only the procedure timing, but also the risk of treating healthy cells, for the better result in the individual treatment.

The whole process is summarized in the following figure which represents the workflow from the acquisition data and to the physical prototype realization (Figure 16).

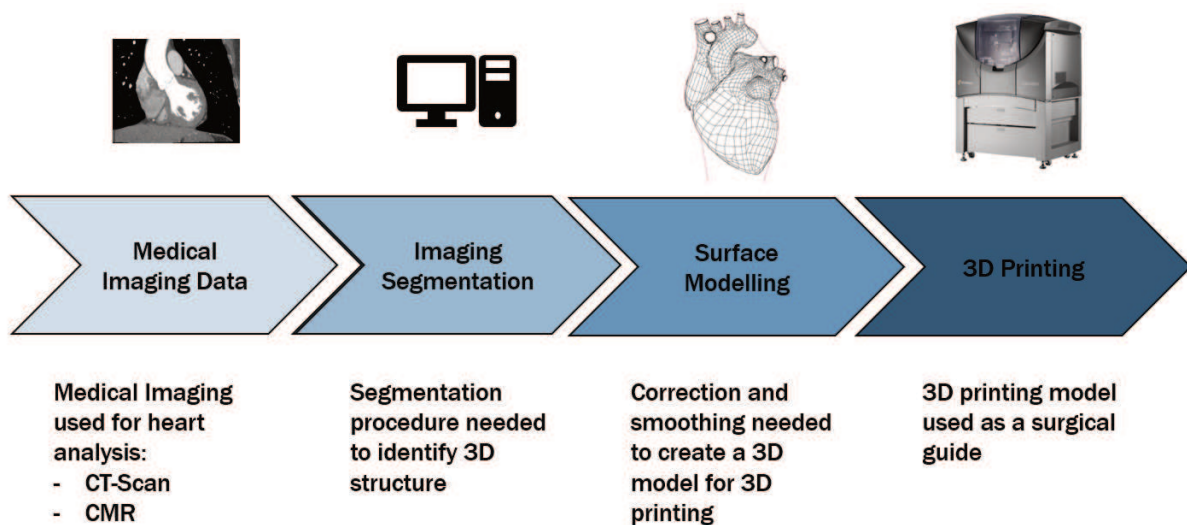


Figure 16. The workflow describes the main steps of surgical guide development process from the acquisition data to 3D printing.

3.3. Requirements

This step involves the designer interpreting and prioritizing needs into product requirements, which essentially identify the objectives of the product.

The main requirement, which cardiac surgeons need, is to obtain a surgical mapping which precisely identify the scar and arrhythmogenic tissue, in order to intervene with a target treatment. Secondly, since the surgical guide will be applied directly on the heart surface, it must be biocompatible and

heart contact safe to avoid any infections or unexpected body reactions, but also flexible and lightweight because the heart is composed by a soft and fragile tissue. In addition, the procedure used in in heart tissue to destroy abnormal electrical pathways that are contributing to a cardiac arrhythmia is the radiofrequency ablation or cryoablation, thus, the guide material must be radiofrequency energy resistant and cryoablation resistant and not conductive, avoiding to damaging the surgical mask and protecting heart tissue.

Furthermore, it is important that it fits as great as possible to heart surface, for the patient-to patient mapping reconstruction, and since the surgical guide will be applied to beating heart, that means moving heart, a good stability must be guaranteed by specific reference points.

In addition, an easy design is required for a rapid application by specialized personnel, avoiding waste of time which could lead to a longer surgery procedure timing.

Finally, it would be desirable that all these requirements could be collected in an efficient design, realised in a minimum manufacturing, with a minimum manufacturing cost. The main requirements in priory order are listed in the following Table 1, highlighting the surgeon's requirements from the engineer's ones.


Table 1. In priority order the main requirements are listed distinguishing the medical from the engineering ones.

Letter	Meaning	Requirements	Medical	Engineering
M	MUST	Precision	X	X
		Biocompatibility	X	
		Contact safety	X	
		Radiofrequency ablation and cryoablation resistant		X
		Electrically safety	X	X
		Flexibility	X	
S	SHOULD	Stability	X	X
		Good fitting		X
		Lightweight	X	
C	COULD	Rapid application	X	
		Easy to use	X	
W	WOULD	Efficient design		X
		Minimum manufacturing time		X
		Minimum manufacturing cost		X

3.4. Function

This step, shown in Table 2, describes engineering action that the product is meant to perform, which, after a correct mask application by user (surgeon), consists in providing a clear identification of pathological area, involving ischemic scar-related ventricular arrhythmias and surrounding arrhythmogenic tissue, which will be treated by ablation procedure.

Table 2. Engineering action performed by surgical guide.

Input		Output
➤ User intervention for the mask application	 Function Box	➤ Pathological area identification

3.5. Specifications

The product specifications are the first step in the process of transforming product ideas into approved product development effort. The product specifications in terms of geometry, materials, safety are listed and divided into subcategories. The Table 3 shows the main items which describe specifications as a metric and/or a value, hypothesizing structure and features of the new device, related to tasks that it will perform.

Table 3. Surgical guide Specifications.

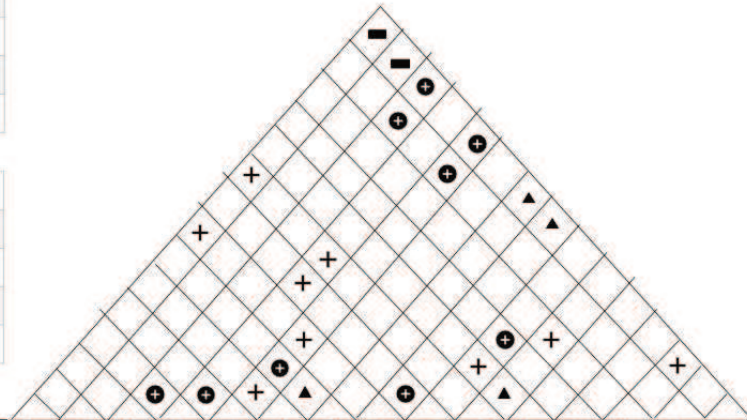
Categories	Items	Value
Geometry	Size of device	120x80x60 mm
	Thickness	3 mm
	Weight of device	500 g
	Pathological area visualization	Specific-patient scar dimensions
	Reference points	Anatomical landmarks
Materials	Shore hardness	Scale A
	Elongation at break	50 %
	Lightweight	Density < 2 g/cm ³
	Temperature Resistant	-70 °C ÷ +70°C
	Color	Transparent
	3D printable	Stratasys Objet260 Connex1
	Washable	With water or soap
	Sterilizable	Hospital sterilization technique
Safety	Electrically safe	Insulated
	Not toxic	Chemical characterization
Recycling	Lifetime	Single use
Manufacturing	Timing	5 days
	Cost	Max 1000 €

3.6. Quality Function Deployment Method

Quality Function Deployment, or QFD, is a method used to identify critical customer requirements and to create a specific link between customer requirements (green rows) and design specifications (blue columns). In the intersection a number among 1, 4, 7 and 10, from the weakest to the strongest level of correlation, is assigned according to the Legend 2. On the top, the triangle describes the correlation among specifications, by distinguishing four levels of relationship: strong positive, positive, negative and strong negative, depending on symbols noted in Legend 1. Immediately below, the arrows suggest when the specification could be minimized or maximized to improve the device quality. Instead, at the base, each specification is detailed in specific measurement. Finally, the absolute rating is computed by summing the product of customer importance weight (in yellow) and the intersection value, while the relative rating describes the correspondent value in percent. The correlation matrix, called House of Quality, is shown in the Figure 17.

Legend 1	
⊕	Strong Positive
+	Positive
■	Negative
▲	Strong Negative

Legend 2	
10	Strongest
7	Strong
4	Fair
1	Weak



Maximize/Minimize			0	↑	0	↓	↓	0	0	↑	↑	0	0	↑	↑	↓	↓	
House of Quality	SPECIFICATIONS		Target area visualization	Reference points	Size	Weight	Thickness	Shore hardness	Elongation	Temperature resistance	Harmless	3D printable	Washable and sterilizable	Electrically safe	Lifetime	Manufacturing time	Manufacturing cost	
	REQUIREMENTS		1	2	3	4	5	6	7	8	9	10	11	12	13	14	15	
1	10	Precision	10	10														
2	10	Biocompatibility									10		4					
3	10	Contact safe									10		10	10				
4	10	Ablation resistance								10				10				
5	7	Flexibility				7	10	10	10		7							
6	7	Stability		10			10	7	7									
7	7	Fitting		10	7		7	4	4									
8	7	Lightweight			10	10	10											
9	7	Rapid to apply		10	7		4	1	10		7							
10	7	Easy to use		10	10		4											
11	7	Efficient design		10	10	10	7			7		10						
12	4	Min manufacturing time			10		10					10	4			10	7	
13	4	Min manufacturing cost			10	10	10					10	7		10	7	10	
CUSTOMER IMPORTANCE			Specific patient scar position	Aorta, pulmonary artery, apex, heart shape	120x80x60 mm	500g	3 mm	Scale A	50%	-70 °C + 70°C	Chemical characterization	Stratasys Objet260 Connex1	Hospital sterilization technique	Insulated	Single use	5 days	Max 1000,00 €	
Absolut Rating			240	450	318	159	444	154	217	149	298	150	44	200	40	68	68	2999
Relative Rating (%)			8	15	11	5	15	5	7	5	10	5	2	7	1	2	2	100

Figure 17. House of Quality.

3.7. Conceptualization

In this step a large quantity of ideas is generated in order to find the best solution for the higher quality of the desired product. It consists of developing as many concepts as possible for each item, drawing up the morphological chart containing all the possible solutions, as shown in Table 4, and then, identifying feasible combinations, which lead to different possible solutions.

The first concept to be considered is the surgical guide geometry, which could be realized in different ways, depending on the covering extension of heart surface: in the full mask, the whole heart surface is covered by the medical device except for the target area, which is leaved empty; the basket one is a lightened version of full mask, in which the scar perimeter is identified by a thicker border, in order to be distinguished by other holes. Instead, the minimal mask is only composed of the main parts, like the target zone and one or more than one reference points, allowing the surgical guide purpose.




Furthermore, for an appropriate application, fitted the heart surface, the choice of reference points is crucial. Among all options the heart surface shaped is the common point, but the stability and the good fitting are increased by adding other focal points. For this reason, also the Aorta, the Pulmonary Artery and the apex are considered. Whereas the surgical guide must be applied directly on the heart surface, it must be clean and sterile. The hospital environment provides several washing techniques: manual, in which the personnel is asked to wash the device with tap water, or machine washing, a specific machine is involved in medical device cleaning under specific conditions, like +95°C for one hour and half. Another option is the composition of two, a sort of hybrid washing: the manual wash is followed the machine one.

Successively, the sterilization method is needed to remove, kill, or deactivate all forms of life (in particular referring to microorganisms such as fungi, bacteria, spores, unicellular eukaryotic organisms such as Plasmodium, etc.) and other biological agents like prions present in a specific surface. Sterilization can be achieved through various means, including heat, chemicals, irradiation, high pressure, and filtration, for this type of medical device, more suitable ways are the autoclave, gamma rays, and Vaporized Hydrogen Peroxide sterilization. After sterilization, an object is referred to as being sterile or aseptic.

To ensure sterile conditions, as well the medical device integrity, usually, proper packaging is required. Among medical device packaging solutions, blisters contain the product in a cavity of hard plastic and sealed shut, usually via an assembly line heating process. Blister packs can be very small or very large, depending on the product in question. Instead, pouch packaging is a flexible packaging product made from barrier film, foil that supports products; pouches are lightweight, compact, and have minimal product waste because of its flexible material that breaks down as it is used. Lastly, flow wrapping is a horizontal-motion process in which product of any shape is wrapped in polypropylene film. The result is a flexible package with a non-lap type seal.

All these options are reported in the following table.

Table 4. Morphological chart provides three options for each item to realize the surgical guide. Among all possible combinations, the green and the blue are considered and analyzed. Other combinations are possible.

<i>Items</i> \ Options	Option 1	Option 2	Option 3
<i>Geometry</i>	Full mask	Minimal mask with a thicker border around target area	Basket mask with a thicker border around target area
<i>Reference points</i>	Heart surface shaped, Apex	Heart surface shaped, Aorta, Pulmonary Artery	Heart surface shaped, Aorta, Pulmonary Artery, Apex
<i>Washing</i>	Manual wash	Machine wash	Hybrid wash
<i>Sterilization method</i>	VHP sterilization	Autoclave sterilization	Gamma rays
<i>Packaging</i>	Blister packaging 	Flow wrap 	Pouch packaging 

3.8. Evaluating Alternatives

Among all possible combinations for the medical device implementation, the blue and the green solutions are considered to evaluate which one satisfies the customer demands (Table 4). Other combinations of previous options are possible candidates, but they are not taken into account.

The green solution of surgical guide is characterized by a minimal geometry, with a thicker border around target area, that allows a minimum expenditure of material, but ensuring a good stability and surface fitting thanks to the heart surface shape, the Aorta, the Pulmonary Artery, and the apex. For this solution, a machine washing is chosen for a good cleaning to ensure sterilant can reach all parts of the device at +95°C for one hour and half, and successively, the surgical guide is submitted to the Vaporized hydrogen peroxide sterilization, a vapor of hydrogen peroxide (H₂O₂) kills microbes by oxidizing amino acids and proteins, at +43°C for 45 minutes. Finally, this option proposes a pouch packaging which allows to maintain the sterile and integrity conditions of medical device in a low-cost solution with a minimum product waste. The sketch of green solution is shown in the Figure 18. Concerning the blue alternative, another geometry is considered: a basket shaped is a lightened version of full mask, in which the scar perimeter is identified by a thicker border, in order to be distinguished by other holes. The reference points that give the stability are the heart surface fitting and the apex. The manual cleaning is chosen to remove all extraneous parts before being undergone to autoclave, that kills the deleterious microorganisms including bacteria, viruses through a machine that makes the object contaminant-free by maintaining pressurized saturated steam under controlled temperature for desired time [17]. The steam pressure and temperature can change, depending on the size of the load and the contents.

Finally, regarding the packaging technique, the blue solution proposes a blister packaging, that is composed of a rigid plastic box which guarantees the sterile and integrity conditions during the transport from sterilization department to operating room, where the surgical guide is applied on patient, and the surgical procedure occurs. The sketch of blue solution is shown in the Figure 19.

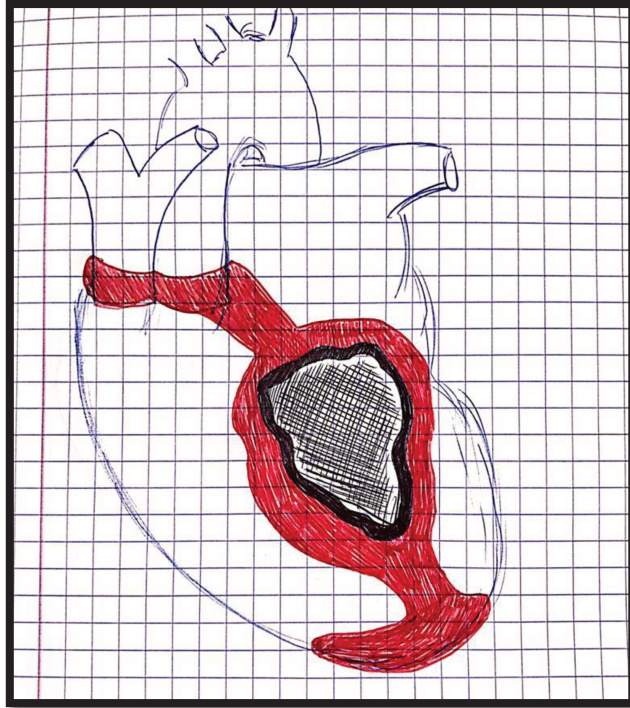


Figure 18. The sketch of green solution: the main reference landmarks are the Aorta the Pulmonary Artery, and the apex, and the thicker border, drawn in black, surrounds and identifies the target zone.

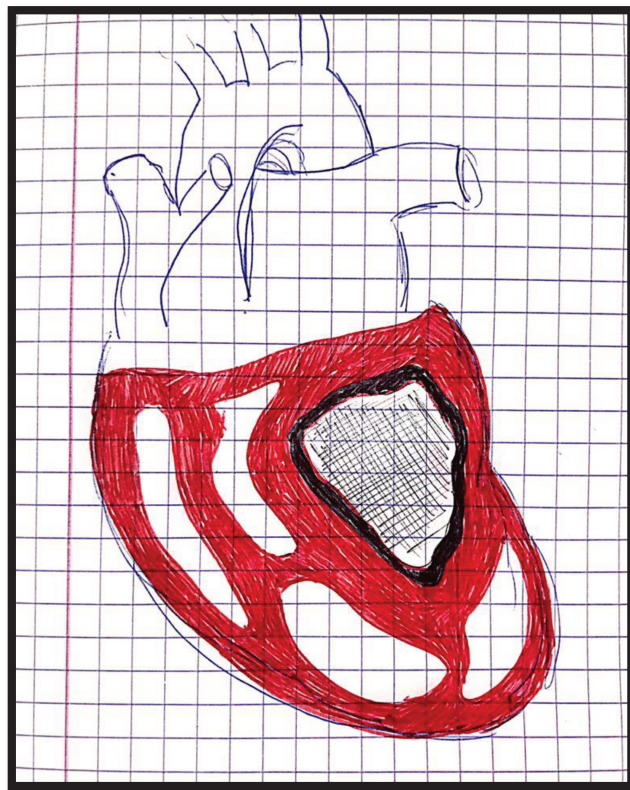


Figure 19. The sketch of blue solution: the basket shape. The reference points that give the stability are the heart surface fitting and the apex. A thicker border, drawn in black, identifies the scar perimeter, distinguishing from other holes.

3.8.1. Concepts and Parameters Evaluation

According to Decision Matrix, reported in Table 5, the green and blue solutions are analyzed, generating a score which allows to find the better tradeoff between concepts. The decision matrix is composed by specifications on columns and solutions on rows. For each specification, a weighting factor (from 0 to 1.0) is assigned according to the importance ratings for each design criteria of the device that we are going to product. Then, a rating factor (from 0 to 10) is given to each specification in relation to the specific solution (green and blue). The final score is generated by a sum among contributions, obtained by multiplying the weighting factor and the rating factor for all specifications. Although both green and blue solutions give high scores (8.77 and 8.18 respectively), the best solution is represented by the green one, which represents a better tradeoff: thanks to a simple shape a surgical guide provides a great pathological zone visualization at low manufacturing time and low-cost manufacturing. The choice of anatomical landmarks like Aorta, Pulmonary Artery, and the apex, together with the heart surface shape, ensuring the fair stability, make a rapid and easy application for a good fitting on the heart. A proper flexibility is given by the polymeric material and its thin thickness. Finally, the VHP sterilization is preferred to autoclave because the high temperature could damage the surgical mask and alter its mechanical and thermal properties.

Table 5. Decision Matrix.

DECISION MATRIX	Multiplier factor	Pathological area visualization	Reference points	Size of device	Weight of device	Thickness	Shore hardness	Elongation at break	Temperature Resistant	Harmless	3D printable	Washable & Sterilizable	Electrically safe	Lifetime	Manufacturing time	Manufacturing cost	Sum
	Weighting	0.11	0.11	0.02	0.04	0.05	0.04	0.08	0.10	0.11	0.11	0.11	0.08	0.01	0.02	0.01	1.0
Blue		9	8	7	9	8	8	9	7	10	10	5	7	8	10	8	
		0.99	0.88	0.14	0.36	0.40	0.32	0.72	0.70	1.1	1.1	0.55	0.56	0.08	0.2	0.08	8.18
green		9	9	6	8	8	8	9	7	10	10	10	7	8	9	9	
		0.99	0.99	0.12	0.32	0.40	0.32	0.72	0.70	1.1	1.1	1.1	0.56	0.08	0.18	0.09	8.77

4. Case Report

In this study a 61-year-old man case is analyzed. He presents different cardiovascular risk factors, like hypercholesterolemia, familiarity of coronary heart disease less than 65 years old, Tabagism, and a sedentary life. The Ischemic Cardiomyopathy and heart failure is diagnosed after performing CMR with contrast and CT angiography. In particular, T2 weighted black blood sequence (in axial), SSFP cine sequences (short axis, 4K, 2K, 3K, LVOT, aortic valve), resting perfusion and delayed enhancement were performed, and a strongly dilated left ventricle with akinesia at the lateral wall from basal to apex is noted.

Some physiological and anatomical features are measured to evaluate left ventricle functionality and structure, such as left ventricle (LV) ejection fraction (EF) of 35%, a LV end diastolic volume (LV EDV) of 354ml, a LV end systolic volume (LV ESV) of 229ml, a LV stroke volume (SV) of 125ml, and a LV myocardial mass of 218g. Delayed enhancement images show transmural lateral infarction and infarction of papillary muscles. Moreover, left ventricle is strongly dilated with akinesia at the lateral wall from basal to apex. Basing on pathological conditions, following a syncope, chest pain, and ventricular tachycardia, the clinical decision suggests the surgical ablation procedure.

4.1. Virtual Prototyping Algorithm

Virtual prototyping is a method in the process of product development, which involves the computer-aided design (CAD) software to aid in the creation, modification, analysis, or optimization of a design before committing to making a physical prototype.

The first and important step to generate a specific patient 3D printed model is to acquire imaging data and the precision of 3D models depends on the quality of the medical imaging used to create them. Regardless of the type of imaging, it is important to consider the purpose of the model being created.

For this purpose, CMR imaging is performed by Philips Medical Systems at 1.5T of magnetic field, at 63MHz of imaging frequency and 2ms of repetition time. Cine CMR recorded in transversal orientation 360 slices of 288x288 pixels, at thickness of 10 mm.

Instead, CT angiography (GE Medical Systems) was performed at 256 slices of 6mm thickness, with 512x512 pixels. After acquisition, all data in Digital Imaging and Communications in Medicine (DICOM) format are stored in PACS Archive.

To generate a patient- specific 3D model of surgical guide two kinds of medical images are uploaded, and separately processed in 3D Slicer, an open-source Software, specialized in medical image visualization and computation:

- CMRI, for the target area identification
- CT image as a template for the surgical guide

CT image is necessary for the 3D model reconstruction, in fact its high signal-to-noise ratio, reasonable soft tissue contrast, and excellent spatial resolution, provides a more reliable 3D heart model it also provided the necessary volumetric data required to create the patient-specific phantom.

The first step of post-processing to create a 3D reconstruction from the medical images is the segmentation, a semiautomatic process, which divides an image into regions with similar properties such as gray level, brightness, and contrast.

Segmentation of medical images to extract anatomical structures is arguably the most important problem in medical image analysis. In this case, the threshold-based segmentation is implemented to separate the anatomical region of interest (ROI) from the background, by setting a threshold range, which identify the cardiac tissue. Regarding the CT scan was set from 1 to 375, while for the CMRI segmentation a range threshold was set at 99 to 509 (Figure 20 and Figure 21, respectively). Nevertheless, the semi-automatic threshold-based segmentation is not enough accurate because of anatomical structures heterogeneity in size, shape, and location and because of boundaries ambiguity due to a low contrast between target organs and the neighboring tissue, a supervised slice-by-slice segmentation through operator interaction is still required for error correction in the event of an inadequate result: it is a time-consuming method, but the operator intervention is fundamental to check if all anatomical heart structures were involved in the process.

Successively, the smoothing step is performed for surface definition, by closing undesired holes and removing distortions, due to noisy acquisition.

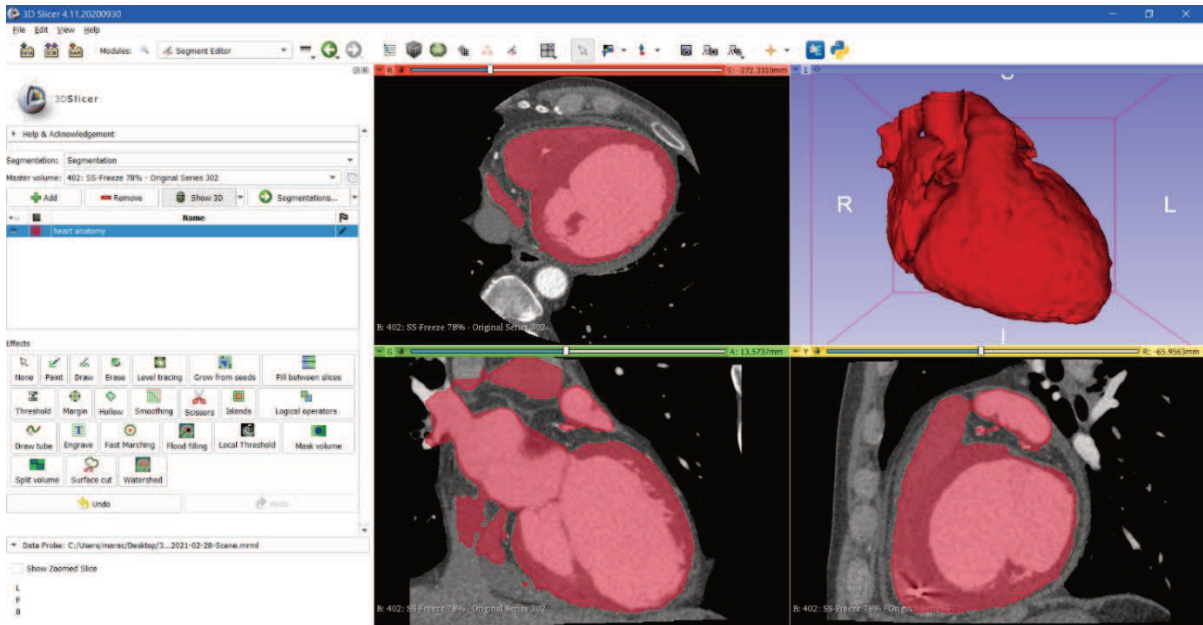


Figure 20. Axial, Sagittal, Coronal and 3D views of CT Segmentation on 3D Slicer Software.

To ensure the 3D reliable reconstruction from CT scan, the heart anatomy is segmented in two parts, cardiac tissue and internal chambers volume separately, which are later combined in an assembly. In parallel, the MRI segmentation is manually performed by distinguishing the pathological area from rest of cardiac tissue thanks to the different contrasts. In this way, the result is a single 3D model characterized by a scar border identification.

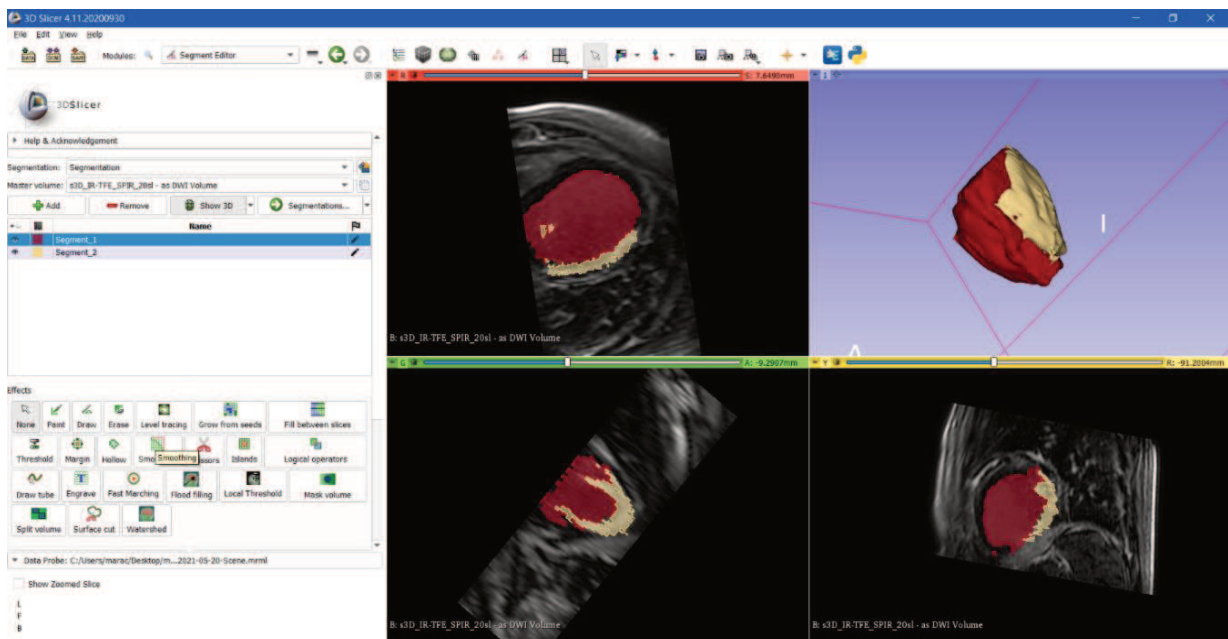


Figure 21. Axial, Sagittal, Coronal and 3D views of MRI Segmentation on 3D Slicer Software.

At the end of this process, two 3D heart models are generated and converted in STL format. In particular, the 3D heart reconstruction generated from CT images has a double purpose: it is used as a template for the surgical guide surface model, and the second one is used to create a heart phantom.

The second part of post processing was performed in Meshmixer Software: for the heart phantom modelling, the creation of additional components is necessary to stabilize the model to be printed, avoiding the collapse (Figure 22).

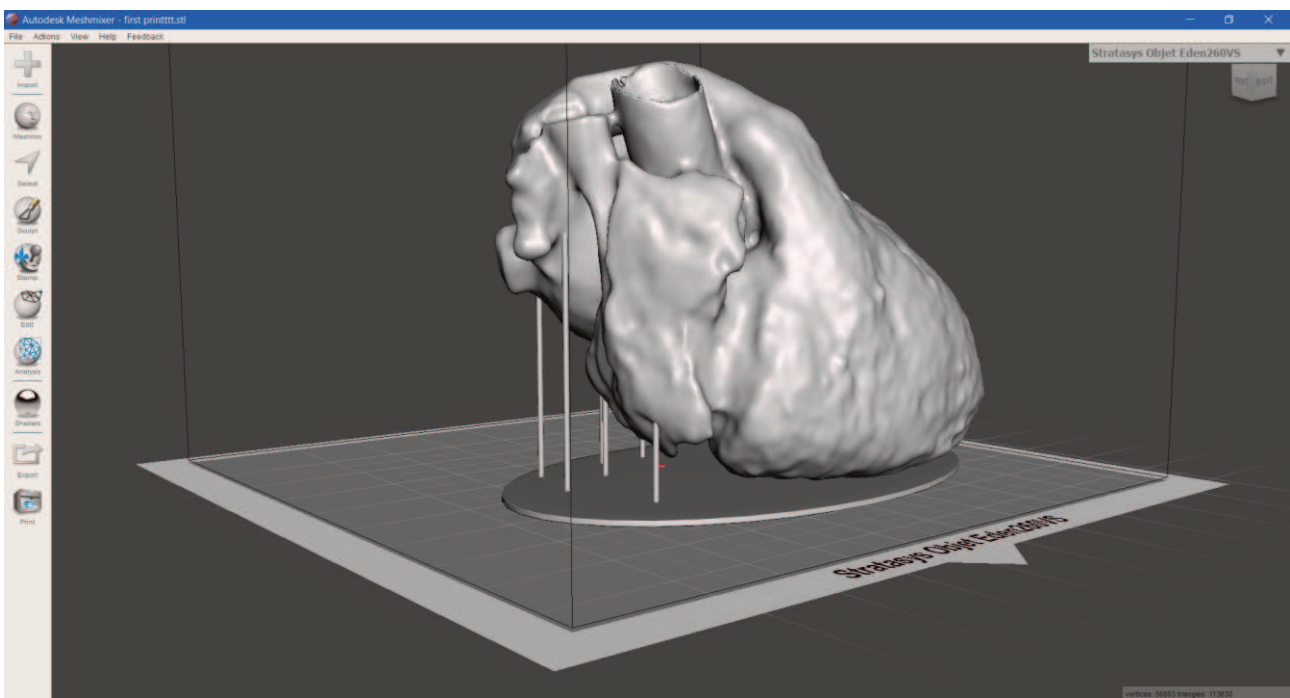


Figure 22. 3D model of heart phantom with additional components to stabilize the model to avoid the collapse during printing.

Regarding the surgical guide modelling, both 3D models from CT and MRI are loaded in Meshmixer and thanks to the left ventricle used as anatomical landmark, the merge of models is achieved (Figure 23).

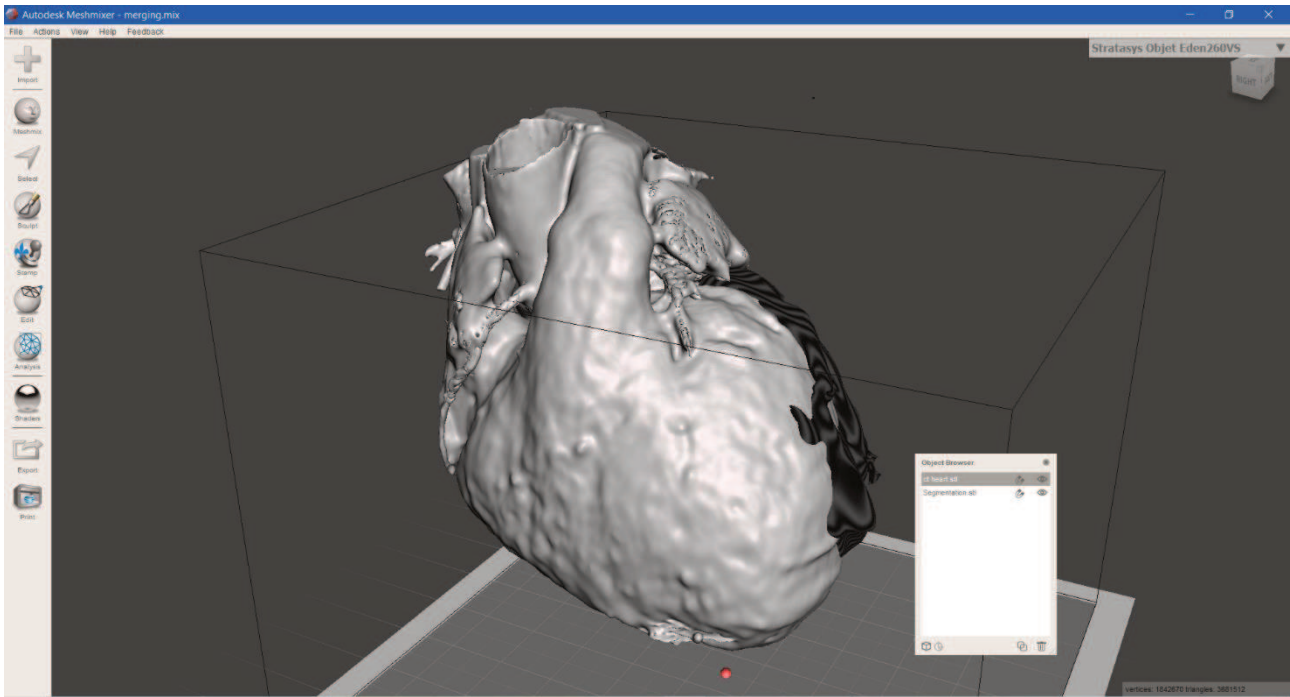


Figure 23. CT and MRI models merging on Autodesk Meshmixer Software.

Then, successive step is represented by the surface mesh modelling of surgical guide: once having imported and merged the STL files in Meshmixer, the CT heart surface is used as a template. The scar border is drawn firstly, then, the anatomical landmarks, such as the aorta ring, the pulmonary artery anulus and heart apex are draft and manually connected to the pathological target area, creating the whole surgical guide surface as stable as possible.

Successively, the surgical guide sheet was extruded to have a 3-dimensional shape of 3 mm of thickness. In addition, for a better identification of target area, and for a higher protection to healthy tissue from surgical procedure, an extra thickness of 3 mm around the target area is added. Moreover, to improve the surface design of mask the “brush” function is performed and the whole mask model is subjected to smoothing phase. Finally, the Meshmixer “make solid” functionality is employed and converted in STL format to create a suitable file to be printed. The figure 24 represents the 3D model of surgical mask from different views (Figure 24). The main virtual prototyping steps are summarized in the following Figure 25. Finally, to verify whether the surgical guide fits on heart phantom, a virtual simulation is performed on Meshmixer Software, as shown in the Figure 26.

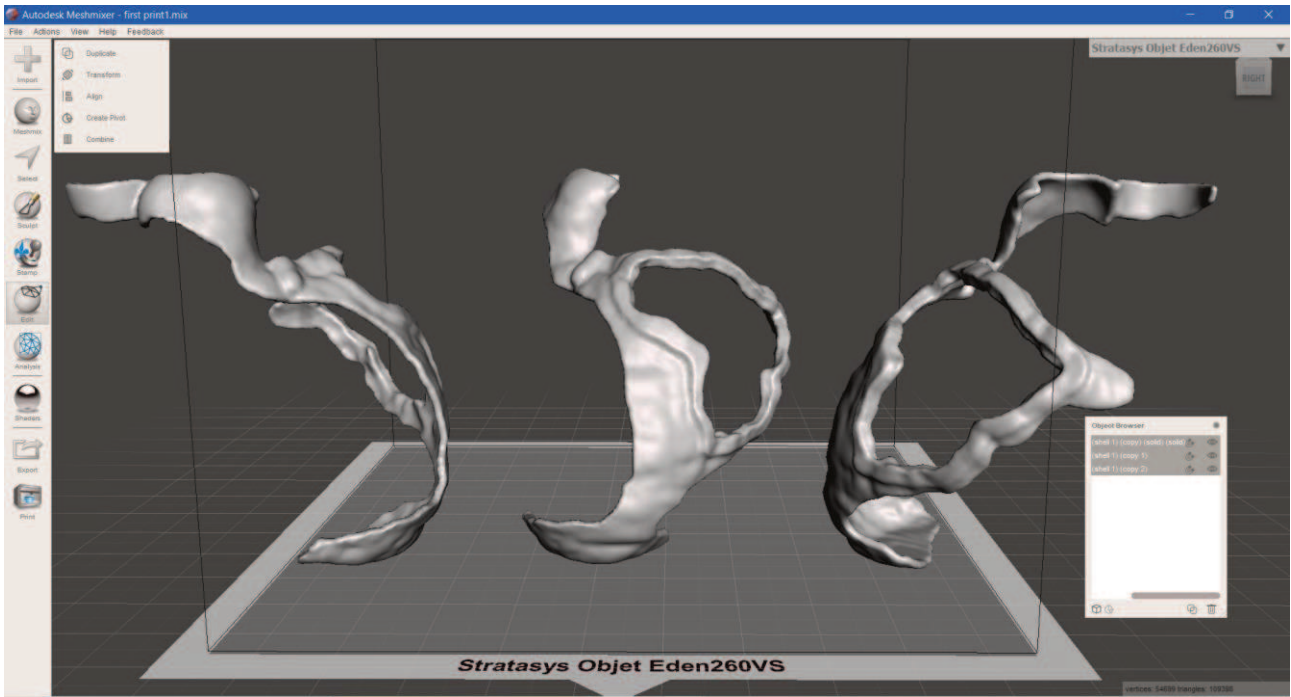


Figure 24. Anterior, lateral and posterior view of the 1st virtual prototype of surgical guide for ischemic scar treatment.

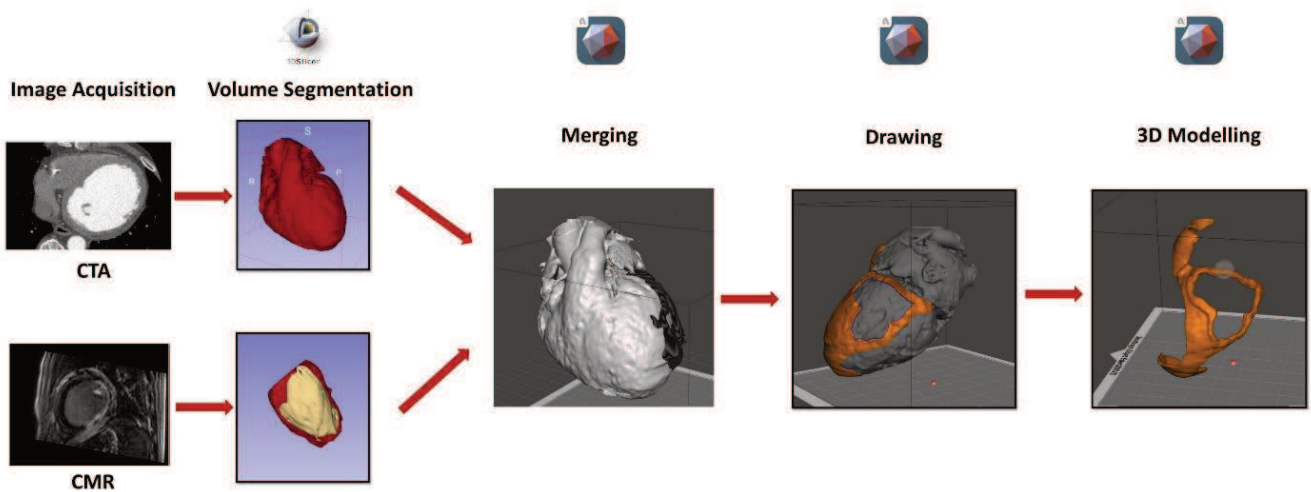


Figure 25. The main virtual prototyping steps from the acquisition data, volume segmentation in 3D Slicer Software, to 3D model visualization in Autodesk Meshmixer Software.

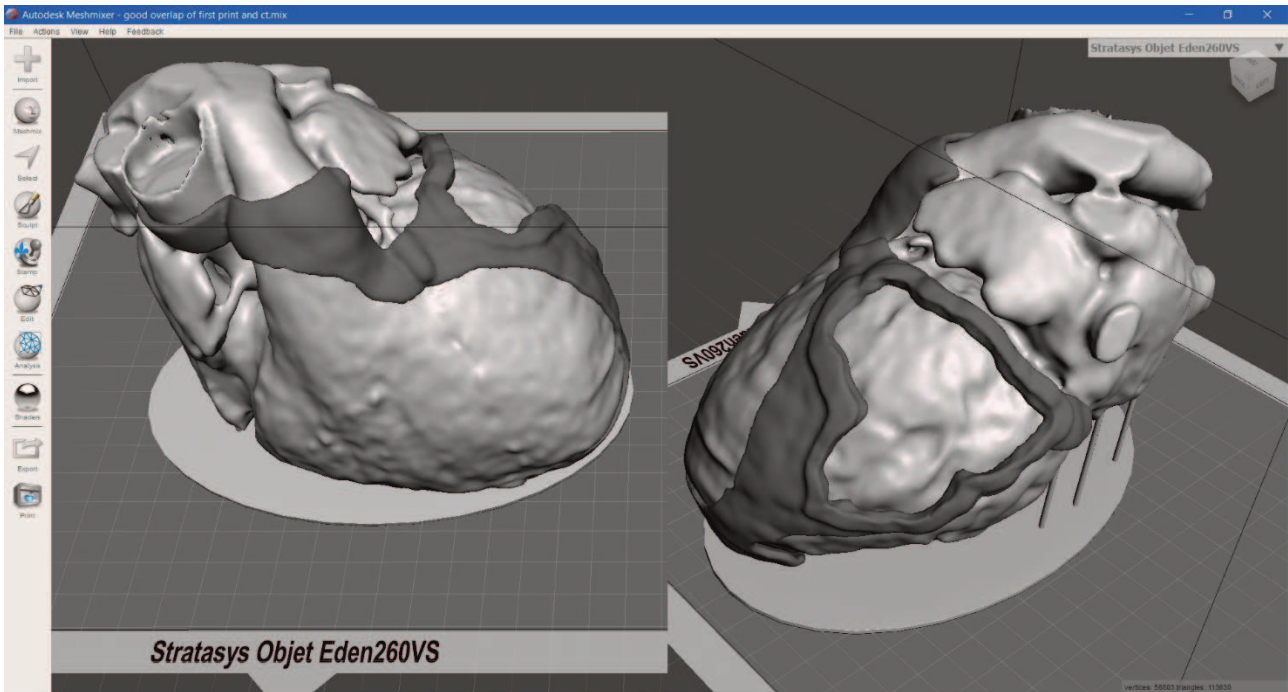


Figure 26. Anterior and posterior view of virtual simulation of surgical guide fitting on the heart phantom in Autodesk Meshmixer Software.

5. Detailed Design

5.1. Process Selection: 3D printing

The advent of additive manufacturing technology and the improved medical imaging techniques, such as high-resolution CT and MRI scanning, enables the translation of digital images on the computer screens into tangible objects. In the biomedical engineering field, additive manufacturing technology can be used for various applications, such as tissue and organ fabrication, production of anatomical structures, drug delivery and implant and surgical guide production. In the clinical research area, especially, 3D-printed anatomical models with realistic anatomical organ shaped structures have been used as experimental models for presurgical planning through rehearsing and preparing complex surgical procedures to reduce the risk and time on the operating table, as well as education and training.

For this work two 3D printers are used: the PRUSA, based on fused deposition modeling technology, to realize the 3D heart phantom, and the Stratasys Objet260, based on Polyjet technology, to create the 3D surgical guide.

5.1.1. Stratasys Objet260 Connex1 3D printer

Once the STL file of model to print is ready, it is imported in Object Studio software, where it is automatically displaced on the virtual tray. After setting of all printing features like material, printing mode, the estimation of time and material consumption is provided, and the printing model starts. Stratasys Objet260 Connex1 is a Polyjet 3D printing, an additive manufacturing process in which layers of acrylic-based photopolymers are selectively jetted at precise coordinates onto a build tray. Figures 27 and 28 are the illustration of Polyjet 3D printing.



Figure 27. Stratasys Objet260 Connex1.

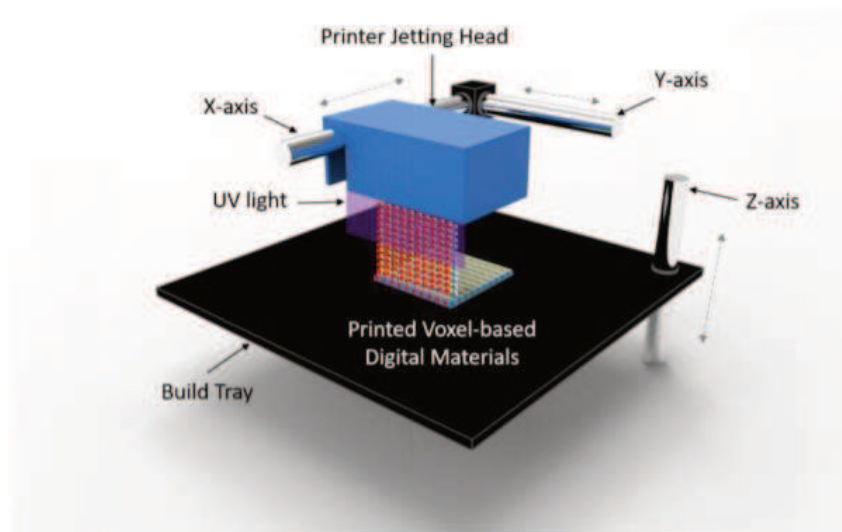


Figure 28. Illustration of Polyjet 3D printing.

The liquid material is jet streamed from the print heads via controlled piezoelectric pulses. UV lamps, mounted on the print block, partially cure the material on each pass. Material is jetted both when the print block travels from left to right and when it travels from right to left. However, when the print block travels from right to left, the Z stage moves upwards slightly, allowing the part to be contacted by the roller mechanism on the print block. The roller, spinning in a clockwise direction, can pick up the partially cured material, thereby leveling the surface of the part for the next printed slice. The roller, on each revolution, is scraped clean by a rollerblade. The tray then moves down again, ready for the next slice to be printed on the next left to right pass. 3D printed model material is inserted in the matrix, the GelMatrix, an alkaline solution soluble material utilized when printing small features. The GelMatrix material is softer and easier to remove, and it allows to realize a small diameter structure previously unattainable by 3D printing. Due to its softness, GelMatrix is printed in conjunction with normal Support material to give model enough support during the printing process. For the Stratasys Objet260 Connex1, is used the SUP705 as GelMatrix [18].

After printing, the 3D model is being subjected to washing in a specific support material removal system, provided by Stratasys, the WaterJet, a compact and affordable system enable to efficiently clean any type of 3D model or prototype. The WaterJet comprises a self-contained cleaning unit and a small, separate pressure pump unit (figure 29).

During washing, it is important to verify the part is fully cleaned to enable its biocompatibility properties, because support material is not biocompatible. It is best to hold the waterjet nozzle a safe distance from the model – approximately 20 cm is considered safe when using a standard water pressure of 750 Psi/50 Bar. If the water pressure used is less than the standard (i.e., due to infrastructure limitations), the safe distance should be decreased accordingly. It is also recommended to move the nozzle with quick movements (not fixed on a single location for more than 2 seconds), to avoid tearing and/or other damage due to high water-model impact.



Figure 29. The WaterJet, a compact system enables to efficiently clean any type of 3D model or prototype from support material.

5.1.2. PRUSA 3D printer

The PRUSA 3D printer, used to create 3D heart phantom, works according to the Fused Deposition Modeling (FDM) technology (Figure 30). FDM is an additive manufacturing process that belongs to the material extrusion family. In FDM, an object is built by selectively depositing melted material in a pre-determined path layer-by-layer. The materials used are thermoplastic polymers and come in a filament form. The basic principles of the technology are presented below.

A spool of thermoplastic filament is first loaded into the printer. Once the nozzle has reached the desired temperature, the filament is fed to the extrusion head and in the nozzle where it melts. Successively, the extrusion head is attached to a 3-axis system that allows it to move in the X, Y and Z directions. The melted material is extruded in thin strands and is deposited layer-by-layer in predetermined locations, where it cools and solidifies. Sometimes the cooling of the material is accelerated through the use of cooling fans attached on the extrusion head. Then, to fill an area, multiple passes are required. When a layer is finished, the build platform moves down (or in other

machine setups, the extrusion head moves up) and a new layer is deposited. This process is repeated until the part is complete and the 3D heart phantom is represented in the figure 31 [19].



Figure 30. PRUSA 3D printer.

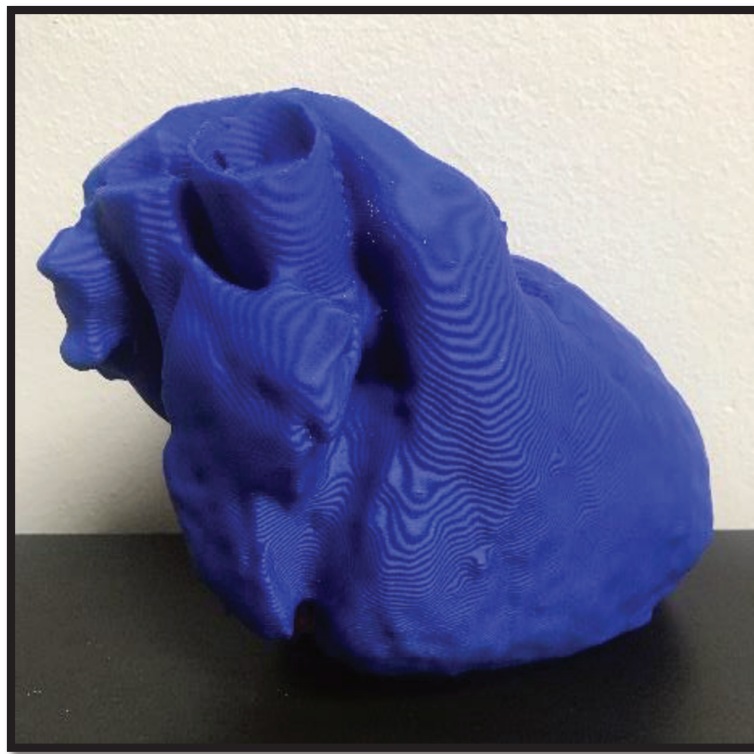


Figure 31. The 3D heart phantom is printed in PLA by PRUSA.

5.2. Material Selection

Despite the large amount of 3D printable materials, provided by Stratasys, the research has been done among all compatible with the Objet260 Connex1.

Moreover, the material selection not only depends on the 3D printer used, but also on action that the surgical guide is meant to perform, taking into account different aspects, like workspace, way to use, surgical procedure associated. Thus, most of material features coincide with surgical guide requirements, previously described. In fact, since the surgical guide will be applied directly on the heart surface, its material must be biocompatible and heart contact safe to avoid any infections or unexpected body reactions, and thus, washable and sterilizable. Whereas the mechanical properties, the material has to be flexible and lightweight to avoid damaging the soft and fragile underlying heart tissue.

Moreover, as the scar treatment consists of radiofrequency ablation or cryoablation, the guide material must be radiofrequency energy resistant and cryoablation resistant and not conductive, avoiding to damaging the surgical mask and protecting heart tissue.

Among all printable materials, the one that reflects most mechanical and thermal properties, as well as biocompatibility and sterilizability features is the MED625FLX, however, as Stratasys has provided a narrow material data sheet because of its recent availability in the market, additional mechanical and thermal tests are needed to demonstrate the product functionality.

5.3. Cleaning, Packaging and Sterilization

Since patients come in contact with surgical tools all the time, sterilizing equipment and medical devices is a vital element of medical care, to ensure the medical safety of environment and medical equipment. Firstly, it is important to define the terms cleaning, disinfecting, and sterilizing. Cleaning corresponds to the removal of visible elements from objects and surfaces (e.g., soil, dirt, dust, organic, and inorganic materials). Generally, a complete cleaning is accomplished using water with detergents or enzymatic products, and it is fundamental before disinfection and sterilization because the presence of inorganic and organic components on the surfaces may interfere with the effectiveness of these processes. Instead, disinfection allows to remove or inactivate the most

pathogenic microorganisms except bacterial spores. And finally, a sterile object is defined as absent of viable microorganisms. The sterilization process leads to death of the microorganisms in the material and is expressed in terms of probability of surviving microorganisms. The safety of a sterilization method is given by statistical probability of a microorganism surviving the sterilization process, the sterility assurance level, which may be reduced to a very low number, but it cannot reach zero.

An efficient sterilization is crucial to minimize the incidence of medical device-related infections, which are a major concern in health care. Moreover, as there is no universal set of conditions for sterilizing, to help the choose of the best sterilization process, the gathering detailed information regarding the material/object properties is fundamental in order to avoid any damages. Thus, among all sterilization methods, each formulation much be tested on a case-by-case basis to select the more suitable conditions that are effective and allow the main properties to remain unaltered [20].

According to the sterilization methods available in the hospital, and taking into account the material properties, the best way to sterilize the surgical guide is a specific gas sterilization, the Sterrad Vaporized Hydrogen Peroxide Gas Sterilization (figure 32). This method is typically used to sterilize materials that would be damaged by high temperature or radiation and the gaseous active agent is the hydrogen peroxide (H_2O_2).



Figure 32. Pouch packaging on the top, Sterrad Vaporized Hydrogen Peroxide Gas Sterilization machine on the bottom.

Before being sterilized, the surgical mask undergoes the pouch type packaging phase, fundamental to ensure sterile conditions, as well the medical device integrity during transport from sterilization department to operating room. The type-pouch wrapping is a flexible packaging product made from barrier film, foil that supports products; pouches are lightweight, compact, and have minimal product waste because of its flexible material that breaks down as it is used.

Once packaged, the surgical guide is placed in the Sterilization Chamber where is subjected to vaporized hydrogen peroxide sterilization process, consisting as follows:

- Liquid H_2O_2 gets converted into vapor,
- The vapor fills the chamber, contacting all surfaces and penetrating lumens,
- After sterilization, the vapor is vacuumed from the chamber and converted into water and oxygen [21].

The following figure 33 shows the scheme of VHP sterilization system components.

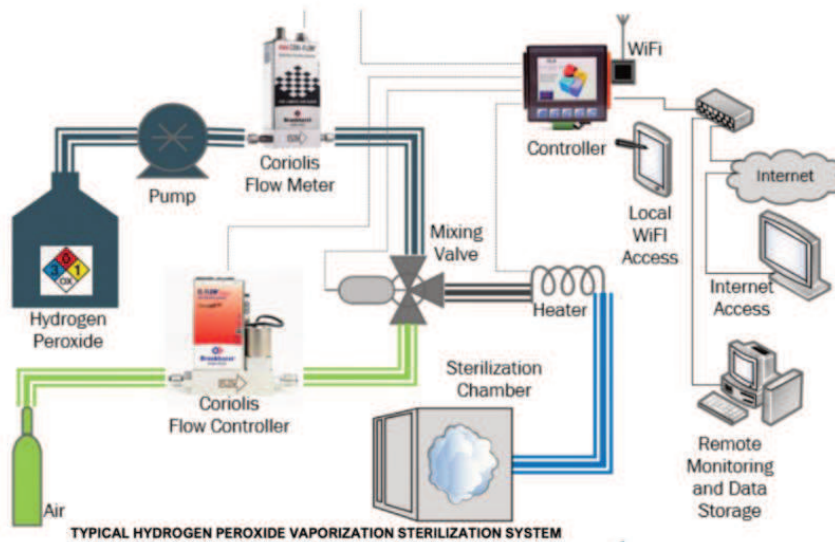


Figure 33. The scheme of VHP sterilization system components.

5.4. Cost Estimation

The surgical guide cost is completely dependent on both MED625FLX cost and SUP705 cost (support material), and the cost estimation is strictly related to surgical guide dimension and thickness. Because the guide is specific patient, its dimension derives from patient heart. Thus, it is obvious that smaller the heart, lower the used material, and reduced will be the manufacturing cost. The following table describes the estimation cost of 1st physical prototype.

Table 6. Cost Estimation of the 1st physical prototype of surgical guide.

Cost Estimation of the 1st Physical Prototype of Surgical Guide

MED625FLX cost	1220€/3.6 kg
SUP705 cost	420€/3.6 kg
1 st Prototype mass	117g
MED625FLX consumption	117g
SUP705 consumption	180g
Tot.	61.60 €

6. Design Analysis

6.1. The First Physical Prototype

In this paragraph the first physical prototype of surgical guide is defined and analyzed. The high-resolution images of CMR and CTA, the CAD software and the current 3D printing technology allowed the development and the realization of 3D surgical guide for a high precise identification of ischemic scar aimed for accurate procedure of personalized ablation treatment.

After being printed by Stratasys Objet260 Connex1 in transparent MED625FLX (Figure 34), the 3D object is subjected to accurate washing in a specific support material removal system, provided by Stratasys, the WaterJet, to verify the part is fully cleaned to enable its biocompatibility properties, because support material is not biocompatible (Figure 35).

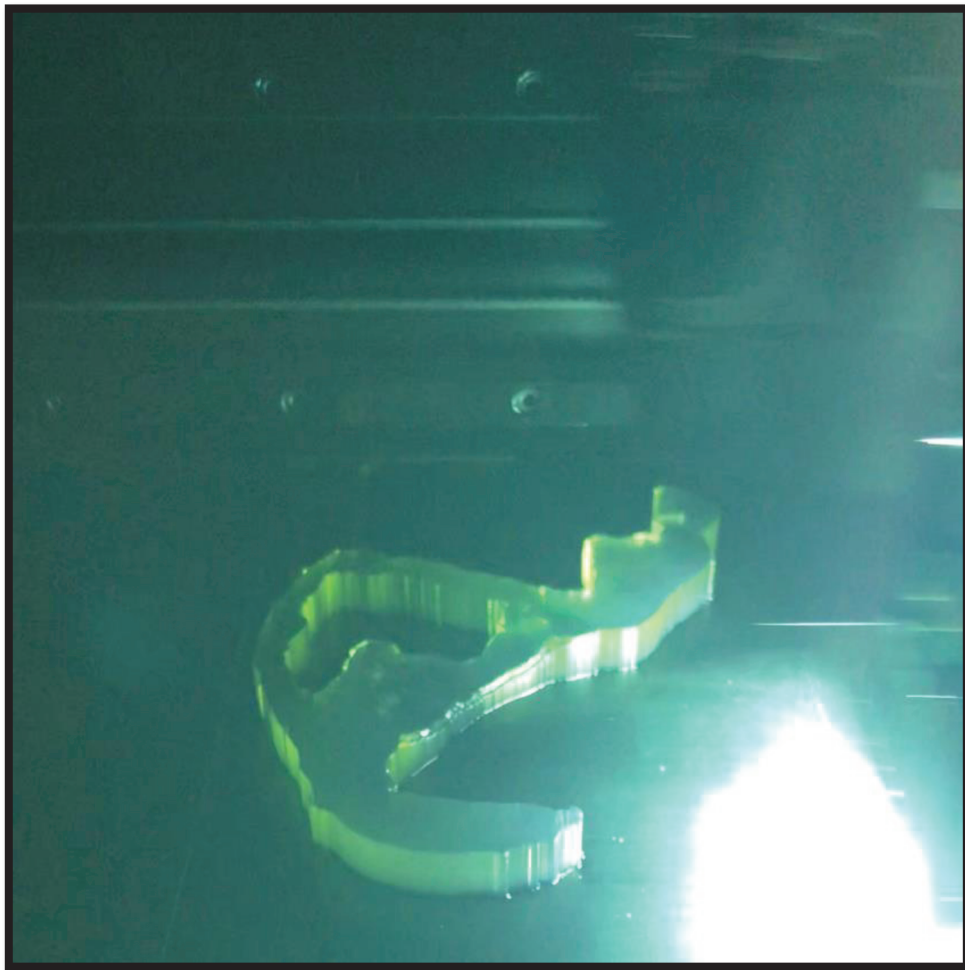


Figure 34. The first prototype representation during printing.

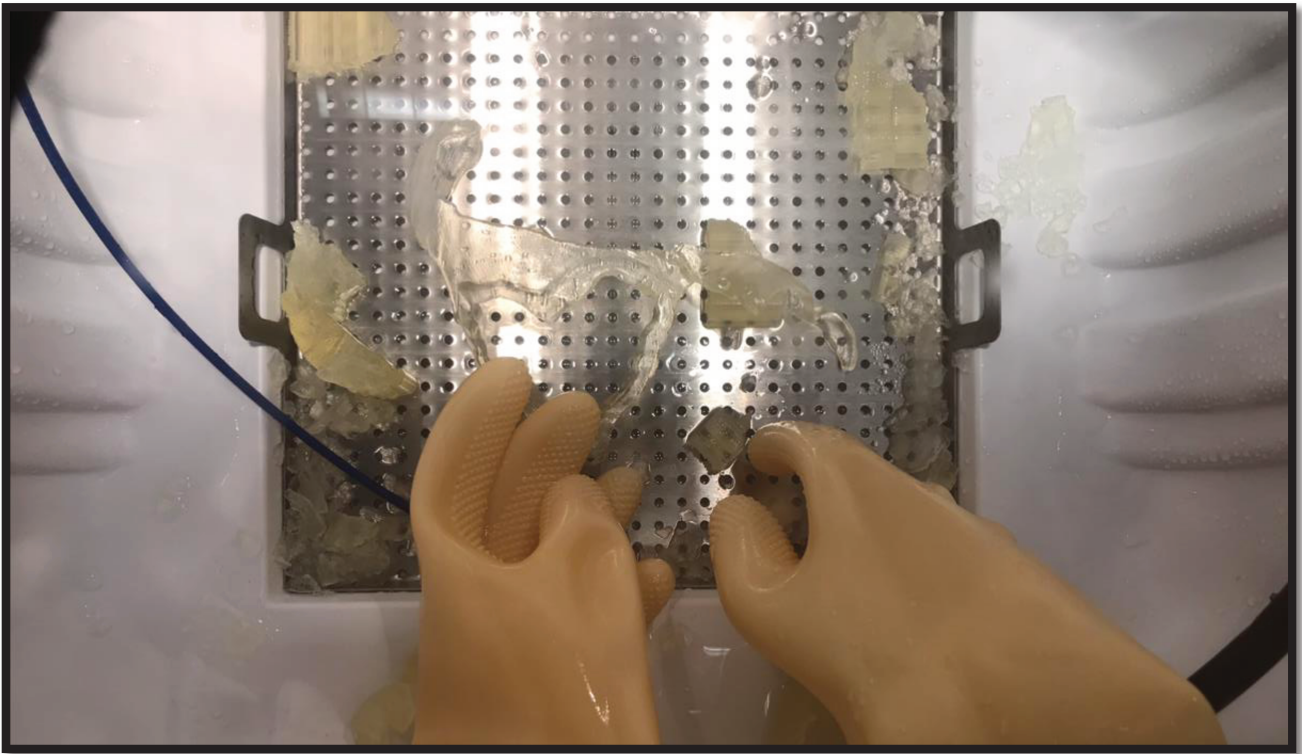


Figure 35. The 1st prototype of surgical guide during cleaning in Waterjet to remove the support material.

The first physical prototype is defined by a minimal geometry, with a thicker border around target area, that allows a minimum expenditure of material, but guaranteeing a good stability and surface fitting thanks to the specific patient heart surface shape, and the landmarks such as the Aorta, the Pulmonary Artery, and the apex. All reference points have properly connected each other, for except of the link between target zone and heart apex, in fact it could represent a critical point, subjecting to rupture.

The surgical guide prototype is characterized by a thickness of 3 mm and a border of 6 mm around the target zone, providing good flexibility for an easy application on heart surface. Moreover, the MED625FLX ensures the biocompatibility as well as the lightweight, avoiding damaging the underlying cardiac tissue. Basing on data sheet provided by Stratasys, MED625FLX contact safe characteristics in terms of biological toxicology, therefore, any unexpected infections or body reactions do not take place.

Finally, being the Radiofrequency ablation or cryoablation, at medical discretion, the treatment procedures for scar-related VT, the temperature resistance has crucially importance not only for the

cardiac tissue protection but also for surgical mask integrity. Nevertheless, by reason of the narrow material data sheet due to its recent availability, additional technical tests are needed to demonstrate the product functionality and feasibility.

The first prototype of surgical guide for treatment of ischemic scar is shown in the following figure, where it is possible to appreciate the target zone for the guided surgery ablation procedure, and the reference points such as Aorta ring, Pulmonary Artery ring and apex, essential for the easy and rapid application on heart surface (Figure 36). Instead, the figure 37 represents a preliminary simulation of surgical mask application on the heart phantom, previously printed in PLA by PRUSA 3D printer.

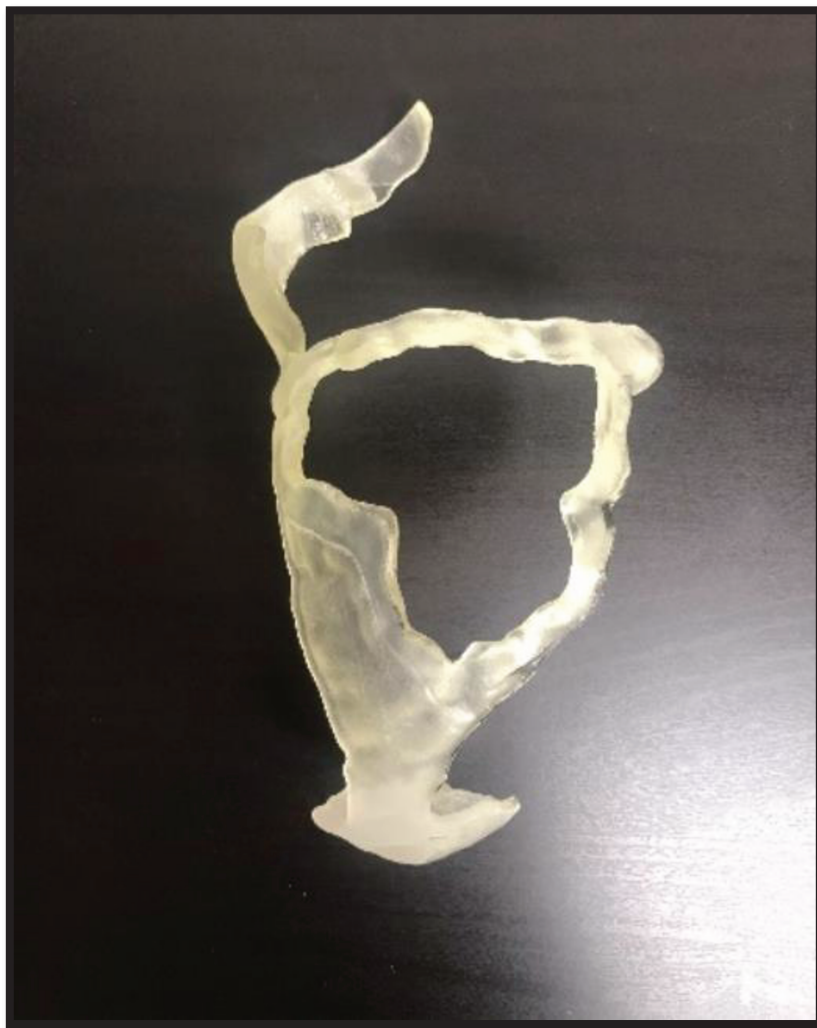


Figure 36. The first prototype of surgical guide for treatment of ischemic scar printed in MED625FLX by Stratasys Objet260 Connex1.



Figure 37. Surgical mask fitting simulation on the heart phantom, previously printed in PLA by PRUSA 3D printer.

6.2. The Second Physical Prototype

After the engineering meticulous design analysis, the surgical guide is undergone to the surgeon judgment. According to his needs, the mask design is approved in terms of geometry, weight, and flexibility, conferred by the polymeric material (MED625FLX), with a thickness of 3 mm. Instead, whereas the cardiac tissue soft and the beating heart during surgery, the surgeon believes that the stability is not completely guaranteed, thus, link adding may make the system more stable.

Furthermore, because the ablation procedure using for the scar treatment is harmful for vessels, the surgeon expressed the need to have an additional information, regarding the coronary arteries identification, which are usually hidden by fat tissue, in order to operate the pathologic area, reducing the risk of damaging.

Consequently, following both surgeon feedback and engineering evaluation analysis, the second physical prototype is developed and realized. The major change of second prototype is represented by a more complex structure, due to links, realizing a more stable system. Moreover, the target zone to ablate is designed larger than 10 mm to include both scar and arrhythmogenic tissue, according to clinical considerations. Instead, surgical guide thickness has remained unchanged as well as the shape of reference points and their interconnections. In addition, thanks to the new links, like the link of the close artery to the scar, the problem of fluctuant apex is solved, not being a critical point anymore. Three views of the second virtual prototype, three views of the second physical prototype, and three views of physical prototype applied on heart phantom are shown in the following figures (Figure 38, 39 and 40, respectively).

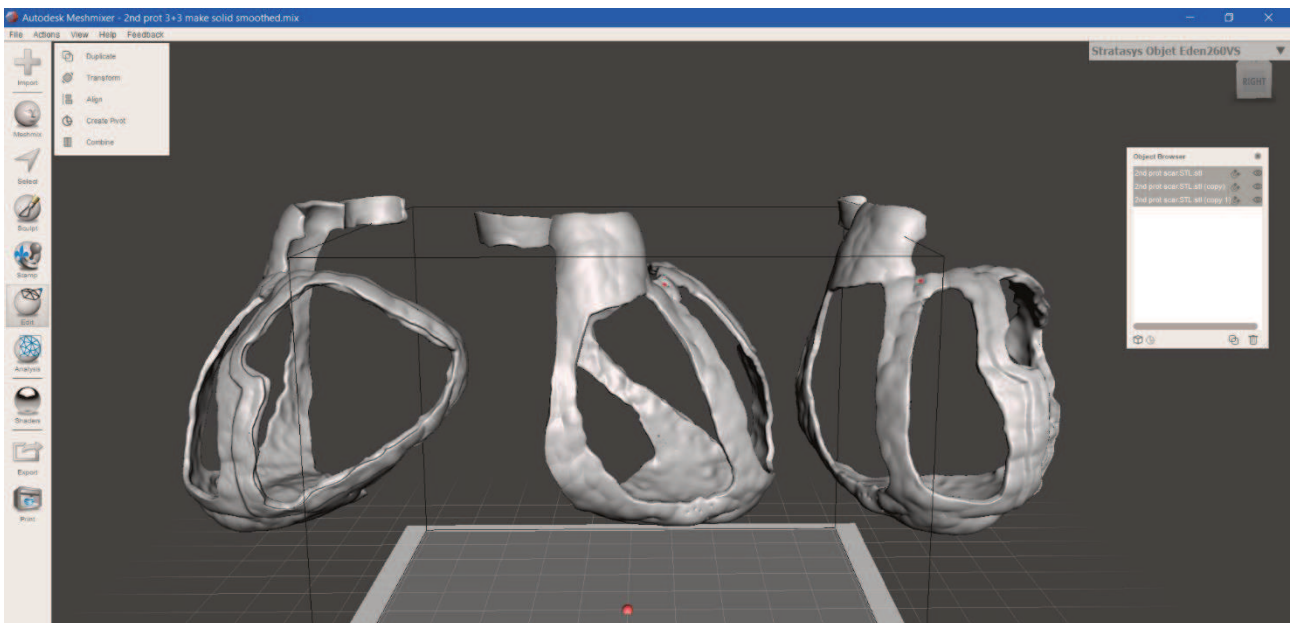


Figure 38. Three views of the 2nd virtual prototype of surgical guide for ischemic scar treatment.

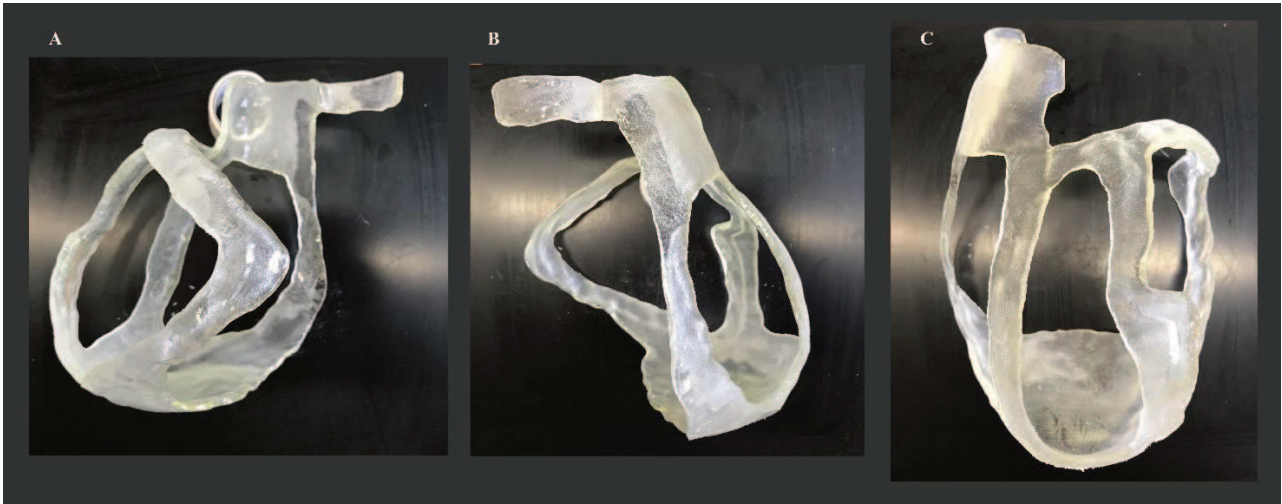


Figure 39. Three views of the 2nd physical prototype of virtual surgical guide for ischemic scar treatment.

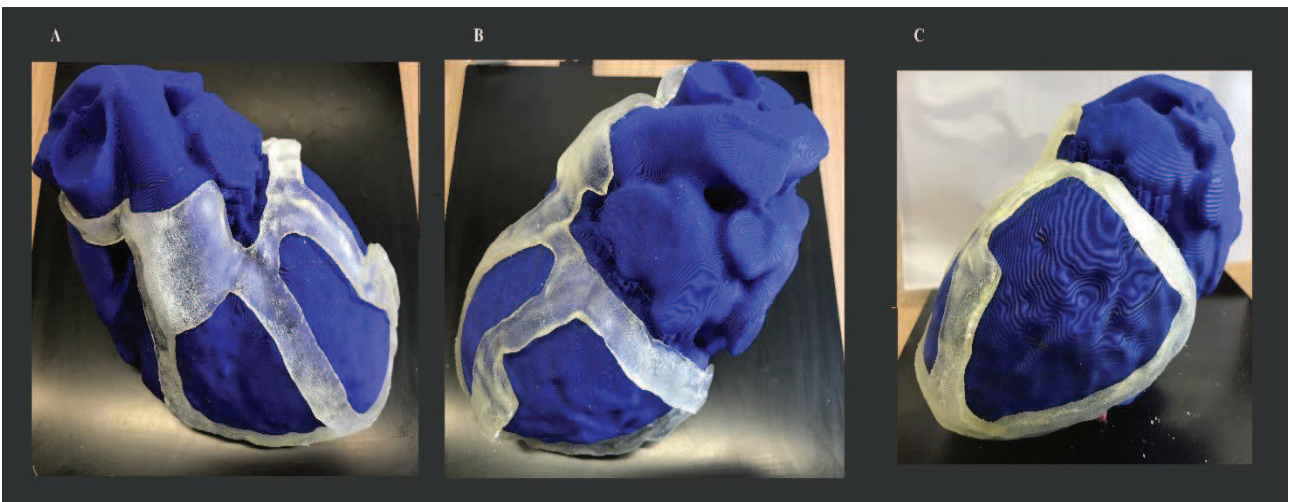


Figure 40. The 2nd physical prototype of surgical mask fitting simulation on the heart phantom, previously printed in PLA by PRUSA 3D printer.

6.3. Comparative Analysis between the first and the second prototype

In this paragraph a comparative analysis between first and second prototype is made, to evaluate whether the second prototype represents an effective improvement of the first one. For a better evaluation, an already done for the Decision Matrix in the paragraph X, at each medical and engineering requirement is assigned a weighting factor (from 0 to 1.0), that defines its importance ratings, and a rating factor (from 0 to 10), to appreciate the quality achieved by the surgical guide

realizing. The final score is generated by a sum among contributions, obtained by multiplying the weighting factor and the rating factor. The final score confirms the superiority of second prototype (9.01 score) with respect to the first prototype (8.77). In the table X are reported the medical and engineering requirements, which surgical guide is asked to perform and related Weighting Factor. The third and fourth column serves to appreciate the quality achieved by 1st and 2nd prototype, respectively, and the last column are collected all notes.

Table 7. Comparative analysis between the first and the second prototype. The final score confirms the superiority of the second with respect to the first one. In the last column come notes are reported.

<i>Requirements</i>	Weighting Factor	1st	2nd	Notes
		Rating Factor	Rating Factor	
<i>Target Area Visualization</i>	0.11	9	10	Specific-patient dependent
<i>Reference points</i>	0.11	9	10	Aorta, Pulmonary Artery and Apex are essential
<i>Size of device</i>	0.02	6	5	Specific-patient heart dimensions dependent
<i>Weight of device</i>	0.04	8	8	Specific-patient heart dimensions dependent
<i>Thickness</i>	0.05	8	8	-
<i>Shore hardness</i>	0.04	8	8	-
<i>Elongation at break</i>	0.08	9	9	It is suggested to carefully handle the surgical mask.
<i>Temperature Resistant</i>	0.10	7	7	Thermal tests are needed
<i>Harmless</i>	0.11	10	10	To be confirmed by thermal tests
<i>3D printable</i>	0.11	10	10	Stratasys Objet260, or 3D printer compatible.

<i>Washable & Sterilizable</i>	0.11	10	10	Hospital availability
<i>Electrically safe</i>	0.08	7	7	User and patient safety
<i>Lifetime</i>	0.01	8	8	Single use
<i>Manufacturing time</i>	0.02	9	8	Specific-patient heart dimensions dependent
<i>Manufacturing cost</i>	0.01	9	8	Specific-patient heart dimensions dependent
		8.77	9.01	

7. Experimental Validation Tests

The MED625FLX is recently available in the market, and because Stratasys has provided a narrow material data sheet, additional mechanical and thermal tests are performed to demonstrate the product functionality and feasibility. For this purpose, the geometry and thermal tests are conducted on the first physical prototype. The geometry test is performed to evaluate material geometry of Cardiac Surgical Guide for ischemic scar treatment before and after the Vaporized Hydrogen Peroxide (VHP) Sterilization to demonstrate whether the VHP sterilization affects geometric structure and mechanical properties. Instead, the Nondestructive tests are aimed to investigate whether MED625FLX do not undergone any mechanical and geometric alterations during and after the RF ablation, LRF ablation and cryoablation procedures and whether there is a change in energy propagation on the tissue underneath the MED625FLX. Finally, a simulation of LRF ablation on porcine heart is performed to evaluate whether the ablator acts within the surgical mask target area, creating the lesion which precisely follows the guide perimeter. Tolerances in the order of millimeter are considered acceptable.

7.1. Geometry Test

7.1.1. Methodology of Geometry Test of Cardiac Surgical Guide for ischemic scar treatment

This paragraph describes the procedures for the evaluation of material geometry of Cardiac Surgical Guide for ischemic scar treatment before and after the Vaporized Hydrogen Peroxide (VHP) Sterilization. The test is performed the 15th of April 2021 at Cardiology Research Department of UZ Brussel, (Health Campus Avenue du Laerbeek 101,1090 Jette, Brussels). Before the VHP sterilization, the tester was cleaned in a specific washing machine at 93°C for 1 hour and 30 minutes, and then it was placed to VHP sterilization machine (Sterrad Sterilization System of Johnson & Johnson) at 45°C for 40 minutes. The geometry test consists in applying the surgical guide on heart phantom, previously printed in PLA, and marking its geometry by grey drawings. To evaluate the shape changes before and after sterilization the marks, made before and after sterilization, are compared. For geometry evaluation the first prototype of surgical guide, printed in MED625FLX through Stratasys Objet260 Connex1, is tested.

7.1.2. Results of Geometry Test



Figure 41. Pouch packaging of the first prototype after the VHP sterilization.

Table 8. Results of geometry test: surgical guide features before (No sterilization) and after sterilization (VHP Sterilization) are reported.

Features	No Sterilization	VHP Sterilization
Material	MED625FLX	MED625FLX
Surgical Guide Thickness	3 mm	3 mm
Thickness of Target Area Border	6 mm	6 mm
Target area dimensions	65x60 mm	65x60 mm

Table 9. On the left side the picture of surgical guide is represented before VHP sterilization (No sterilization is performed yet). On the right side the picture of surgical guide after VHP sterilization. In both cases grey marker defines the surgical guide perimeter.

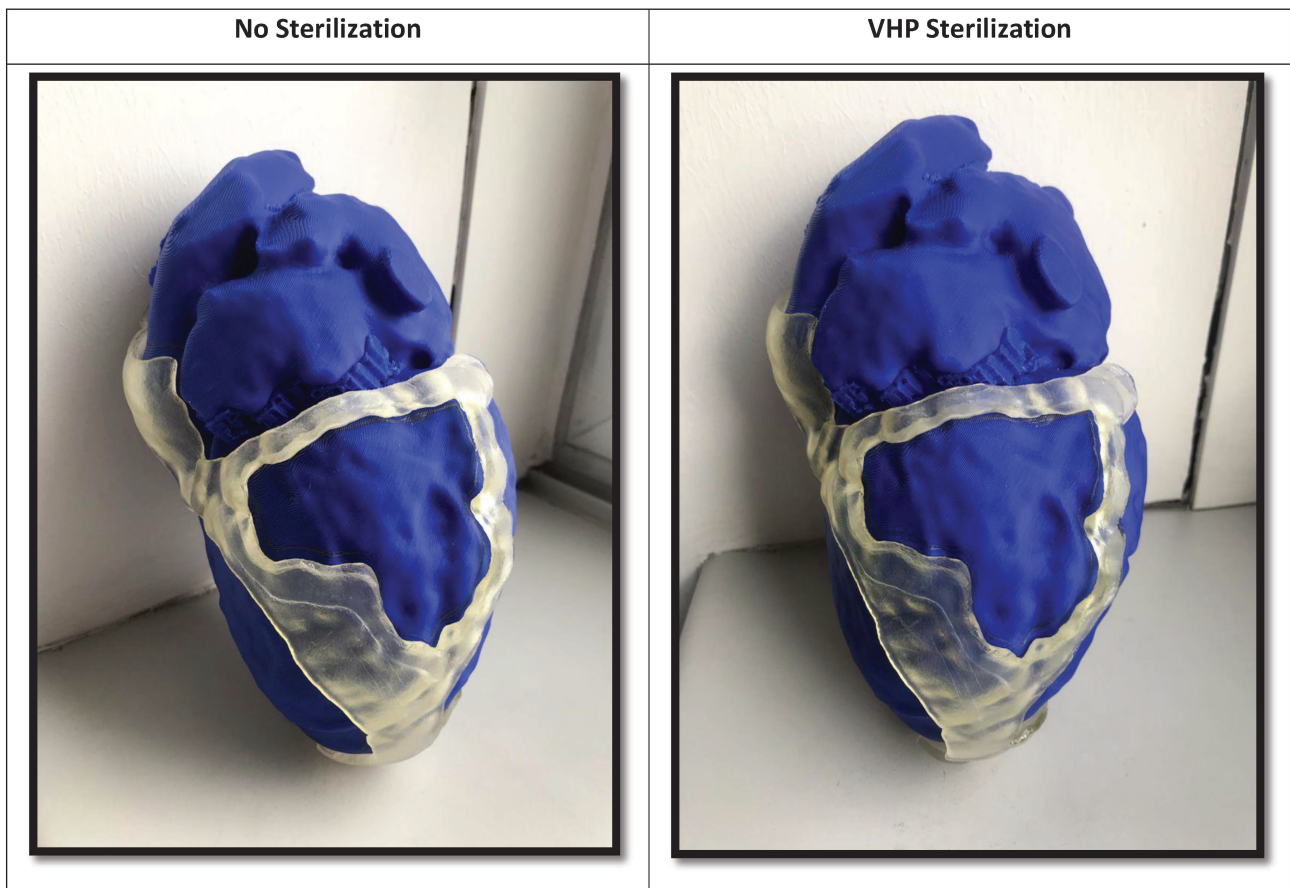


Table 10. The grey marker on the heart phantom (indicated by the white arrows), printed in PLA, defines the surgical guide perimeter before (No sterilization) and after sterilization (VHP Sterilization).

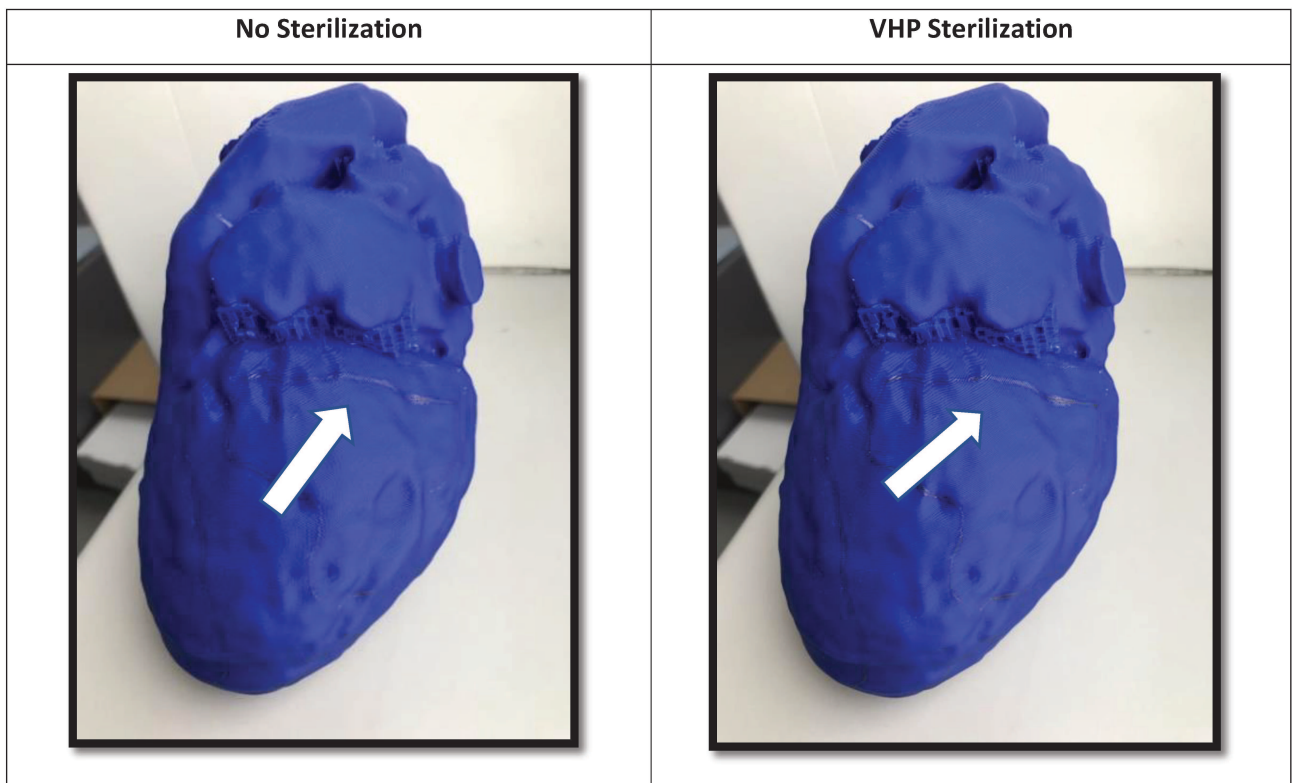
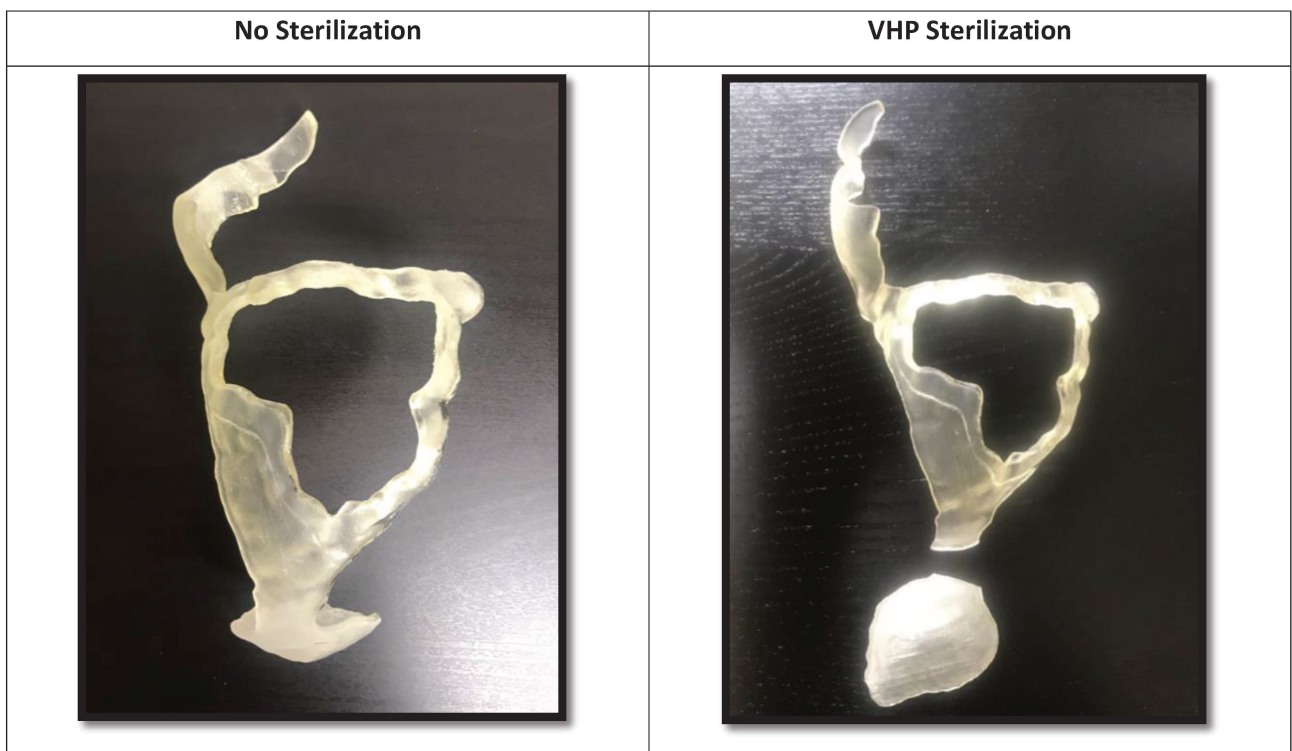


Table 11. surgical guide is shown before (No sterilization) and after sterilization (VHP Sterilization). After sterilization technique the bottom part of surgical guide has reported a rupture in correspondence to critical point.



7.2. Nondestructive Tests: Thermal and Contact Safe evaluation in Wet Lab

7.2.1. Methodology of Nondestructive Tests

The purpose of this methodology is to facilitate the management and standardize the execution of the tests as part of the additive manufacturing (AM) Scar-VT project. The first part is a description of each of the components needed to carry out the test. The second part is a description of simple procedures for each measurement necessary for the projects. For the methodology the following elements were needed:

- Voltcraft thermometer PL-125-T4 with 4 thermocouples type K
- CJ101 Digital Probe Thermometer
- Meat samples of h=10 mm
- N. 1 Porcine Heart
- Plexiglass box
- AM prototype

Table 12. AM scar-VT features.

Prototype	Material	Units	Thickness
AM scar-VT	MED625FLX	1	3 mm + 3 mm

- Samples (test coupon) in the Figure 42:

Table 13. Material samples features.

Half circular sector samples

Material	Units	Thickness
MED625FLX	3	1 mm
MED625FLX	3	2.5 mm
MED625FLX	3	3 mm + 3 mm
	Tot. 9	



Figure 42. Half circular sector samples of 1 mm, 2.5 mm and 3 mm+ 3 mm of thickness.

- Catheter ablators:

Table 14. Ablators' settings.

Ablation catheter	Units	Power (W)	Temperature (°C)	Time (s)
<i>Linear Radiofrequency ablator</i>	1	70	+70	30
<i>Radiofrequency ablator 4 mm</i>	1	50	+70	15
<i>Cryoablator</i>	1	-	-70	120

➤ **Phase 1: Materials validation and temperature measurement**

The aim of the Phase 1 test is to investigate whether MED625FLX do not undergone any mechanical and geometric alterations during and after the RF, LRF and cryoablation procedures and whether there is a change in energy propagation on the tissue underneath the sample, depending on sample thickness. For this test phase 1 are used a Plexiglas box, meat samples, digital probe thermometer, thermocouple thermometer, ablators, water heater.

The phase 1 is divided into 3 steps:

1. *Preparation*, which consists in:
 1. Take a Plexiglas box and fill it with water, heated at +34°C, through the water heater.
 2. Place the meat sample inside the Plexiglas box.
 3. Place a digital probe thermometer on the meat sample.
 4. Wait until the meat sample reaches the temperature of $T \sim +29^{\circ}\text{C}$.
2. *Control-Procedure (Meat temperature measurement without material sample)*

1. Place the material sample to be tested, on the meat sample.
2. Define the Ablation Point (AP), represented by the black dots and black rectangle in the Figure 1.
3. Mark the highlighted points (D_1 and D_2) across the material sample, as described in the following table and figure (Table 15 and Figure 43):

Table 15. The table describes the distances (D_1 and D_2) from the source, depending on the ablation procedures.

Ablation procedure	Cryo	RF	LRF
1 st distance from source (D_1)	1 mm	1 mm	1 mm
2 nd distance from source (D_2)	11 mm	11 mm	11 mm

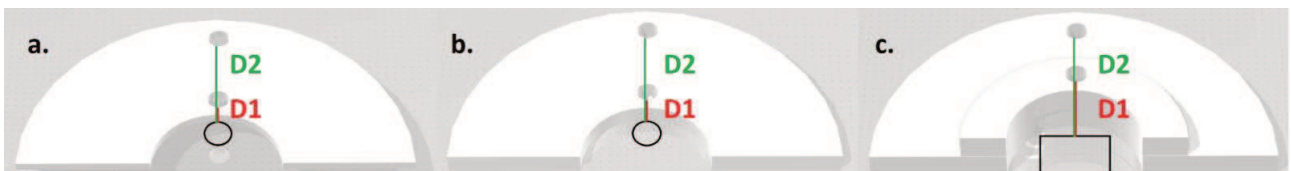


Figure 43. The figure represents the material samples to be tested with different thickness: a. 1 mm, b. 2.5 mm, c. 3 mm + 3 mm. D_1 and D_2 are the distances from the sources. The black circles represent the cryoablator and the RF ablator, while the rectangle represents the linear RF ablator.

4. Remove the material sample.
 5. Place the 2 K-type probes of thermocouple thermometer in the previously marked points and turn on the thermocouple thermometer.
 6. Turn on the catheter ablator and Set the ablator according to the information in the table "Ablators settings" (Table 1).
 7. Place the ablator in the AP, perform the ablation and measure the temperature of meat sample at 0, 10, 15 and 30 seconds after the ablation.
 8. Repeat all steps of "Control-Procedure" for each ablator.
3. Procedure (Temperature measurement of meat sample under the material sample)
1. Take the material sample to be tested.
 2. Manually clamp it on the meat sample.

3. Place the 2 K-type probes of thermocouple thermometer in the specific holes created on the material sample, as shown in the following figure (Figure 44).
4. Define AP and AP_{contact}, represented in the Figure 44 by the black dots and black rectangle, and by the blue dots and blue rectangle, respectively.
5. The ablation procedure is performed 4 times:
 - 5.1. Perform the ablation in AP and measure the temperature of the underlying meat sample 0, 10, 15 and 30 seconds after the ablation.
 - 5.2. Repeat the step 5.1. in a different AP, but at the same conditions defined in the Table 16 and Figure 44.
 - 5.3. Perform the ablation in AP_{contact} and measure the temperature of the underlying meat sample 0, 10, 15 and 30 seconds after the ablation.
 - 5.4. Repeat the step 5.3. in a different AP_{contact}, but at the same conditions defined in the Table 3 and Figure 2.
6. Repeat all steps of “Procedure” for each MED625FLX material sample with each ablator.

Table 16. The table describes the distances (D1 and D2) from the Ablation Point (AP) when the procedure is performed not in contact with the material sample, and from the Ablation Point contact (AP_{contact}), when the procedure is performed in contact with the material sample.

Ablation procedure		Cryo	RF	LRF
1st distance from source (AP)	D ₁	1 mm	1 mm	1 mm
2nd distance from source (AP)	D ₂	11 mm	11 mm	11 mm
Ablation procedure		Cryo	RF	LRF
1st distance from source (AP_{contact})	D ₁	0 mm	0 mm	0 mm
2nd distance from source (AP_{contact})	D ₂	10 mm	10 mm	10 mm

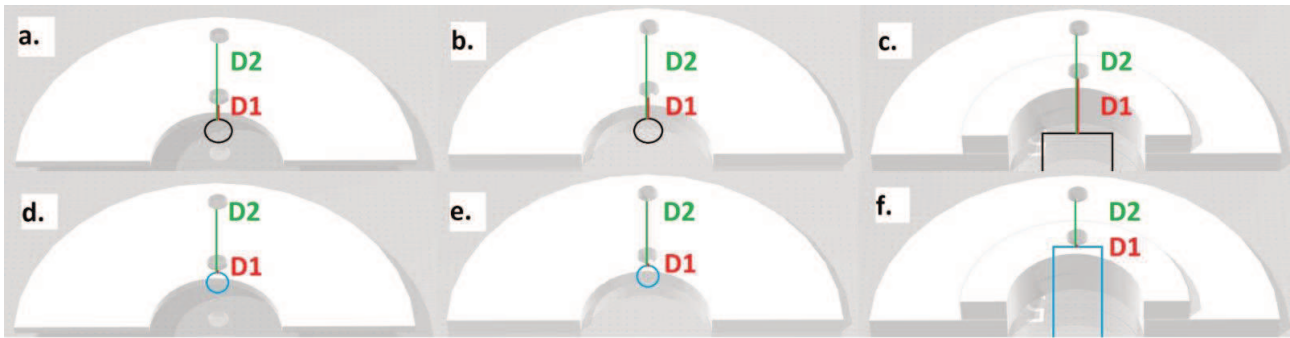


Figure 44. The figure represents the material samples to be tested with different thickness: a. and d. 1 mm, b. and e. 2.5 mm, c. and f. 3 mm + 3 mm. D1 and D2 are the distances from the sources. The black dots represent the cryoablator and the RF ablator, while the black rectangle represents the linear RF ablator, during the ablation performance not in contact with the material samples (a., b., and c.). The blue dots represent the cryoablator and the RF ablator, while the blue rectangle represents the linear RF ablator, during the ablation performance in contact with the material samples.

➤ Phase 2: Measurements of AM Scar-VT prototype

The aim of the Phase 2 test is to simulate real Linear Radiofrequency ablation using AM Scar prototype (the first prototype) directly on porcine heart. For this phase, a Linear Radiofrequency Ablator, a Plexiglas box, a porcine heart, and water heater, are needed. The phase 2 is divided into 2 steps:

1. Preparation

1. Take a Plexiglas box and fill it with water heated at +34°C, through the water heater.
2. Place the porcine heart inside the Plexiglas box.
3. Wait until the porcine heart reaches the temperature of +34°C.
4. Turn on and set the Linear Radiofrequency Ablator according to the table "Ablator settings" (Table 14).

2. Procedure

1. Place the prototype over the porcine heart.
2. Manually maintain the prototype in place.
3. Perform the Linear Radiofrequency Ablation within the selected area (in purple) as shown in the Figure 45.

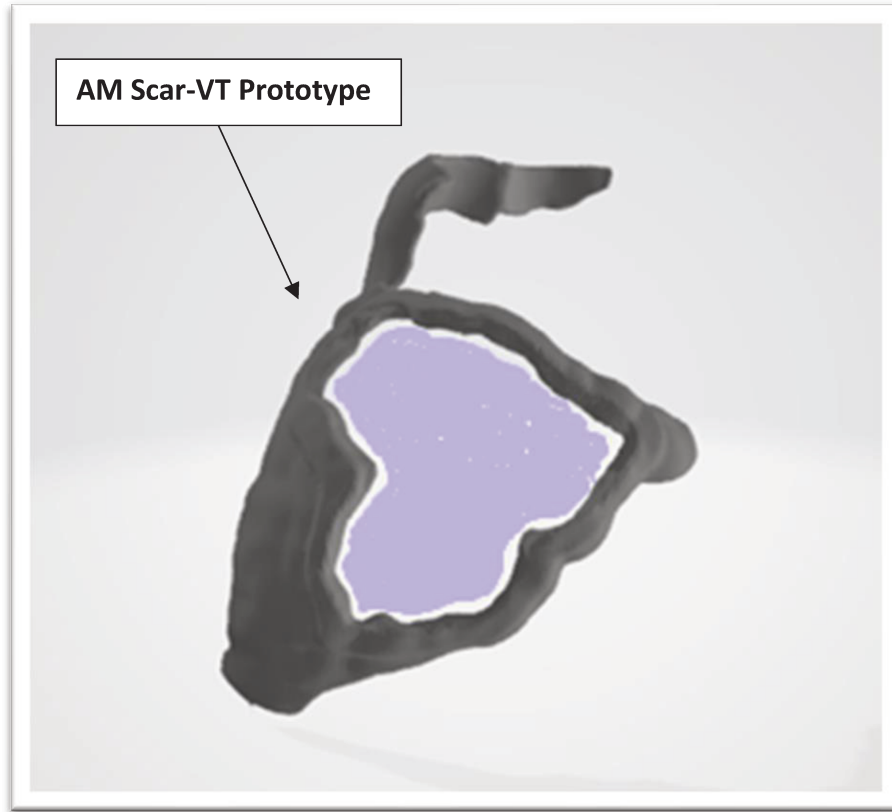


Figure 45. The AM Scar-VT Prototype. The area to be ablated is in purple.

7.2.2. Results of Nondestructive Tests

The results of the first phase of Nondestructive Tests are reported in Appendix A, by distinguishing the response of MED625FLX to three different procedures: Radiofrequency ablation, Linear Radiofrequency ablation and Cryoablation. For all ablations 3mm+3mm, 2.5 mm and 1 mm of MED625FLX samples are tested. T_1 (at D_1) and T_2 (at D_2) are the temperatures of underlying tissue measured at different distances from the source at 0 s, 10 s, at 15 s, 30 s and 60 s after ablation. The control refers to temperatures' measurement of meat sample without material sample. Each star (*) identifies the number of ablations performed. For the first two stars (* and **) the ablations are performed not in contact with material sample, while for the last stars (***) and ****) the ablations are performed in contact with material sample.

The T_1 and T_2 Results, related to RF ablation, are reported in the Table 17, results related to Cryoablation are reported in Table 18, T_1 and T_2 in response to LRF are reported in the Table 19.

Furthermore, the Appendix A contains the temperature graphs, highlighting T_1 and T_2 behaviors and comparing values among different thickness of MED625FLX when undergone to ablations. Also, in the Appendix A, through the figures of MED625FLX samples, it is possible to appreciate not macroscopically evident changes after procedures (Appendix A, Figure 50, 51 and 52).

The graphs, shown in the figures 53, 54, and 55 in the Appendix A, describes T_1 and T_2 temperatures behaviors of tissue under MED625FLX sample with a thickness of 2.5 mm, during RF ablation, LRF and Cryoablation procedures, respectively. The blue line represents T_1 , while the orange line represents T_2 . The X-axis shows the time in seconds, while the Y-axis shows the temperature in °C.

In the Appendix A, the figures 56, 57, and 58 analyze the T_1 behavior during time, depending on sample thickness, after RF, LRF and Cryoablation procedures: the orange, the grey and the yellow lines represent T_1 of tissue underlid the MED625FLX of 3mm+3mm, 2.5mm and 1 mm, respectively, instead, the Control temperature of T_1 is shown in blue. The X-axis shows the time expressed in seconds, while the Y-axis the temperature expressed in °C. In the same manner the results of T_2 at D_2 distance from the source, are reported in the figures 59, 60, and 61 of Appendix A, highlighting how the different thicknesses of MED625FLX effect the temperature of underlying tissue, according to the ablation procedures (RF, LRF and cryoablation), with respect to the control.

Instead, the results of phase 2 are shown in the figures below, representing:

- Placement of surgical guide on porcine heart (Figure 46)
- Application of LRF ablation on target area for the ischemic scar treatment (Figure 47)
- Visualization of cardiac treated area with surgical guide (Figure 48)
- Visualization of cardiac treated area without surgical guide (Figure 49)

It is interesting to notice how the ablator creates the lesion, following the surgical guide perimeter: it is particularly visible by comparing the grey scar in the figures 48 and 49.

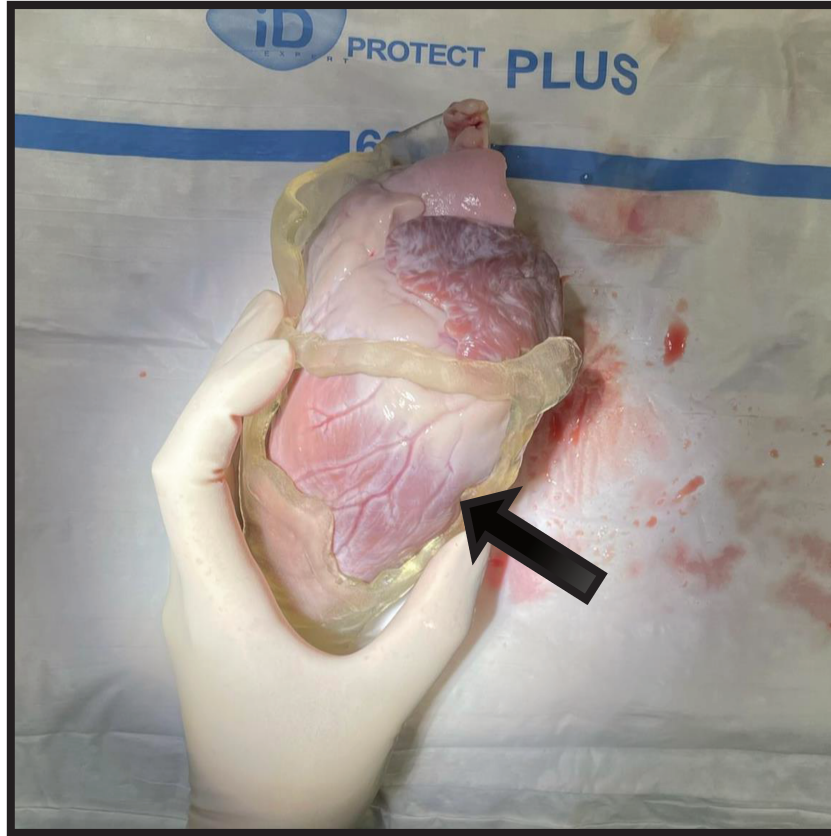


Figure 46. Application of first prototype of surgical guide on the porcine heart for the LRF treatment. The black arrow indicates the area to treat.

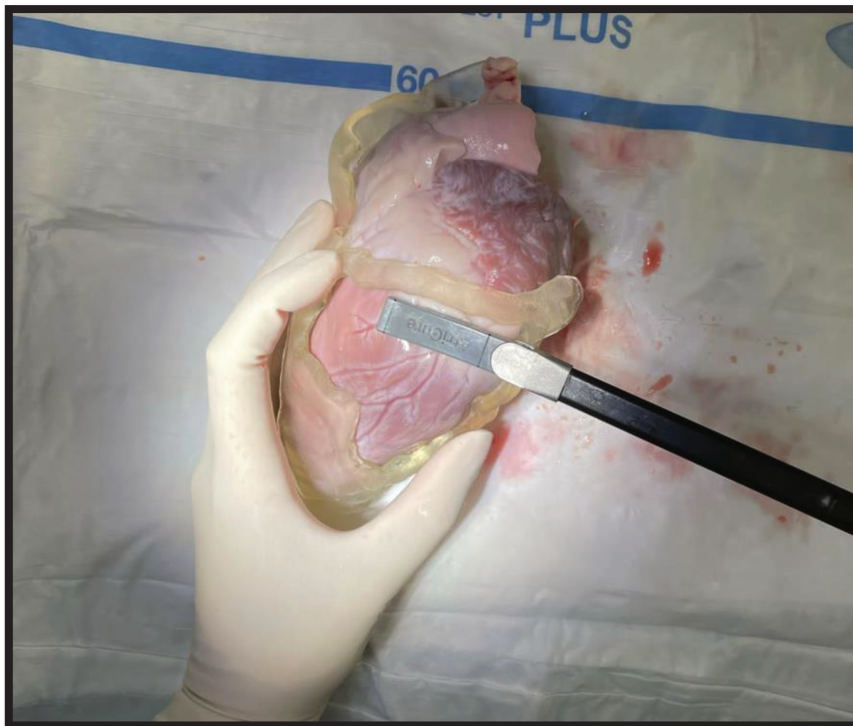


Figure 47. LRF ablation procedure on porcine heart with the first prototype of surgical guide.

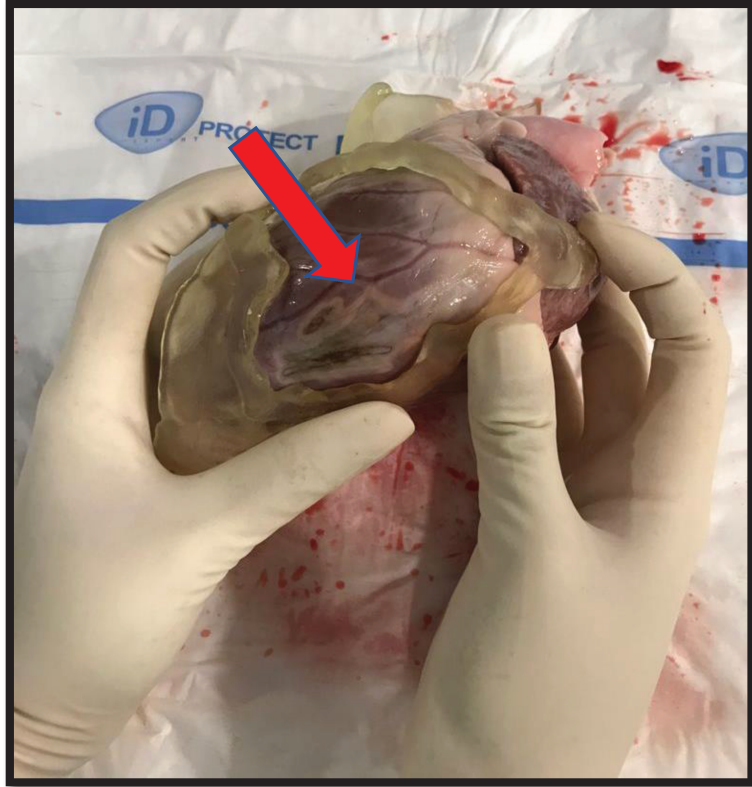


Figure 48. Porcine heart after the LRF procedure with mask. The red arrow shows the effect of ablation.

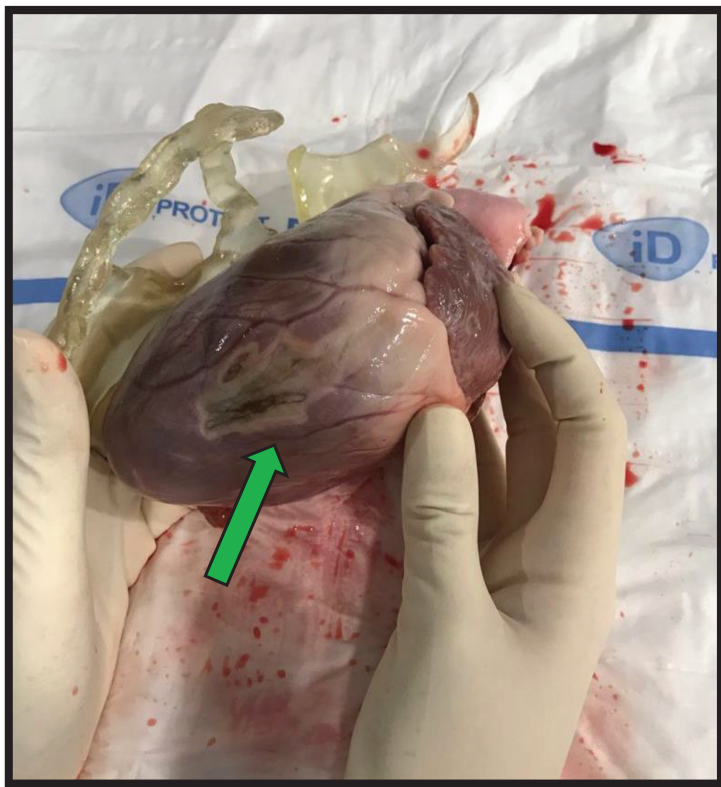


Figure 49. Porcine heart after the LRF ablation. The green arrow indicates the grey lesion created by the LRF ablator.

8. Discussion

The concept of specific-patient surgical guide, for personalized ischemic scar-related VT treatment in patients post-myocardial infarction, derived from the need to have a precise visualization of pathological area to make sure to assess the necrotic extent of ablation lesions, because an incomplete ablation of arrhythmogenic substrate causes subsequent recovery of tissue with restoration of conduction and recurrent arrhythmias like ventricular tachycardia (VT), which represent a common cause of morbidity and mortality. As a rapid developments of 3D reconstruction as surgical guide in orthopedic surgery, the purpose of this project is to apply the additive manufacturing technique in cardiac surgery, in order to reduce the medical procedure timing, improving the treatment result.

Starting from the state of art, and according to the medical and engineering requirements and the function performing in base of the medical procedure associated, the design of surgical guide has been developed. The process of surgical mask development starts from the medical imaging data acquisition from Computed Tomography (CT) and Cardiac Magnetic Resonance (CMR) and, using post-processing software, such as 3D Slicer and Meshmixer software, the region of interest undergoes segmentation, modelling and conversion into a STL file format, which the 3D printer can interpret, transforming the virtual prototype into physical prototype. Currently, different printing technologies are used to create the models, which may be made of a number of different materials that possess different mechanical and chemical properties, and the choose of material, according to the 3D printer availability, is strictly dependent to the surgical guide task.

After an accurate engineering evaluation, according to action that the product is meant to perform, among all printable materials compatible with Stratasys Objet260 Connex1, the one that reflects most mechanical and thermal properties, as well as biocompatibility and sterilizability features is the MED625FLX. However, because of its recent availability in the market, Stratasys has provided a narrow material data sheet, therefore, additional mechanical and thermal tests are performed to demonstrate the product functionality and feasibility.

For this purpose, the geometry and thermal tests are conducted on the first physical prototype. The geometry test is performed to evaluate material geometry of Cardiac Surgical Guide for ischemic scar treatment before and after the Vaporized Hydrogen Peroxide (VHP) Sterilization. Through the

geometry test it is possible to demonstrate that the VHP sterilization does not affect either geometric structure (about a millimeter) and mechanical properties: in fact, the grey markers, obtained after VHP sterilization, perfectly matches to the previous one and not evident changes are reported (Table 9, 10). Nevertheless, even though the material color is slightly changed from white transparent before VHP to light yellow transparent after VHP, it is considered negligible.

Far from negligible is, instead, the rupture in correspondence with the critical point represented by the link between target zone and heart apex, in the bottom part of surgical guide, after cleaning, during VHP sterilization and despite its uncompromised functionality, any type of damage must be absolutely avoided (Table 11).

Concerning the nondestructive test in Wet Lab, the experiment aims to investigate whether MED625FLX do not undergo any mechanical and geometric alterations during and after the radiofrequency ablation, linear radiofrequency ablation and cryoablation procedures and whether there is a change in energy propagation on the tissue underneath the MED625FLX. The first part of experiment tests different MED625FLX samples with 3 mm + 3 mm, 2.5 mm, and 1 mm of thickness.

Though the overcomes of nondestructive tests, as we expected, by comparing T1 and T2, independently of the med thickness, the temperatures are inverse proportional to the distance from the ablation source during RF and LRF (Figure 53, 54). The logically opposite happens using cryoablation (figure 55). Only the MED625FLX of 2.5mm is reported in response to each ablation procedures, because other samples have the same behavior.

Instead, focusing on underling tissue temperature at 1 mm (T1), after the RF and LRF ablation, it is possible to notice that all trials with MED625FLX samples, independently of thickness, have higher temperature with respect to the control (measures without MED625FLX); nevertheless, at 0s, that is the end of ablation, during RF the T1 reaches the highest value, and then, decreases, instead, during LRF ablation, the highest temperature is reached after 30s (figure 56, 57).

Concerning the T2, during LRF ablation and cryoablation, the temperature of underlying tissue is higher than the control, and it maintains constant (figure 59, 60).

Instead, T2 after RF ablation has different behavior, depending on the thickness: in MED625FLX 3 mm + 3 mm is higher and then decreases, the opposite occurs in other cases. It could be explained by the fact that the higher thickness of MED625FLX (3+3mm) holds more heat with respect the lower (Figure 59).

Focusing on the cryoablation, the procedure does not significantly affect the T2, even though the temperatures maintain higher with MED625FLX with respect to the control (Figure 61).

What that is important to underline is the maximum and the minimum temperatures after ablations, in fact, to ensure safe conditions, avoiding any tissue damage, the temperature must be below 40-45°C during RF and LRF and, above -40°C during cryoablation. However, these safe conditions are guaranteed in all trials, except for T1 at 0 s during RF ablation. This phenomenon suggests that the RF ablation leads to MED625FLX become warmer, which in turn heats the underlying tissue, leading to cell damaging. Thus, it would be appropriate to not be in contact with the surgical mask and maintain at least 1 mm of distance from the mask during ablation, to avoid cell death by heat.

After the ablation trials, all MED625FLX samples are placed on millimetric paper and, the comparison between samples before and after each ablation is used to verify whether the samples have undergone changes (Figure 50, 51, 52). Through the comparison it is possible to appreciate that all samples have not any visible changes. Moreover, to verify whether the underlying tissue have chemical changes, additional biological tissue analysis is needed.

Moreover, the second phase of nondestructive tests simulates LRF ablation with surgical mask on porcine heart (Figure 46, 47). Overcomes have demonstrated the surgical mask functionality: during Linear RF procedure, the ablator acts within the surgical mask target area, creating a visible grey lesion which precisely follows the guide perimeter with tolerances in the order of millimeter, considered acceptable (Figure 48, 49). Also, through the simulation on porcine heart, it is possible to appreciate the easy and rapid application, conferred by MED625FLX flexibility, but a carefully handle is recommended.

Thus, basing on results of mechanical and thermal tests already described, following the engineering evaluation analysis and surgeon feedback, a 2nd prototype is developed: weight, thickness, and flexibility, conferred by the polymeric material (MED625FLX), are maintained, instead, coronary artery identification, close to the scar, and other links are added improving the prototype in terms of provided information, reducing the risk of vessels damaging and guaranteeing a better stability, during surgery. Moreover, other important change is represented by a wider than 10 mm target zone to ablate, including the ischemic scar and the arrhythmogenic tissue, considered the predominant substrate causing the majority of ventricular tachycardias (VT) post-MI.

Instead, reference points choosing has demonstrated to be satisfying, but the 2nd prototype design is realized focusing on critical points represented by interconnections, and making stronger and more stable, as the problem of fluctuant apex is solved, not being a critical point anymore.

Finally, according to a comparative analysis described in the precedent paragraph, the 2nd prototype is proven to be improved with respect to the 1st one, in terms of stability, geometry, and coronary arteries identification (Table 7). Considering the sterilization process and the treatment procedures at which the surgical mask is undergone, the MED625FLX, previously based on the data sheet proved by Stratasys, successively supported by geometry and non-destructive tests, is a rather functional material, but presents some limitations. In fact, the MED625FLX can be subjected to cleaning and VHP sterilization without any mechanical or geometrical changes, only in case of accurate design, avoiding critical points in correspondence to the interconnections.

In conclusion, the 2nd prototype of surgical guide printed in MED625FLX is proven to be functional for the ischemic scar identification and its biocompatibility and contact safety is guaranteed during and after LRF ablation and cryoablation, but, regarding the RF, it is recommended to be not in contact with mask and maintain at least 1 mm of distance from the ablation source, otherwise the surgical mask becomes warmer, leading to temperature increasing, which damages the underlying healthy tissue.

9. Conclusion and Future Developments

The purpose of this work is to propose a surgical guide as improved solution for ischemic scar treatment, reducing the medical procedure timing, and improving the treatment result. In fact, work findings indicate that the 3D surgical guide is a reliable technology that contributes to more precise and rapid treatment of ischemic scar post MI, but a medical support for identification of target area to treat from diagnostic images is essential.

Nevertheless, as a supervised slice-by-slice segmentation through operator interaction is required, because of boundaries ambiguity due to a low contrast between target organs and the neighboring tissue, an automatic segmentation process could reduce the post-processing timing, decreasing the operator error. Anyway, the operator control and correction in the event of an inadequate result will be necessary. Moreover, considering the already described MED625FLX limitations, in terms of

thermal and mechanical properties, it could be useful to investigate other material for AM realization, focusing on temperature resistance.

In conclusion, further studies are needed to make a trustworthy evaluation of the position accuracy obtained, and further trials could demonstrate the efficiency of the patient-specific surgical mask, for the treatment of ischemic scar, concerning the surgical procedure timing, and the quality of executed treatment.

Finally, to improve the surgical guide stability during ablation procedure, it might be interesting to introduce some support systems, already used in surgery, like wall-suction system. Inevitably, the integration of this structure will involve some engineering considerations and design changes but could allow to maintain the heart in desired position.

Appendix A

Phase 1 of Nondestructive Tests: Results

- MED625FLX response to Radiofrequency Ablation Procedure

Table 17. Radiofrequency Ablation (RF) Procedure. 3mm+3mm, 2.5 mm and 1 mm of MED625FLX samples are tested. T1 and T2 are the temperatures of underlying tissue measured at different distances from the source at 0 s, 10 s, at 15 s, 30 s and 60 s after ablation. The control refers to temperatures' measurement of meat sample without material sample. Each star (*) identifies the number of ablations performed. For the first two stars (* and **) the ablations were performed not in contact with material sample, while for the last stars (***) the ablations were performed in contact with material sample.

RF	MED625FLX	D ₁	D ₂	D ₁	D ₂	D ₁	D ₂	D ₁	D ₂	D ₁	D ₂
Time		0 s	0 s	10 s	10 s	15 s	15 s	30 s	30 s	60 s	60 s
		T₁	T₂	T₁	T₂	T₁	T₂	T₁	T₂	T₁	T₂
	Control*	36.3	30.1	38.3	30.8	38.4	31.4	38.2	31.1	-	-
	Control**	35.8	31.6	37.5	33.2	37.9	33.8	38.4	34.9	-	-
	Control***	34.0	32.2	35.9	33.4	36.3	34.4	36.6	35.3	37.2	36.8
	Control****	32.6	30.5	33.6	31.1	33.8	31.1	34.5	31.4	35.2	32.7
	Mean	34.7	31.1	36.3	32.1	36.6	32.7	36.9	33.2		
Time		0 s	0 s	10 s	10 s	15 s	15 s	30 s	30 s	60 s	60 s
	3mm+3mm	T₁	T₂	T₁	T₂	T₁	T₂	T₁	T₂	T₁	T₂
	Sample N										
	7*	41.7	31.7	40.2	31.3	40.1	31.2	39.7	30.8	38.2	30.8
	7**	34.6	31.3	36.0	31.1	36.0	30.8	36.4	30.4	36.3	30.4
	7***	60.0	31.6	50.0	31.9	47.1	32.5	41.6	33.5	37.1	34.8
	7****	61.0	30.4	38.9	30.6	38.7	30.9	38.7	31.4	38.0	31.5
	Mean	49.3	31.3	41.3	31.2	40.5	31.4	39.1	31.5	37.4	31.9
Time		0 s	0 s	10 s	10 s	15 s	15 s	30 s	30 s	60 s	60 s
	2.5 mm	T₁	T₂	T₁	T₂	T₁	T₂	T₁	T₂	T₁	T₂
	Sample N										
	10*	44.5	35.3	45.6	32.1	45.0	31.6	42.3	31.1	38.9	30.8
	10**	50.6	34.4	46.0	32.5	44.3	31.7	42.1	30.8	39.3	30.7
	10***	75.2	31.8	65.4	31.9	60.0	32.0	52.9	32.3	45.2	33.0

	10****	66.0	33.1	45.5	33.3	48.8	33.2	46.2	33.1	43.0	33.2
	Mean	43.9	31.3	41.3	31.2	40.5	31.4	39.1	31.5	37.4	31.9
Time		0 s	0 s	10 s	10 s	15 s	15 s	30 s	30 s	60 s	60 s
	1 mm	T ₁	T ₂	T ₁	T ₂	T ₁	T ₂	T ₁	T ₂	T ₁	T ₂
	Sample N										
	13*	39.2	34.5	39.4	33.8	39.6	33.7	39.4	33.3	38.6	33.1
	13**	33.8	33.6	35.2	33.4	35.5	33.3	35.8	34.0	36.7	34.6
	13***	60.0	35.1	48.7	34.4	47.0	34.0	44.5	34.1	41.9	34.1
	13****	68.0	37.3	55.0	36.8	51.7	36.5	47.0	36.5	42.2	36.5
	Mean	50.3	35.1	44.6	34.6	43.5	34.4	41.7	34.5	39.9	34.6

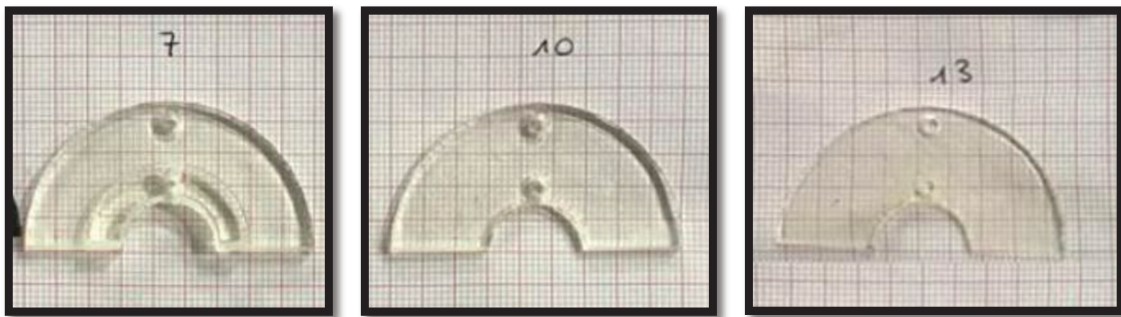


Figure 50. 3mm+3mm (sample 7), 2.5 mm (sample 10) and 1 mm (sample 13) of MED625FLX samples are tested in response to the RF ablation.

- MED625FLX response to Cryoablation Procedure

Table 18. Cryoablation Procedure. 3mm+3mm, 2.5 mm and 1 mm of MED625FLX samples are tested. T1 and T2 are the temperatures of underlying tissue measured at different distances from the source at 0 s, 10 s, at 15 s, 30 s and 60 s after ablation. The control refers to temperatures' measurement of meat sample without material sample. Each star (*) identifies the number of ablations performed. For the first two stars (* and **) the ablations were performed not in contact with material sample, while for the last stars (***) the ablations were performed in contact with material sample.

Cryoablation	MED625FLX	D₁	D₂	D₁	D₂	D₁	D₂	D₁	D₂
Time		0 s	0 s	10 s	10 s	15 s	15 s	30 s	30 s
		T ₁	T ₂	T ₁	T ₂	T ₁	T ₂	T ₁	T ₂
	Control*	14.5	23.0	14.2	22.4	12.9	22.6	11.2	22.4

	Control**	9.7	23.9	9.1	23.5	8.7	23.4	8.0	22.7
	Control***	8.0	24.4	8.5	23.9	9.1	23.7	10.8	23.3
	Control****	1.0	16.3	0.9	16.6	1.0	16.6	2.1	16.4
	Mean	8.3	21.9	8.2	21.6	7.9	21.6	8.0	21.2
Time		0 s	0 s	10 s	10 s	15 s	15 s	30 s	30 s
	3mm+3mm	T₁	T₂	T₁	T₂	T₁	T₂	T₁	T₂
	Sample N								
	9*	20.5	30.0	20.5	29.8	20.2	29.7	19.9	29.6
	9**	3.9	28.1	6.1	26.2	7.0	26.4	10.5	26.6
	9***	-6.0	25.4	-2.1	25.1	-1.2	24.9	0.1	24.1
	9****	-9.4	22.6	-2.8	22.2	-1.5	21.8	-0.5	22.0
	Mean	2.3	26.5	5.4	25.8	6.1	25.7	7.5	25.6
Time		0 s	0 s	10 s	10 s	15 s	15 s	30 s	30 s
	2.5 mm	T₁	T₂	T₁	T₂	T₁	T₂	T₁	T₂
	Sample N								
	12*	11.0	29.0	10.3	28.8	10.2	28.5	11.3	28.3
	12**	16.0	27.0	15.4	26.8	14.2	26.7	17.4	26.3
	12***	-8.7	19.3	-3.0	18.9	-2.2	18.6	-0.8	18.3
	12****	-15.8	19.4	-3.2	19.1	-1.5	18.8	-0.1	18.2
	Mean	0.6	23.7	4.9	23.4	5.2	23.2	7.0	22.8
Time		0 s	0 s	10 s	10 s	15 s	15 s	30 s	30 s
	1 mm	T₁	T₂	T₁	T₂	T₁	T₂	T₁	T₂
	Sample N								
	15*	5.9	29.0	5.7	28.5	6.1	28.4	6.9	27.2
	15**	15.4	27.3	15.2	27.2	15.2	27.0	15.3	26.8
	15***	-20.8	17.5	-4.0	16.7	-2.8	16.6	-2.2	15.8
	15****	-3.9	18.6	-1.1	18.5	-0.8	18.3	0.1	17.8
	Mean	-0.9	23.1	4.0	22.8	4.4	22.6	5.0	21.9

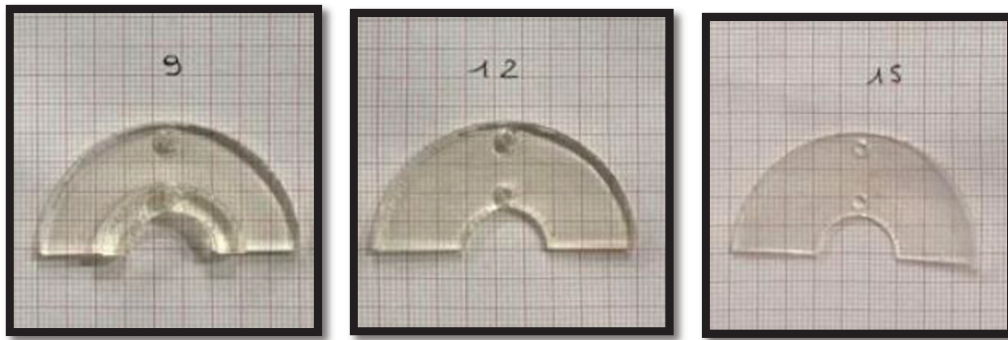


Figure 51. 3mm+3mm (sample 9), 2.5 mm (sample 12) and 1 mm (sample 15) of MED625FLX samples are tested response to the cryoablation procedure.

- MED625FLX response to Linear Radiofrequency Ablation Procedure

Table 19. Linear Radiofrequency Ablation Procedure. 3mm+3mm, 2.5 mm and 1 mm of MED625FLX samples are tested. T1 and T2 are the temperatures of underlying tissue measured at different distances from the source at 0 s, 10 s, at 15 s, 30 s and 60 s after ablation. The control refers to temperatures' measurement of meat sample without material sample. Each star (*) identifies the number of ablations performed. For the first two stars (* and **) the ablations were performed not in contact with material sample, while for the last stars (***) and ****) the ablations were performed in contact with material sample.

LRF	MED625FLX	D ₁	D ₂	D ₁	D ₂	D ₁	D ₂	D ₁	D ₂
Time		0 s	0 s	10 s	10 s	15 s	15 s	30 s	30 s
		T ₁	T ₂	T ₁	T ₂	T ₁	T ₂	T ₁	T ₂
	Control*	34.4	-	34.5	29.7	34.5	29.7	34.7	29.8
	Control**	27.9	27.0	28.2	27.0	28.2	27.1	28.7	27.2
	Control***	32.5	30.5	32.9	31.1	33.1	31.3	33.7	31.6
	Control****	30.9	30.1	31.2	30.2	31.4	30.2	31.6	30.5
	Mean	31.4	Nan	31.7	29.5	31.8	29.6	32.2	29.8
Time		0 s	0 s	10 s	10 s	15 s	15 s	30 s	30 s
	3mm+3mm	T ₁	T ₂	T ₁	T ₂	T ₁	T ₂	T ₁	T ₂
	Sample N								
	8*	30.8	32.4	30.4	31.9	31.3	31.9	31.0	30.4
	8**	33.9	31.4	34.8	31.5	35.2	31.8	35.0	31.8
	8***	37.0	31.9	39.2	31.6	38.9	31.4	40.9	31.2
	8****	37.7	29.3	39.7	30.6	39.7	30.4	40.9	30.1
	Mean	34.9	31.3	36.0	31.4	36.3	31.4	37.0	30.9

Time		0 s	0 s	10 s	10 s	15 s	15 s	30 s	30 s
	2.5 mm	T ₁	T ₂	T ₁	T ₂	T ₁	T ₂	T ₁	T ₂
	Sample N								
	11*	31.8	29.2	32.8	29.2	32.8	29.2	33.9	29.2
	11**	33.4	29.6	33.8	29.4	33.9	29.5	34.5	29.7
	11***	35.0	29.7	36.2	29.8	36.2	29.8	37.1	29.8
	11****	32.3	30.3	32.8	30.5	33.4	30.6	33.7	30.9
	Mean	33.1	29.7	33.9	29.7	34.1	29.8	34.8	29.9
Time		0 s	0 s	10 s	10 s	15 s	15 s	30 s	30 s
	1 mm	T ₁	T ₂	T ₁	T ₂	T ₁	T ₂	T ₁	T ₂
	Sample N								
	14*	33.2	32.5	33.5	32.5	33.7	32.6	34.1	32.6
	14**	32.4	32.1	33.0	32.2	33.3	32.2	33.9	32.1
	14***	37.8	32.3	40.0	32.1	39.8	32.1	38.4	32.3
	14****	33.3	31.1	33.1	31.0	33.7	31.0	34.0	31.1
	Mean	34.2	32.0	34.9	32.0	35.1	32.0	35.1	32.0

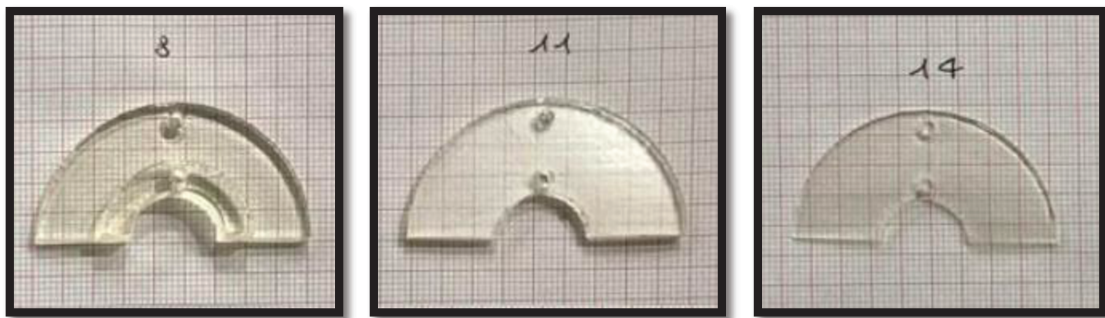


Figure 52. 3mm+3mm (sample 8), 2.5 mm (sample 11) and 1 mm (sample 14) of MED625FLX samples are tested response to the Linear Radiofrequency ablation procedure.

RF MED 2.5mm

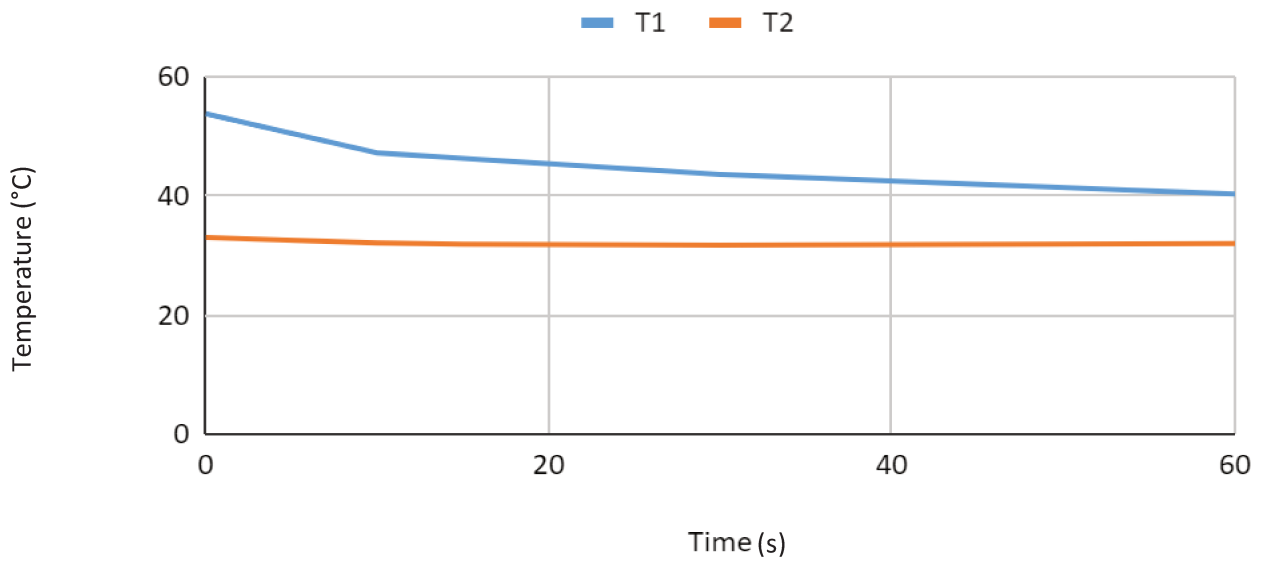


Figure 53. Radiofrequency effect on MED625FLX of 2.5 mm at 1 mm (T1) and 10 mm (T2).

LRF MED 2.5mm

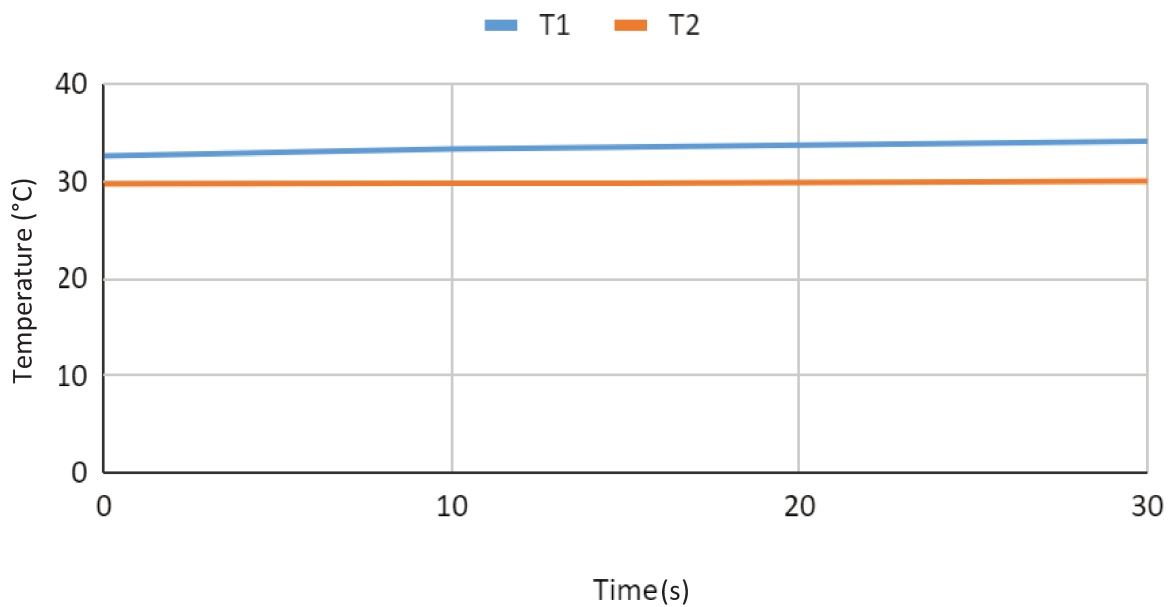


Figure 54. Linear Radiofrequency effect on MED625FLX of 2.5 mm at 1 mm (T1) and 10 mm (T2).

Cryo MED 2.5mm

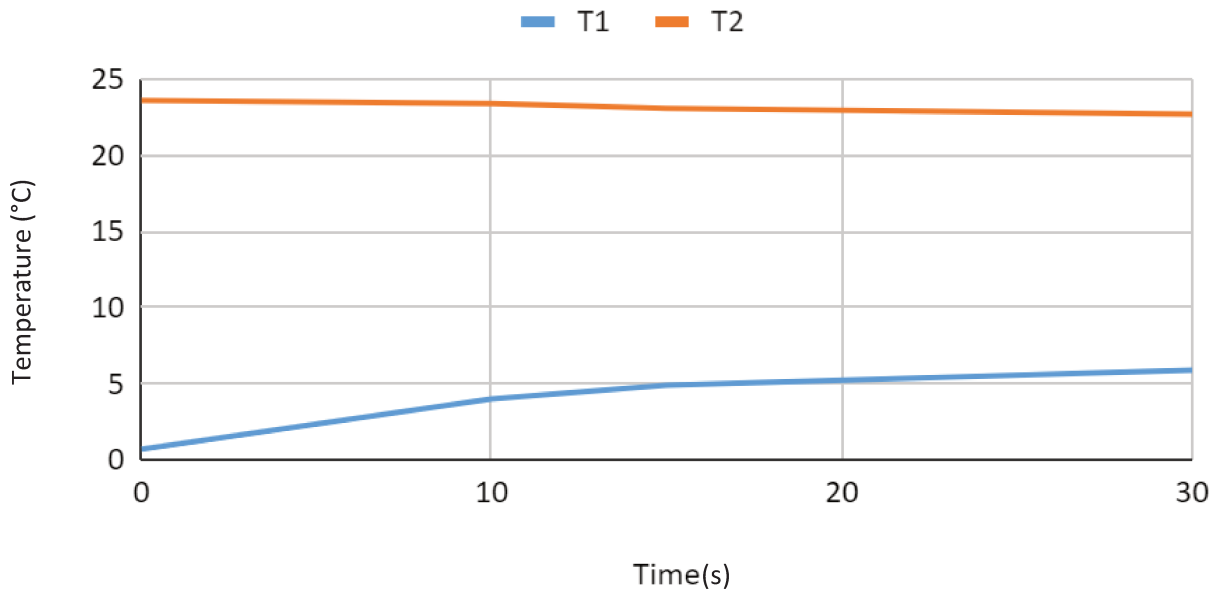


Figure 55. Cryoablation effect on MED625FLX of 2.5 mm at 1 mm (T1) and 10 mm (T2).

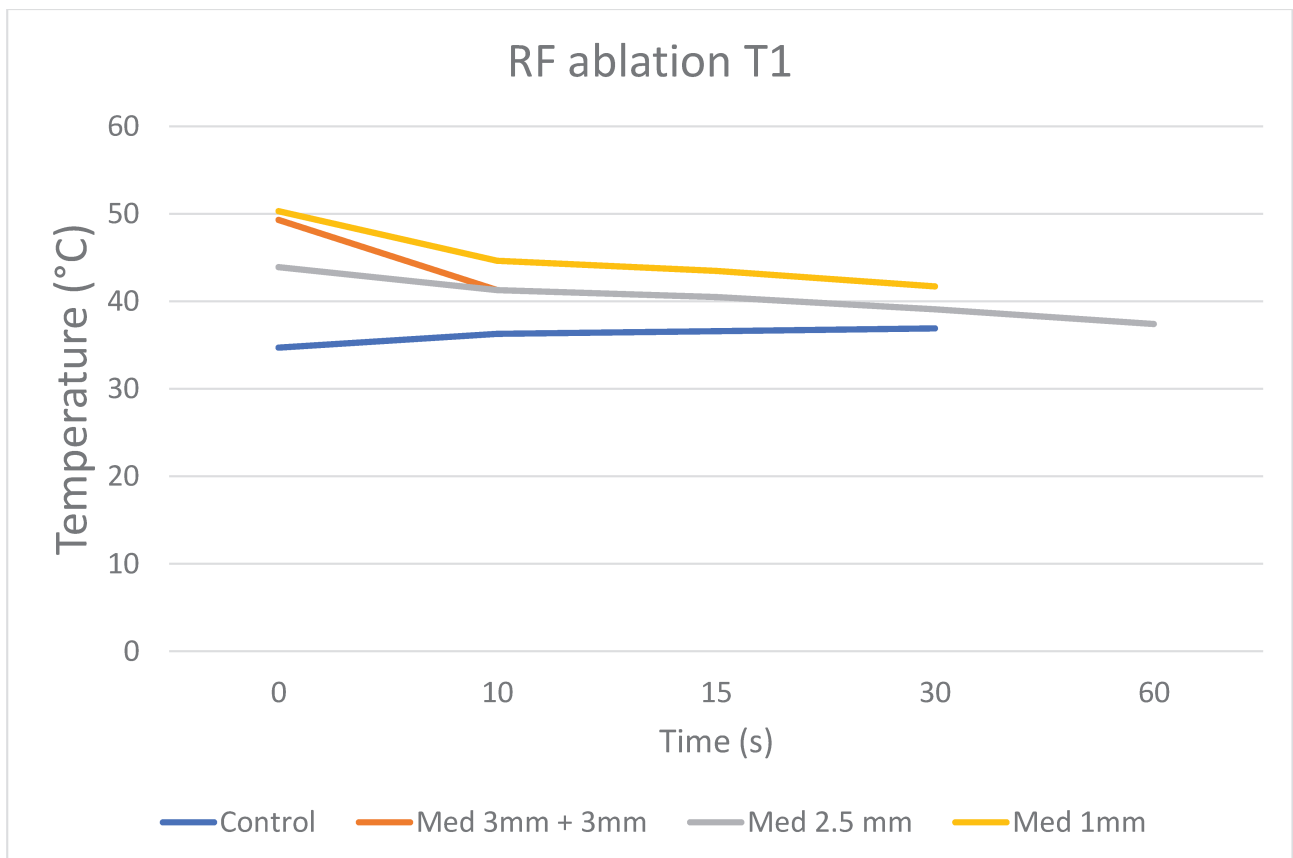


Figure 56. Radiofrequency effect at 1 mm (T1).

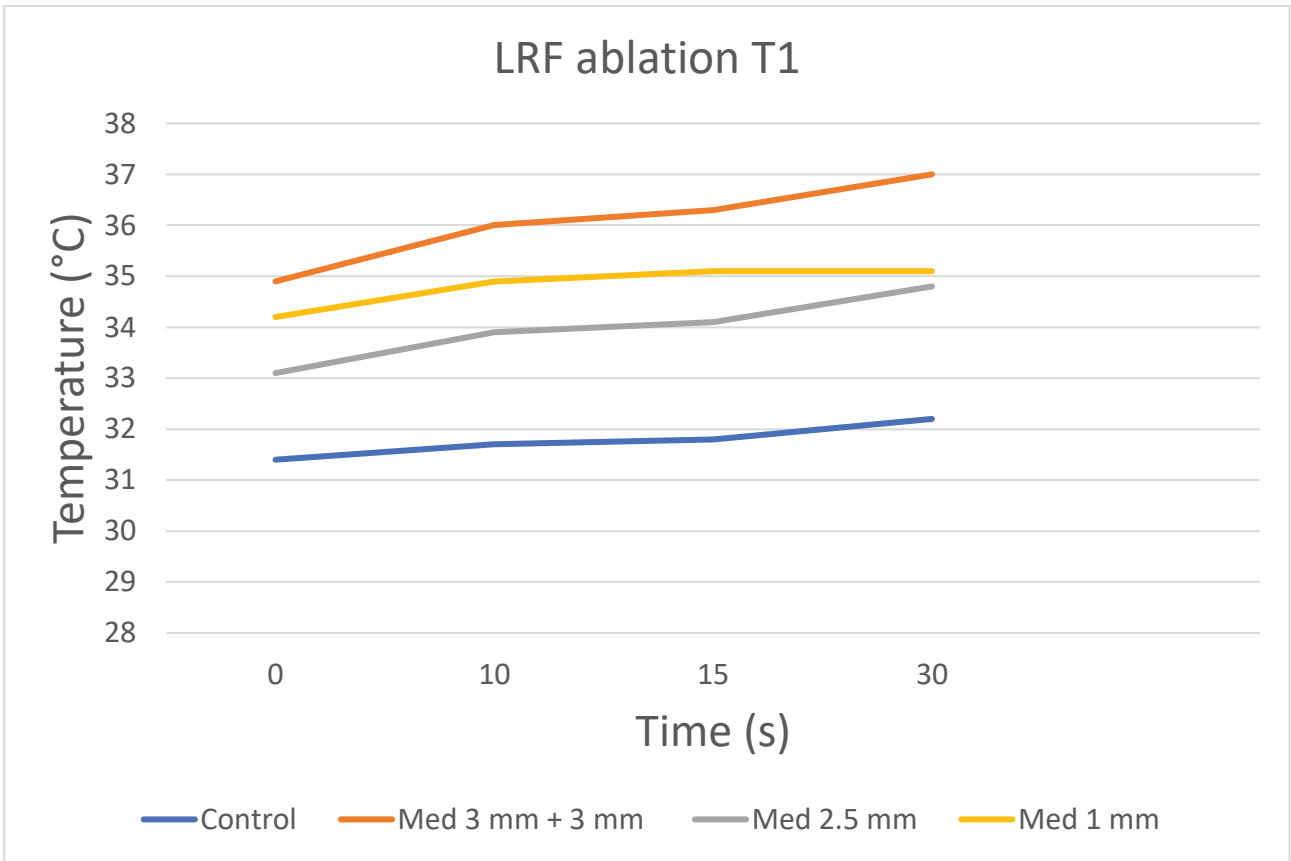


Figure 57. Linear Radiofrequency effect at 1 mm (T1).

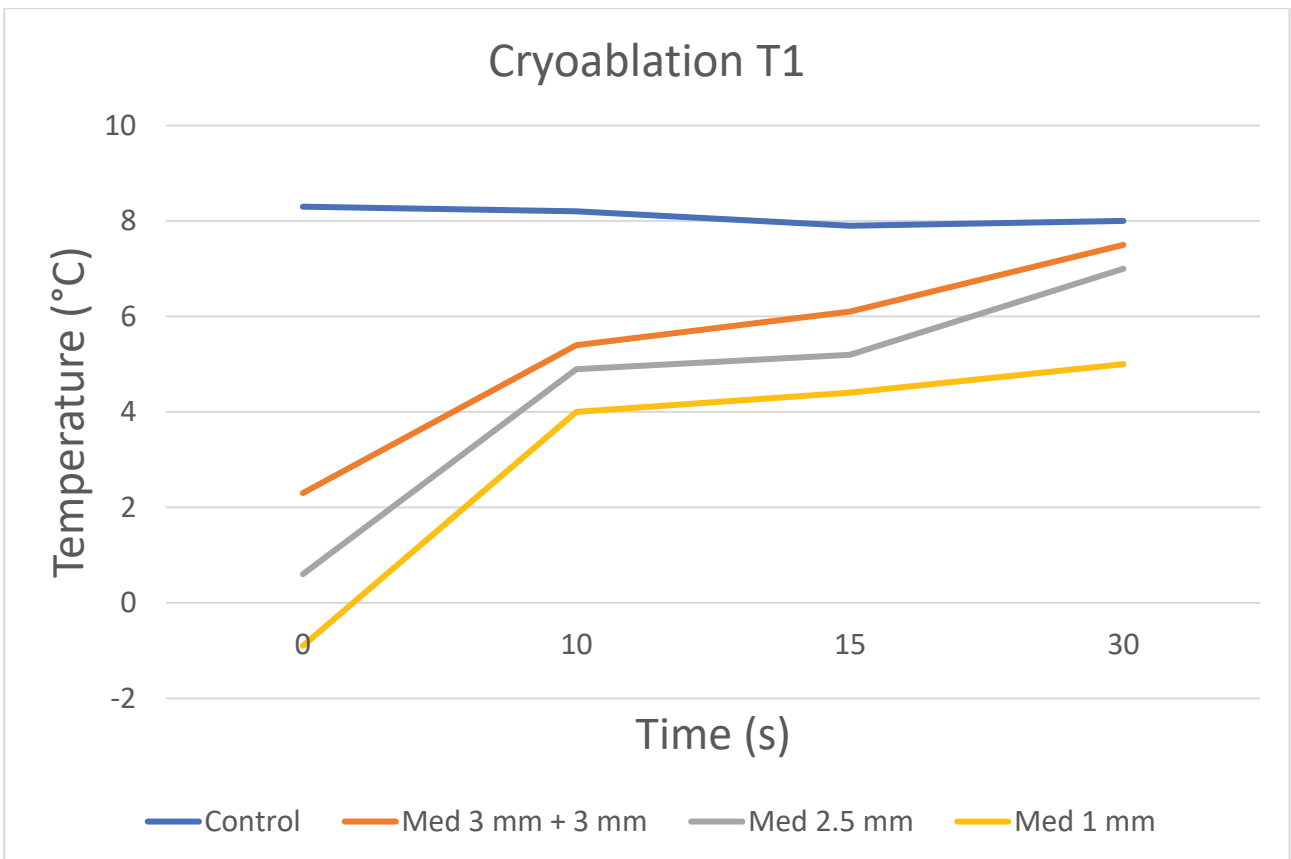


Figure 58. Cryoablation effect at 1 mm (T1).

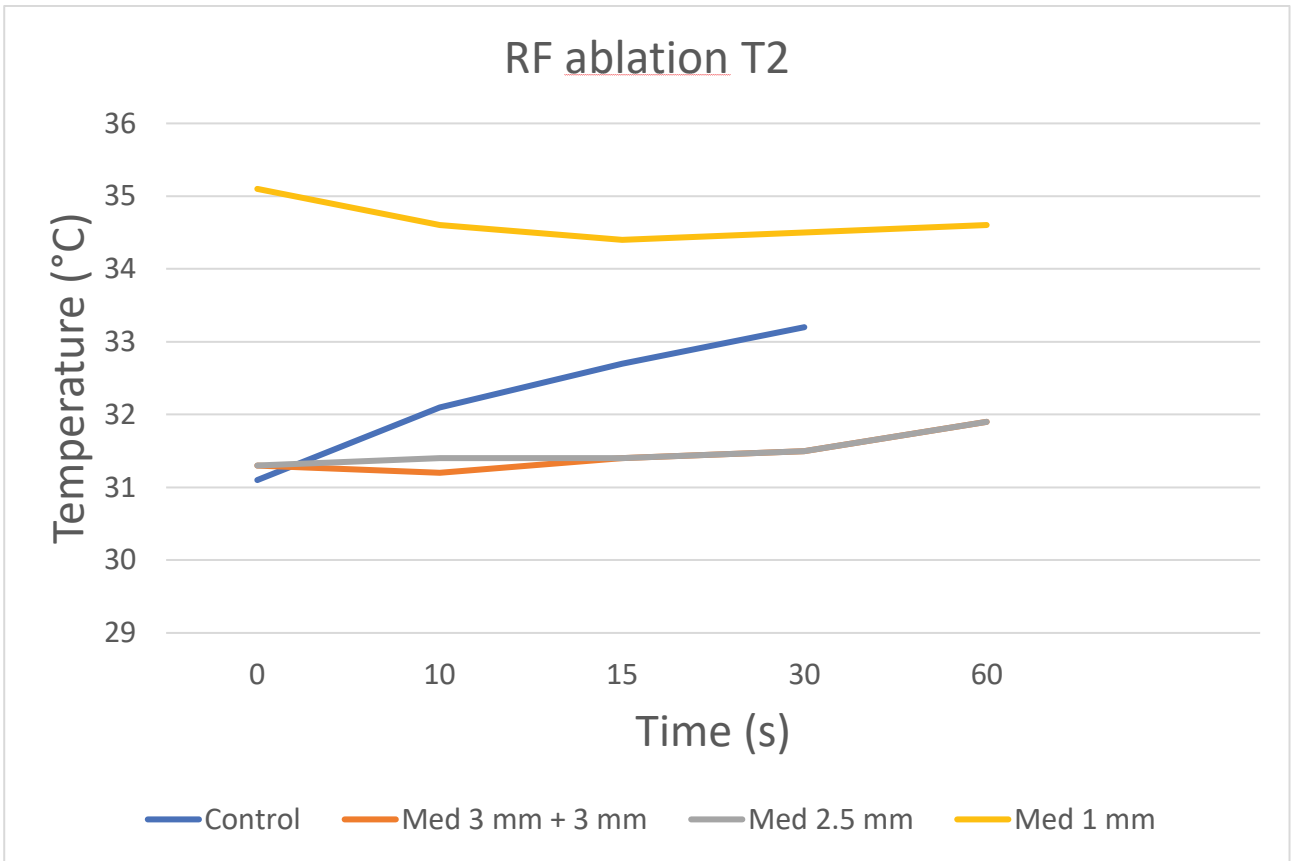


Figure 59. Radiofrequency effect at 10 mm (T2).

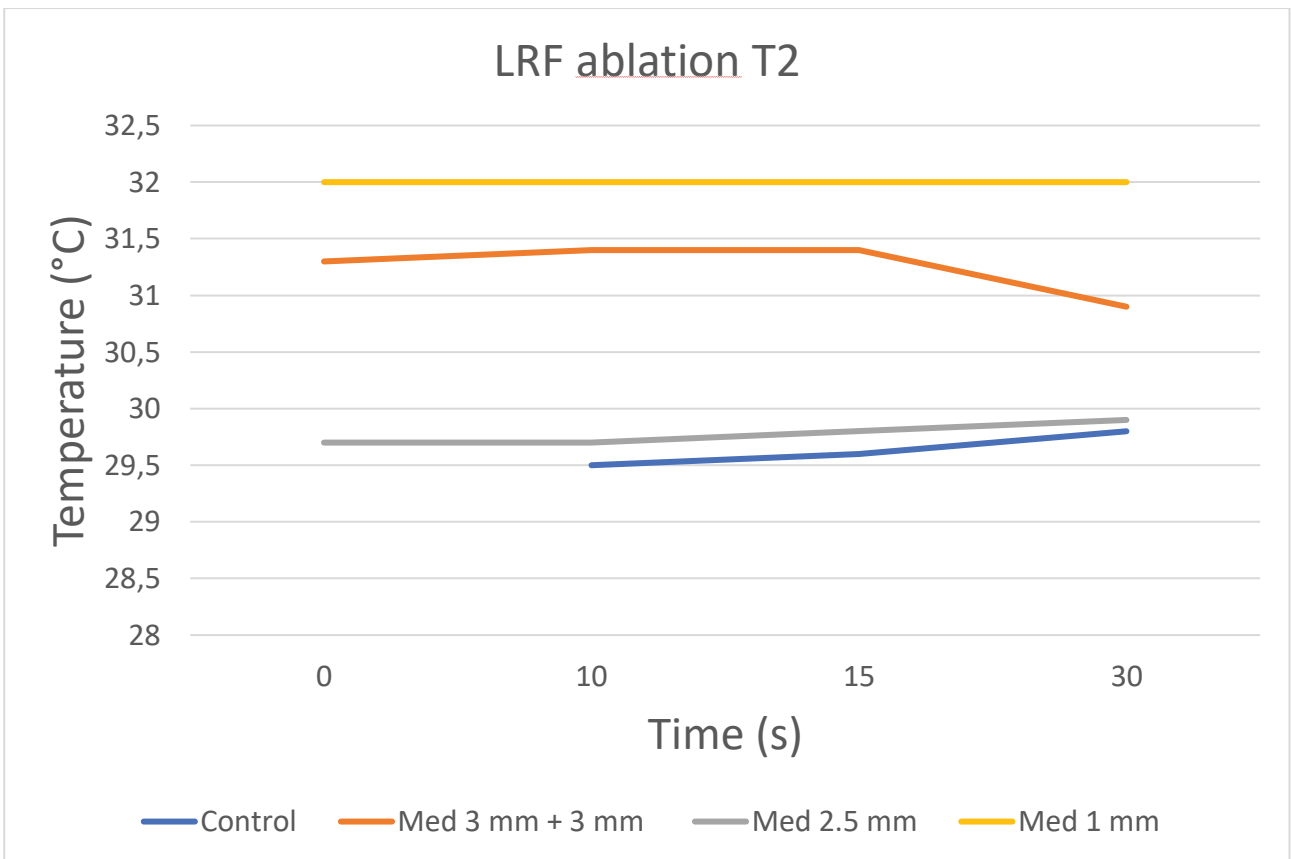


Figure 60. Linear Radiofrequency effect at 10 mm (T2).

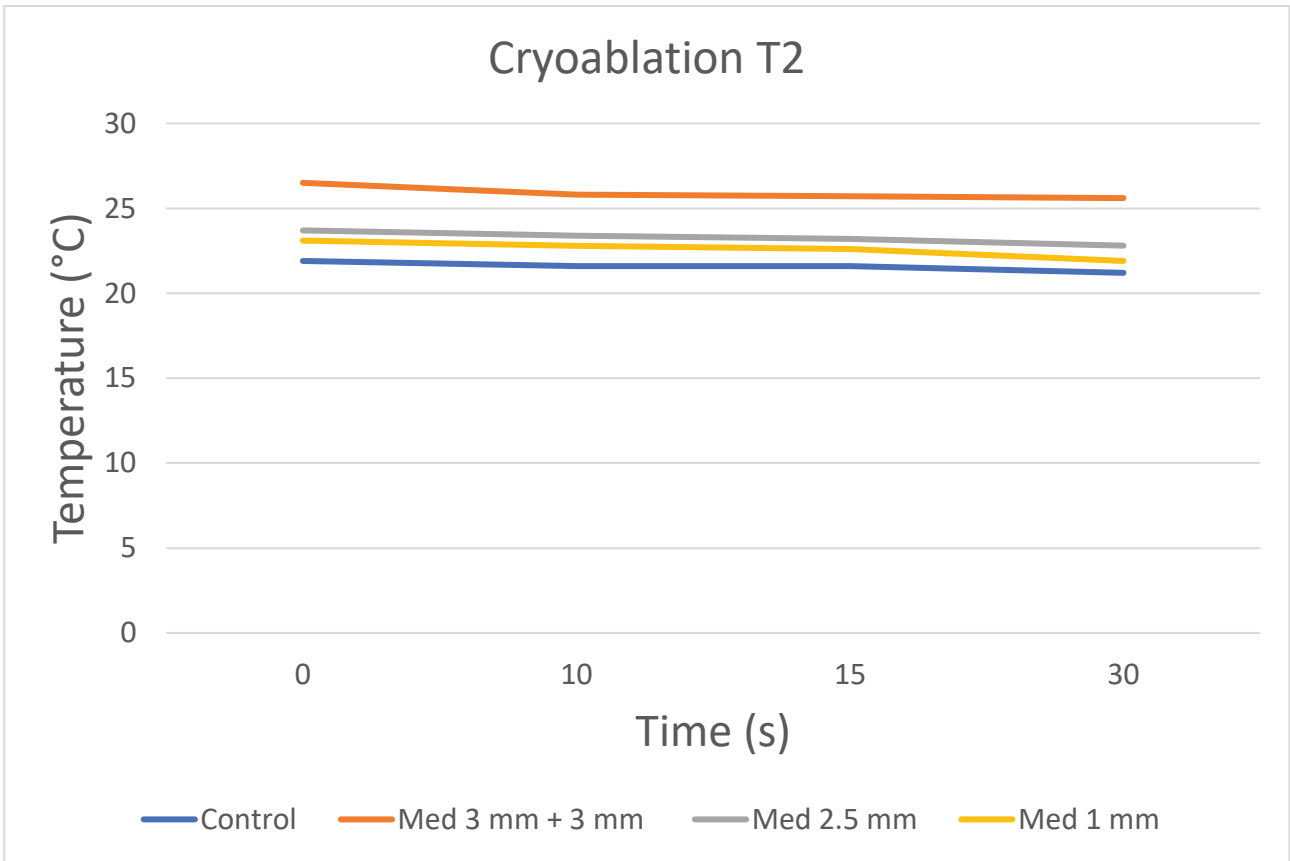


Figure 61. Cryoablation effect at 10 mm (T2).

III. References

- [1] Zhonghua Sun. Clinical Applications of Patient-Specific 3D Printed Models in Cardiovascular Disease: Current Status and Future Directions. *Biomolecules* 1,34, 2020.
- [2] Nan Chen, Kai Zhu, Chunsheng Wang, Xiaoning Sun. 3D printing technique for guiding complicated cardiovascular surgery. *Journal of Thoracic Disease*, 9, 10, 945-946, 2017.
- [3] Atul Verma, Nassir F Marrouche, Robert A. Schweikert, Walid Saliba, Oussama Wazni, Jennifer Cummings, Ahmad Abdul-Karim, Mandeep Bhargava, J. David Burkhardt, Fethi Kilicaslan, David O. Martin, Andrea Natale. Relationship Between Successful Ablation Sites and the Scar Border Zone Defined by Substrate Mapping for Ventricular Tachycardia Post-Myocardial Infarction, *Journal of Cardiovascular Electrophysiology*, 16, 5, 465-71, 2005.
- [4] Cristian Rosu, Philippe Demers. Three-dimensional printing in cardiovascular surgery: logical next step after three-dimensional imaging. *Journal of Thoracic Disease*, 9, 9, 2720-2722, 2017.
- [5] Daniele Gabriel-Costa. The pathophysiology of myocardial infarction-induced heart failure. *Pathophysiology* 25, 277–284, 2018.
- [6] Guangtao Yao, Guohai Su, Keqing Li, Bin Li, Hongwei Dong. Comparative study of ticagrelor and clopidogrel in therapeutic effect of acute myocardial infarction patients undergoing percutaneous coronary intervention. *Saudi Journal of Biological Sciences*, 24, 1818–1820, 2017.
- [7] J. Gordon Betts, Peter DeSaix, Eddie Johnson, Jody E. Johnson, Oksana Korol, Dean Kruse, Brandon Poe, James A. Wise. *Anatomy and Physiology*, 2013.
- [8] Yuki Tanabe, Akira Kurata, Takuya Matsuda, Kazuki Yoshida, Dhiraj Baruah, Teruhito Kido, Teruhito Mochizuki, Prabhakar Rajiah. Computed tomographic evaluation of myocardial ischemia. *Japanese Journal of Radiology* 38, 411–433, 2020.
- [9] John G. Webster, John W. Clark, Michael R Neuman, Walter H. Olson, Robert A Peura, Frank P. Primiano. *Medical Instrumentation Application and Design*. Fourth edition, 2010.
- [10] A.A. Qayyum, J. Kastrup. Measuring myocardial perfusion: the role of PET, MRI and CT. *Clinical Radiology* 70, 576-584, 2015.
- [11] Buxton RB. *Nuclear magnetic resonance; introduction to functional magnetic resonance imaging: principles and techniques*. New York, Cambridge University Press 64-85, 2002.

- [12] Chantal E. Stern. Principles of Functional Magnetic Resonance Imaging and its Applications in Cognitive Neuroscience. *New Technologies in Neurology* 8-26, 2005
- [13] Amardeep Ghosh Dastidar, Jonathan CL Rodrigues, Anna Baritussio, Chiara Bucciarelli-Ducci. MRI in the assessment of ischemic heart disease. *Article in Heart (British Cardiac Society)*, 239–252, 2015.
- [14] Pavel S. Yarmolenko, Eui Jung Moon, Chelsea Landon, Ashley Manzoor, Daryl W. Hochman, Benjamin L. Viglianti, and Mark W. Dewhirst. Thresholds for thermal damage to normal tissues: An update. *International Journal of Hyperthermia*, 27, 4, 320-343, 2011.
- [15] Alan K. Schaer, San Jose, EP CATHETER, national library of medicine, 2001.
- [16] G. Andrade, Paul Khairy Marc Dubuc. Catheter Cryoablation: Biology and Clinical Uses, *Circulation Arrhythmia and Electrophysiology*, 6, 1, 218-27, 2013.
- [17] Francesca Iacono, Jorge Lo Presti, Irene Schimpfern, Sara Ferretti, Andrea Mezzadra, Lalo Magni, Chiara Toffanin. Improvement of manufacturing technologies through a modelling approach: an air-steam sterilization case-study. *Procedia Computer Science* 180, 162–171, 2021.
- [18] Hyeonu Heo, Yuqi Jin, David Yang, Christopher Wier, Aaron Minard, Narendra B. Dahotre and Arup Neog. Manufacturing and Characterization of Hybrid Bulk Voxeled Biomaterials Printed by Digital Anatomy 3D Printing. *Polymers*, 13, 123,1-10, 2021.
- [19] Yan Epelboym, Paul B. Shyn, Ahmed Hosny, Tatiana Kelil, Jeffrey Forris Beecham Chick, Nikunj, R. Chauhan, Beth Ripley, Richard D. Nawfel, Francis J. Scholz. Use of a 3D-Printed Abdominal Compression Device to Facilitate CT Fluoroscopy Guided Percutaneous Interventions. *Vascular and Interventional Radiology, Technical Innovation*, 209, 435-441, 2017.
- [20] Raquel Sofia Cardoso Galante, Terezinha J. A. Pinto, Rog erio Colac, Ana Paula. Sterilization of hydrogels for biomedical applications: A review. *Journal of Biomedical Materials Research Part B Applied Biomaterials*, 00B, ISSUE 00, 1-21, 2017.
- [21] Sterris healthcare. Hydrogen Peroxide Sterilization. 2017.